BAPVC BAY AREA PHOTOVOLTAIC CONSORTIUM

Bay Area Photovoltaic Consortium Project Catalogue 2015

Acknowledgment: "This material is based upon work supported by the Department of Energy through the Bay Area Photovoltaic Consortium under Award Number DE-EE0004946.

Cover Photo: Carolin Sutter-Fella, BAPVC Post-doc in the Javey Group at Berkeley, is removing a sample from the thin-film vapor-liquid-solid (TF-VLS) growth chamber.

BAPVC Project Catalogue

2015

TABLE OF CONTENTS

Bay Area Photovoltaic Consortium 2015

Yi Cui, Co-Director Stanford

Ali Javey, Co-Director U. C. Berkeley

John Benner, Executive Director

About the Bay Area Photovoltaic Consortium

BAPVC is a consortium led by Stanford University (SU) and University of California Berkeley (UCB) that is funded by the U.S. Department of Energy (DOE), industry members and the participating universities. The consortium provides a vibrant forum for interaction among PV industry and academic experts to address the critical challenges in converting the U.S. leadership in PV R&D into leadership in PV manufacturing. The collective efforts of manufacturing and academic experts working together can spark great innovation. BAPVC draws on this innovation to conduct research and development in universities to produce technologies that industry members will use.

BAPVC was created in response to DOE's PV Manufacturing Initiative to provide a direct channel for exchange of PV manufacturing information among industry, universities and government. After a multi-year gestation period, the consortium is now achieving its goals. BAPVC established a strong community that has bridged these groups and created a working platform that enables truly disruptive research performed in the leading academic and National laboratories under the guidance of US PV companies. Building from its foundation of strong interaction between industry members and research participants, BAPVC has become highly effective in delivering research collaborations, innovation and intellectual property.

BAPVC's research impacts high-volume PV manufacturing, produces a highly trained workforce, and accelerates commercialization of cutting-edge PV technologies. BAPVC develops and test innovative new materials, device structures, and fabrication processes necessary to produce cost-effective PV modules in high volumes. The research aims to find technologies which can increase photovoltaic conversion efficiencies and simultaneously reduce manufacturing cost. Success in research is measured by transfer of the technologies for development in industry.

Industry Members of the consortium identify research priorities, inform the scope of RFPs, review and rank proposals, and monitor the progress of research. Industry members are the first to learn of inventions and will be in the best position, potentially in partnership with other member companies, to adopt and build on those inventions in their own laboratories and factories.

BAPVC Technical Scope

BAPVC projects have aggressive goals set to develop disruptive technologies. Such projects frequently present multi-faceted challenges needing collaborative, consortium-sized efforts to advance to the next technology readiness level. BAPVC brings together materials scientists, device engineers, manufacturing specialists and equipment suppliers to capture the revolutionary advantage of our technologies.

BAPVC research is composed of the following thrusts: 1) High performance and multijunction cells; 2) Silicon absorbers and cells; 3) Thin film absorbers and cells; 4) Photon management and transparent

conductors; and, 5) Encapsulation and reliability. This catalogue includes a brief description of the thrust strategy followed by the annual reports for relevant projects.

Direction for the Future

Manufacturing costs associated with photovoltaic module production have decreased dramatically over the past decade, uncannily tracking projections extrapolated from the well-known learning curve. The learning curve plots the record of industry's ability to incorporate new technologies in each generation of production as cumulative production expands to meet global demand. Many of the innovations that are moving into production today were invented twenty or more years ago in university laboratories. Incorporating these advancements into new generations of production required additional innovation from industry's engineers. This is the fundamental learning process portrayed in the ubiquitous learning curve for photovoltaics. The key issue in photovoltaics today is that the industry must be growing and adding new capacity with new technology in order to be learning. At the current levels of capital expenditure needed for new capacity, installation of new equipment for replacement or expanded capacity – the "learning experiment" – cannot be sustained from cash flow. It is essential that we develop new technologies to produce high efficiency, durable, low-cost photovoltaic modules from factories costing far less than the $1.00/Wp per annum. This has the direct effect of reducing production costs for equipment depreciation and the more important benefit in maintaining the steep slope of the learning curve.

BAPVC's industry members developed guidance for the next phase of BAPVC research that places much greater emphasis on exploration of technologies that will reduce the capital intensity of PV manufacturing. New technologies with very low CapEx and production cost, based on defensible intellectual property created in the U.S., will enable renewed growth of a sustainable and competitive domestic PV manufacturing industry.

Research will focus on the development of PV devices, materials, manufacturing methods, and understanding of reliability that enable disruptively-lower costs and rapid scaling. A reduction in capex has extra leverage toward these goals because it reduces costs, enables cash-flow-positive growth at lower margins, and enables old-technology-capacity to be replaced by new capacity thus accelerating industry progress. High reliability and confidence in the reliability is required to be able to scale a new technology and have that product be financeable at low interest rates. A module which addresses these needs would have the following characteristics as targets:

- Very low CapEx intensity (target <$0.25/$W_p$ p.a.)
- High conversion efficiency (target >20%)
- Very low product manufacturing cost (<$0.25/$W_p$)
- Excellent environmental profile
- Long module lifetime (>35 years) with low degradation (target < 0.3%/year)

Achieving these goals requires new structures and approaches from those in production or in near term development within industry. Pathways to reaching these goals encompass research on both the traditional as well as new material classes that can challenge the dominance of incumbent PV technologies. Industrial R&D, in the face of decreasing profit margins, is confined by a 5-year development horizon to incremental improvements of the incumbent technology. BAPVC's industry members bring industrial expertise to the consortium to increase academic researcher's understanding of manufacturability. Guidance from industry assists BAPVC to identify avenues of investigation just beyond industry's own mission critical research while avoiding technologies that have been tested and discarded in the course of proprietary industrial research.

BAPVC Annual Project Report

Project Title:
Technoeconomic Analysis in Support of the Bay Area Photovoltaics Consortium
PI: Michael Woodhouse
E-mail: Michael.Woodhouse@nrel.gov

Summary:
NREL's technoeconomic analysis group has worked extensively with a number of other groups within the BAPVC. The analysis results have been used within presentations and posters by other BAPVC principal investigators, and in peer-reviewed publications. The group looks forward to continued analysis in support of BAPVC researchers and member companies.

Key Accomplishments:
In addition to assisting other BAPVC principal investigators with targeted cost estimates of their specific processes, NREL's technoeconomic analysis group continues to enjoy the benefits of close collaboration with Professor Tonio Buonassisi. This collaboration has most recently resulted in a successfully submitted and accepted article to *Energy and Environmental Science* on the topic of capital intensity of Photovoltaics manufacturing and how this may present barriers to scale (as well as opportunities for innovation).

In this study the variable cost elements of materials, labor, electricity, and maintenance are detailed for crystalline silicon manufacturing; as are the fixed cost elements of research and development (R & D); and sales, general, and administrative (S, G, & A). The other fixed cost element of depreciation—the one that belies the CapEx—is also detailed for all major steps of the supply chain, including polysilicon and wafer, cell, and module conversion.

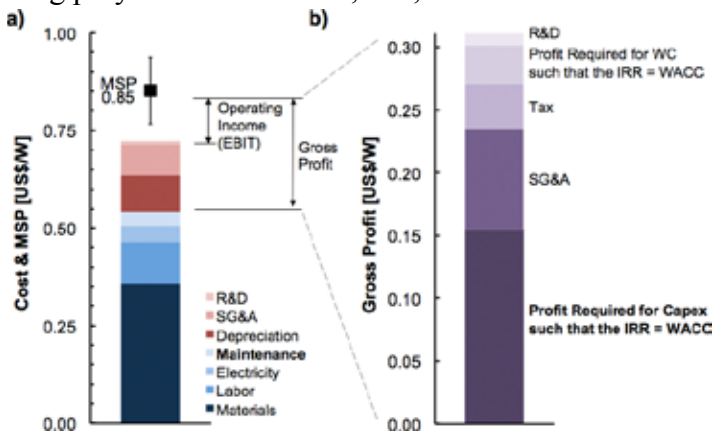

Figure 1: (a) Breakdown of U.S. standard monocrystalline silicon cost components and minimum sustainable price calculations that factor into gross profit and operating income (earnings before interest and taxes, EBIT). (b) Breakdown of gross profit, equal to the MSP minus variable costs. CapEx-related items are bolded. The profit required to generate the required return for CapEx in (b) is approximately double the straight-line depreciation expense in (a) due to the required rate of return on the initial capital investment. If the WACC is increased (from 14% in this example), the disparity between these factors increases.

The other consideration that is significantly influenced by CapEx is the minimum sustainable margin requirement between the price and costs for manufacturing. This is because the CapEx is, by definition, the amount of initial investment required to institute new capacity; the higher the amount of initial investment required, the greater the financing needs. In order to pay back debt and equity investors, increased financing needs for more fixed assets translates to higher calculated sustainable margins. The analysis with MIT shows one example, that for a monocrystalline silicon supply chain within the United States, of the benefits of lowering the CapEx in order to lower these margins.

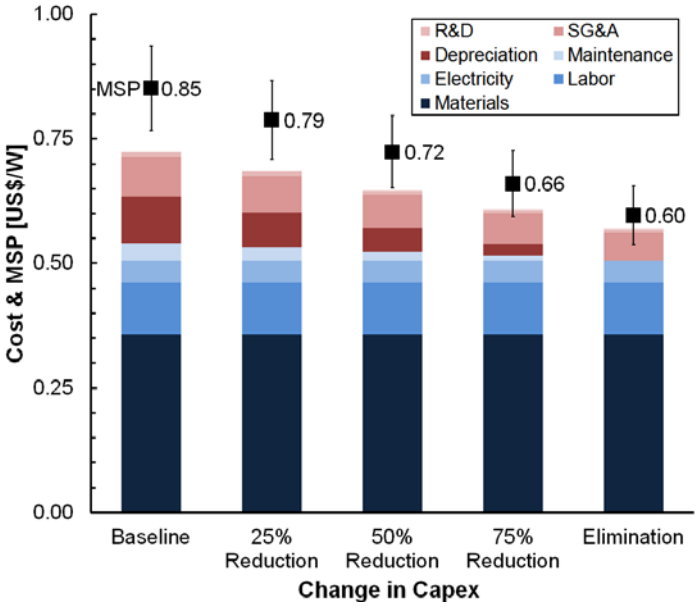

Figure 2: Decreasing CapEx has a large impact on the minimum sustainable price (MSP) of module manufacturing and provides the potential to reduce MSP by up to 0.25 $/W in the modeled scenario. Halving CapEx provides a 15% reduction in MSP. The gross margin requirement drops significantly with reduced CapEx.

Future Work:

NREL's technoeconomic analysis group looks forward to continued assistance to other investigators. Together we can develop a better understanding of how research could be translated into incumbent and novel manufacturing processes. One success from the previous year that should be developed further is in studying the mechanisms for reducing the CapEx. By leveraging prior work for a number of photovoltaics technologies, the group is looking forward to sharing information on the subject of costs accounting. The group hopes that these collaborations will be beneficial, insightful, and informative to other researchers, and that they will provide useful results for inclusion in peer-reviewed publications. It also hoped that the results would be informative for the member companies. The group hopes to work across the consortium in order to identify and pursue research opportunities that may enable solar generated electricity to become competitive with traditional energy sources.

Thrust: High Performance and Multijunction Cells

Key Challenges

The goal of this thrust is to explore new growth processes, material systems, and device architectures for offering high device efficiencies at low processing costs. In particular, two parallel approaches are being explored, one relying on reducing the processing costs of III-V single junction solar cells and the other exploring tandem device architectures based on Si bottom cells. The key challenge for the field is developing disruptive growth and processing technologies that would drastically lower the cost without sacrificing the device efficiencies. In parallel, tremendous opportunities are present in exploring tandem cells based on Si (or CIGS, CdTe, or III-V) bottom cells to enhance the efficiency of the existing PV technologies, but with careful consideration of the costs to ensure a balance approach is developed. Cost analysis, device modeling, and experiments are being performed in parallel in a collaborative manner to ensure success.

Existing Projects in our Thrust

- *High Performance, Low Cost, III-V Photovoltaics on Metal Foils,* Ali Javey (Berkeley)
- *Ultra High Efficiency Thin Film Multijunction Solar Cell,* Jim Harris (Stanford)
- *Thin Film Compound Semiconductor Solar Cells via Templated Growth,* Paul McIntyre (Stanford)
- *Low-Cost Tandem Solar Cells with Greater than 20% Power Conversion Efficiency,* Mike McGehee (Stanford)
- *High Voc Solar Absorbers for High-Efficiency, Spectral-Splitting, Solar Cells,* Eli Yablonovitch (Berkeley)
- *Si/II-VI Double-Heterostructure Solar Cells,* Yong-Hang Zhang (Arizona State)
- *Design Principles and Defect Tolerances of Silicon / III-V Multijunction Interfaces,* Tonio Buonassisi (MIT)
- *Exploratory Photovoltaic Modeling and Simulation,* Peter Bermel (Purdue)

Potential New Areas of Interest

- More cost analysis of the explored research projects in collaboration with NREL. Currently 2-3 of the projects within the thrust have had cost analysis discussions with NREL. More projects can follow this path.
- Exploring the device processing and manufacturability of the new III-V growth technologies, such as the thin-film VLS process.
- Exploring surface passivation effects and back-contact reflectors for the new III-V growth technologies, such as the thin-film VLS process.
- Better understanding (experiments and modeling) of the types of defects that their correlation to performance for the new III-V growth technologies, such as the thin-film VLS process.
- Development of high bandgap (III-V, II-VI, perovskite or other) solar cells for performance in tandem devices
- Defect mitigation during silicon cell fabrication, for improved multijunction bottom-cell performance.

- Defect recognition and characterization in high-quality Czochralski silicon for high-efficiency PV devices.
- Light management in tandem and other high performance solar cells.
- Development of tunnel junctions, recombination layers, polymer electrolytes, or other transparent contacts that will enable current matching between silicon solar cells and a high bandgap solar cell.

BAPVC Annual Project Report

Project Title: Properties of TF-VLS InP Solar Cells on Metal Substrates
PI: Ali Javey
E-mail: ajavey@berkeley.edu

Summary:

The work focuses on the successful development and characterization of first generation solar cell devices based on thin-film vapor-liquid-solid (TF-VLS) grown InP absorbers. Promising conversion efficiencies exceeding 12 % are demonstrated. For the employed device architecture, an ex-situ doping process was established to convert the as grown n-InP to p-InP by Zn incorporation. In depth device analysis has been performed to extract the limiting parameters and is complemented by an ongoing collaboration with Oregon University.

Key Accomplishments:

An ex-situ p-type doping process was developed to convert the as-grown n-InP to p-InP by Zn doping via closed space sublimation. Low temperature PL measurements were used to track the different doping stages, Figure 1a. To evaluate the solar cell performance of TF-VLS InP the following device architecture was successfully tested: Mo foil back contact/p-InP/TiO_2/ITO window layer. Cross sectional SEM micrographs of a representative device and a zoom-in image are depicted in Figure 1b.

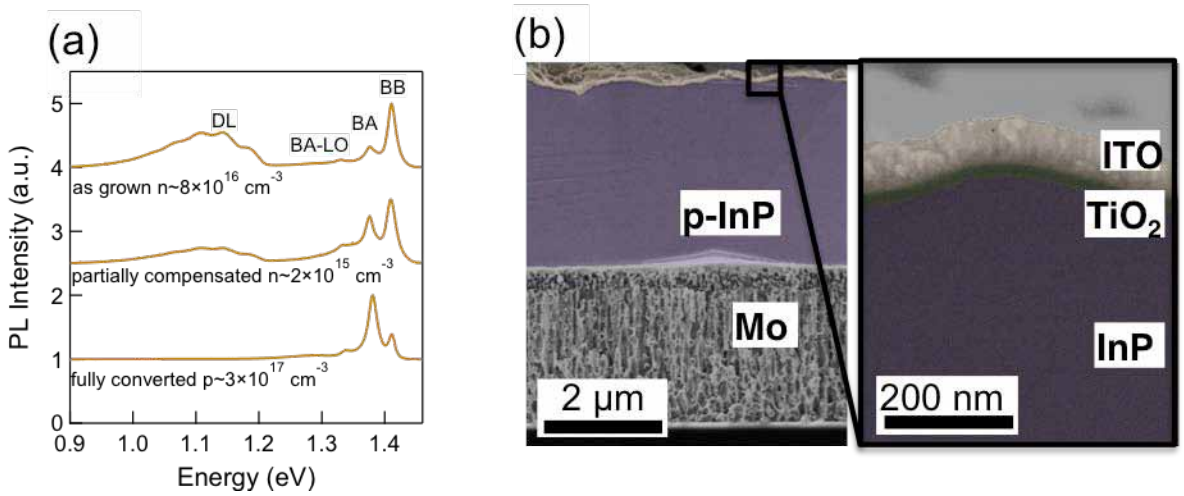

Figure 1. (a) PL spectra of InP taken at 8 K. From top to bottom: as-grown (n~ 8×10^{16} cm^{-3}), partially compensated (n~2×10^{15} cm^{-3}) and fully converted to p-type (p~3×10^{17} cm^{-3}). (b) Cross section SEM image of a completed cell and a higher magnification cross section SEM image of the surface region (SEM images are false colored).

The first generation of TF-VLS devices exhibits efficiencies up to 12.1 % with V_{oc} = 692 mV, J_{sc} = 26.9 mA/cm^2 and FF = 65.0 % (see Figure 2a). The corresponding EQE and 1-R of the cell is shown in Figure 2b.

To investigate the effect of the grain boundaries, electron beam induced current (EBIC) mappings and line measurements were performed on full devices. The dark regions in the EBIC map (Figure 2c) correspond to lower carrier collection. Variations along grains can be seen as well as poor carrier collection at the grain boundaries. EBIC line scans across gain boundaries were used to extract the grain boundary recombination velocity and the minority carrier diffusion length, Figure 2d. The obtained diffusion length is in the range of 1-3 um and is comparable to reported values for CdTe and CIGS based thin film solar cells. However, the extracted grain boundary recombination velocity is about two to three orders of magnitude higher in TF-VLS InP.

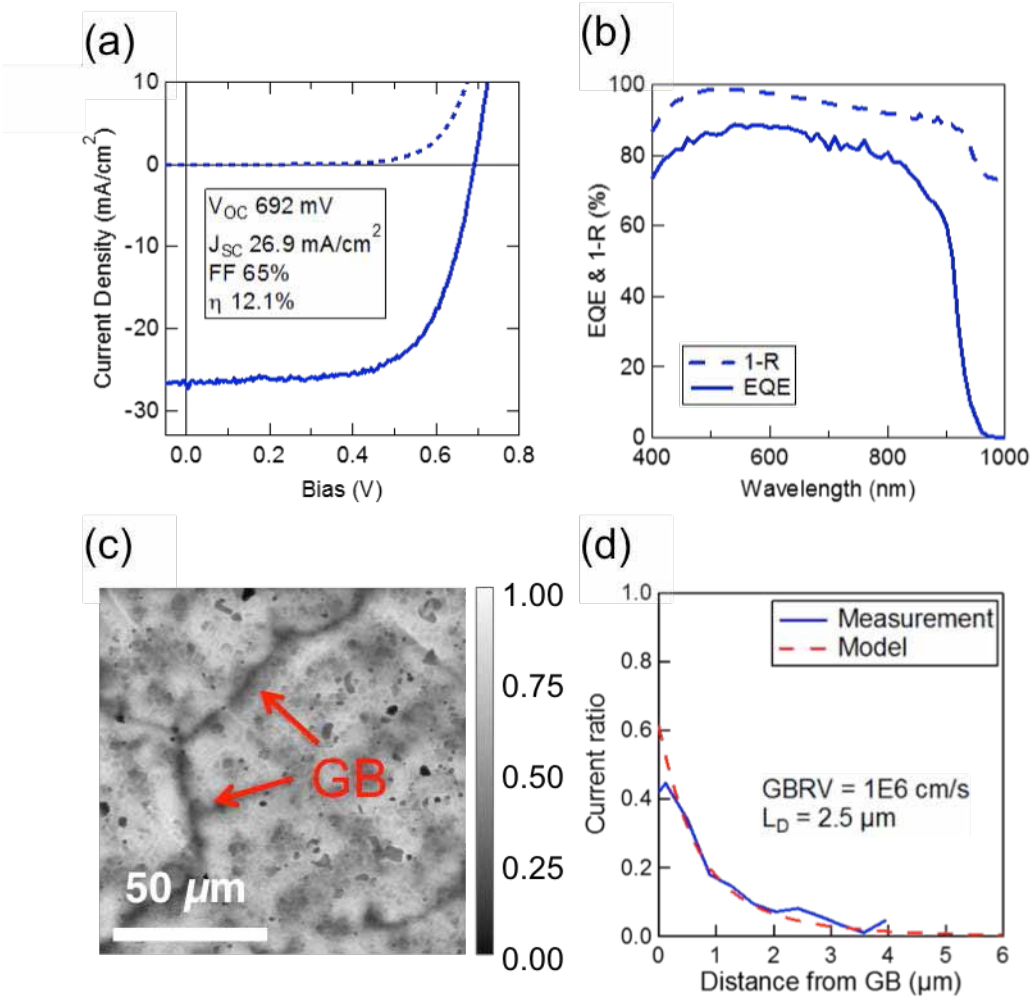

Figure 2. (a) JV measurement under 1 sun illumination and in the dark. (b) Corresponding EQE and 1-R curve. (c) EBIC map on a TF-VLS solar cell device where dark areas represent reduced charge carrier collection. (d) EBIC line scan over a grain boundary.

Future Work:

Future work will focus on the improvement of device efficiency as well as the development of in-situ doping processes and the role of impurities in TF-VLS InP.

Project Title: Ultra high efficiency thin film multi-junction solar cell
PI: James S. Harris
E-mail: jharris@stanford.edu

Summary:

The Harris group proposed to develop significantly higher efficiency thin film multi-junction solar cells by combining multi-junctions and advanced nano-scale light management concepts in ultra-thin film devices that lend themselves to very large scale, low cost manufacturing. In the past year, they developed thin-film nanostructured solar cell modeling, epitaxial growth and fabrication. A nanostructured ultra-thin-film GaAs solar cell (300 nm) demonstrated improved Jsc, Voc, fill factor and efficiency. The voltage enhancement on a 5-μm-thick Si cell was demonstrated, which achieves a V_{oc} of 649 mV. They also developed bonding process and luminescent coupling modeling for multi-junction solar cells based on Si.

Key Accomplishments:

An ultra-thin-film 'nanowindow' solar cell (figure 1a, b) was developed that combines a nanostructured window layer with an ultra-thin-film (300 nm) planar absorber/junction. This ultra-thin cell consists of a nano-structured $Al_{0.8}Ga_{0.2}As$ window layer on the front side to reduce the reflection and to trap the light, and a metal reflector on the back side to further increase the light path. The 300 nm thick GaAs cell with $Al_{0.8}Ga_{0.2}As$ nano-window shows a broad band absorption enhancement from the visible to near infrared (NIR), achieving a spectrally averaged absorption of 94% under normal incidence (figure 1c). Different from the Fabry-Perot oscillations of the planar control sample, flat, broad-band absorption of the nano-structured sample is observed, which is a result of the more confined optical modes formed in the nano-structured film. In addition, this cell shows excellent angular absorption properties, achieving over 85% spectral averaged absorption at up to 60 degrees off normal incidence (figure 1d). Meanwhile, this structure with a planar junction and nano-window has solved the issue of poor fill factor and low open-circuit voltage in nano-structured GaAs solar cells. Because of the anti-reflection and light trapping of the nano-window layer, J_{sc} of the nanostructured cell is improved from 11.9 mA/cm^2 in the planar control sample to 13.8 mA/cm^2 for the nano-structured sample (figure 1e). The overall efficiency is increased from 7.41 % to 9.00 %.

In a second part of our high-efficiency solar cell development, we have focused on the voltage enhancement of thin-film c-Si solar cells due to vertical carrier confinement. The physical mechanism of vertical carrier confinement was theoretically studied with simulations (figure 2a). Furthermore, the voltage enhancement in a 5-μm-thick c-Si cell was experimentally demonstrated, which achieves a 9 mV higher V_{oc} than a 50-μm-thick cell (figure 2b). This is also the highest V_{oc} among recently reported sub-25-μm-thick cells. Together with the nanostructured dielectric layer (NDL) of SiN_x on c-Si, the overall energy conversion efficiency will be further improved. This work provides a solid foundation for the continued development of future high-efficiency and low-cost thin-film crystalline solar cells.

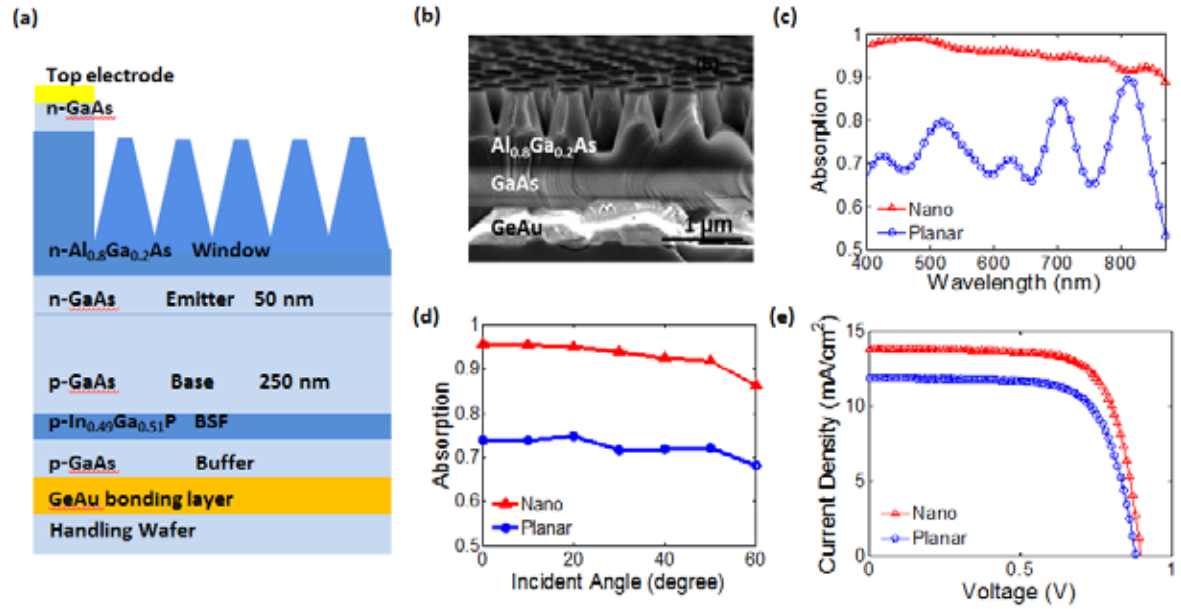

Fig. 1. Overview of the structure and measured characteristics of an ultra-thin-film AlGaAs/GaAs nanostructured window solar cell. (a) Schematic of the cell structure. (b) SEM cross-section image of the solar cell active region with $Al_{0.8}Ga_{0.2}As$ nanocone window layer. The GaAs solar cell is only 300 nm thick. (c) The measured absorption spectrum of ultra-thin-film GaAs cells with nano-window (red) and planar window (blue). (d) The measured spectrally averaged absorption versus incident angle of ultra-thin-film GaAs cells with nano-window (red) and planar window (blue), weighted by AM 1.5G spectrum. (e) J-V characteristics of the ultra-thin-film GaAs solar cells with nano-structured (red) and planar (blue) window layer.

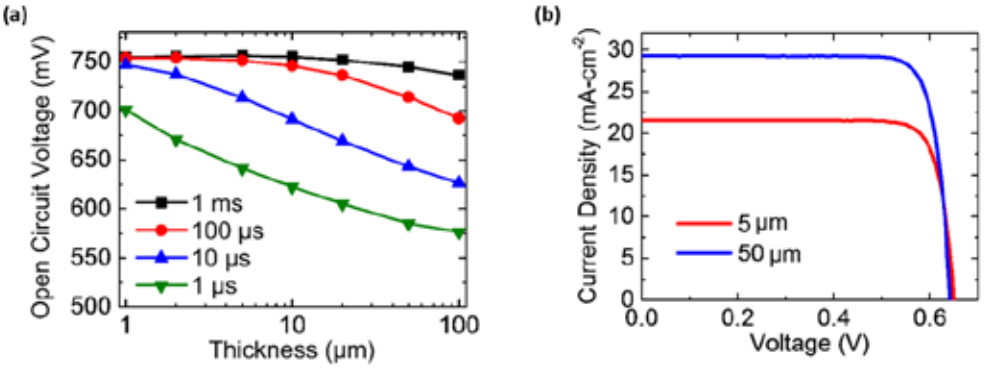

Fig. 2. Overview of the voltage enhancement of thin-film c-Si solar cells. (a) Simulation V_{oc} as function of cell thickness (W) and minority-carrier life time (τ). (b) J-V characteristics of 5-μm-thick and 50-μm-thick c-Si solar cells.

In addition, an In-Au metal bonding process has been developed to replace the Ge-Au bonding process. This bonding process lowers the bonding temperature to below 250°C, reducing damage to the ultra-thin film GaAs cell. Since indium forms a thinner, small bandgap layer rather than a very highly Ge doped region, this process also prevents the shunting effects caused by germanium diffusion and phase segregation. In-Au bonding of bulk materials has been demonstrated with very good bonding strength and uniformity (figure 3). Combined with the subsequent substrate-removal process, which is under development, this bonding process can produce a very promising pathway to a high-efficiency multi-junction device on c-Si.

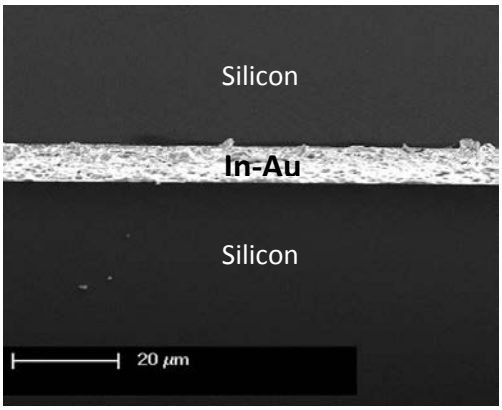

Fig. 3. Result of In-Au bonding process. (a) Bonded silicon pieces. Very good bonding strength has been observed. (b) SEM image of the cross-section of the bonding layer. Uniform In-Au bonding layer has been achieved with no void or peeling.

In order to optimize the device design, advanced multi-junction modeling with luminescent coupling effects has been investigated. In the process of developing the model, the bias-voltage-dependence of luminescent coupling efficiency has been discovered and studied (figure 4). This work will potentially lead to more accurate performance prediction for multi-junction solar cells and greatly improve the cell design process.

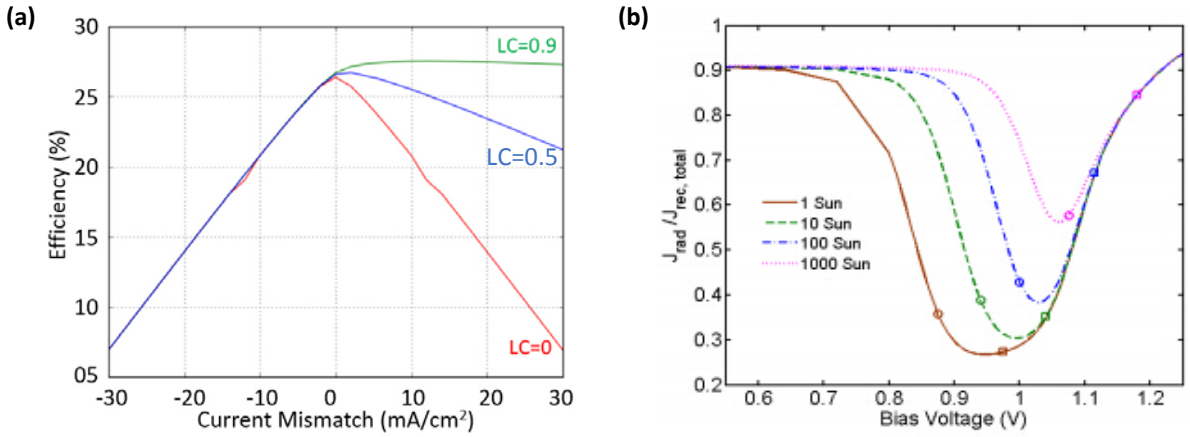

Fig. 4. Modeling results of luminescent coupling effects. (a) Efficiency of a 2-junction solar cell with different photocurrent mismatch of the two junctions. Red, blue and green curves show the cases for luminescent coupling efficiency equal to 0, 0.5 and 0.9 respectively. (b) Change of the luminescent coupling efficiency, expressed as a ratio between the radiative and total recombination current in the top junction, with the bias voltage of the top junction.

Future Work:

The Harris Group will continue to optimize a nanostructured single junction ultra-thin-film GaAs solar cell with a high short circuit current extraction of over 20mA/cm^2 with an overall energy conversion efficiency of over 18%. In order to achieve this, the low-temperature indium bonding process will be integrated into the ultra-thin-film solar cell fabrication process. They'll also fabricate multi-junction solar cells based on ultra-thin nanostructured GaAs and thin c-Si, trying to achieve >30% overall energy conversion efficiency.

BAPVC Annual Project Report

Project Title: Thin Film Compound Semiconductor Solar Cells via Templated Growth
PI: Paul C. McIntyre
E-mail: pcm1@stanford.edu

Summary:

Combining normal Al-induced crystallization (AIC), a thin oxide layer, and rapid thermal annealing (RTA), MOCVD GaAs thin films having maximum grain size ~ 400 μm^2, with an areal coverage of 60% of the film by (100) grains were templated on crystallographically-textured poly-Ge films on glass substrates. The hole mobility of templated poly-GaAs films is similar to that of single crystal bulk GaAs at a similar doping level (~ 10^{18} cm^{-3}). Photoluminescence spectra at room temperature and 80 K measured from templated poly-GaAs films show strong band edge luminescence, indicating that defects resulting from the polycrystalline structure of GaAs are insufficient to suppress radiative recombination.

Key Accomplishments:

Large-grained (100) oriented poly-Ge thin film templates are achieved through normal AIC at relatively low annealing temperature, 250 ˚C, for 10 hours. Placing a thin layer of Al oxide between Al and a-Ge layers in the initial structure is critical to lower the required annealing temperature and shorten the annealing duration for layer exchange crystallization of Ge. In this study, RTA has proved to be effective to increase the Ge grain size in poly-Ge films after exchange. Combining normal AIC, a thin oxide layer, and RTA, the resulting poly-Ge thin films have grain sizes ≤ 124 μm^2, with an areal coverage of 57% of the film by (100) grains.

Poly-GaAs thin films seeded by poly-Ge templates have reasonably good crystal quality and electronic properties. The percentage of (100) grains in templated poly-GaAs film is > 60%, and the maximum single crystal grain size is ~ 400 μm^2. Such improved crystal quality compared with the poly-Ge template indicates the potential to further improve grain sizes and orientations by tuning the GaAs deposition recipe. Templated poly-GaAs thin films are p-type conductive, and the high hole doping is attributed to Ge atoms that dissolve in GaAs from the template. The hole mobility of templated poly-GaAs film (Figure 1) is as high as that in single crystal bulk GaAs at a similar doping level (~ 10^{18} cm^{-3}). Photoluminescence spectra (Figure 2) at room temperature and 80 K of templated poly-GaAs films show strong band edge luminescence, indicating that the defects resulting from the polycrystalline structure of GaAs are insufficient to suppress the strong radiative recombination.

Future Work:

Project completed; graduate student research assistant (Y. Li) completed her doctorate in Applied Physics.

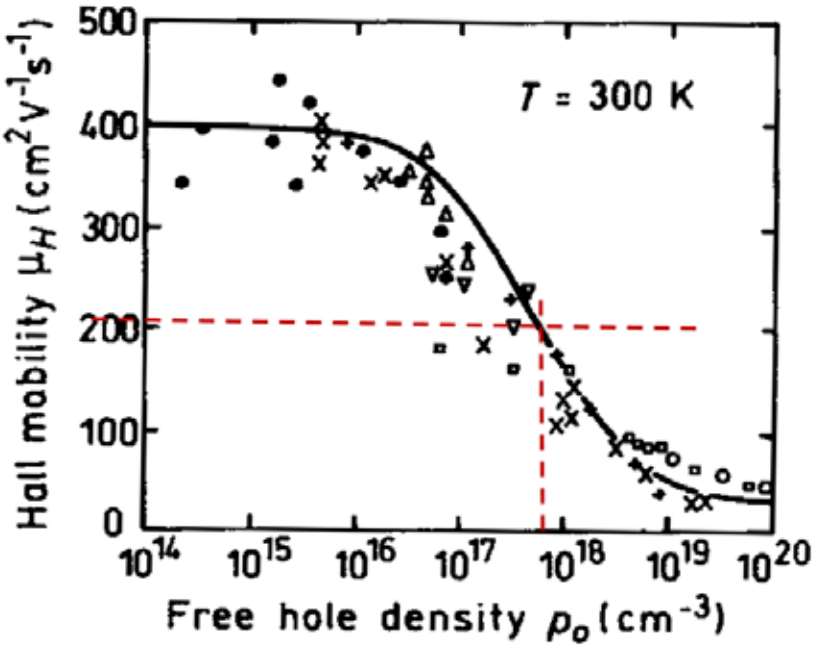

Figure 1 **Hall mobility vs. hole density in single crystal bulk GaAs. The dashed line marks the hole density level of the poly-GaAs thin films seeded by poly-Ge template and their corresponding hole mobility.**

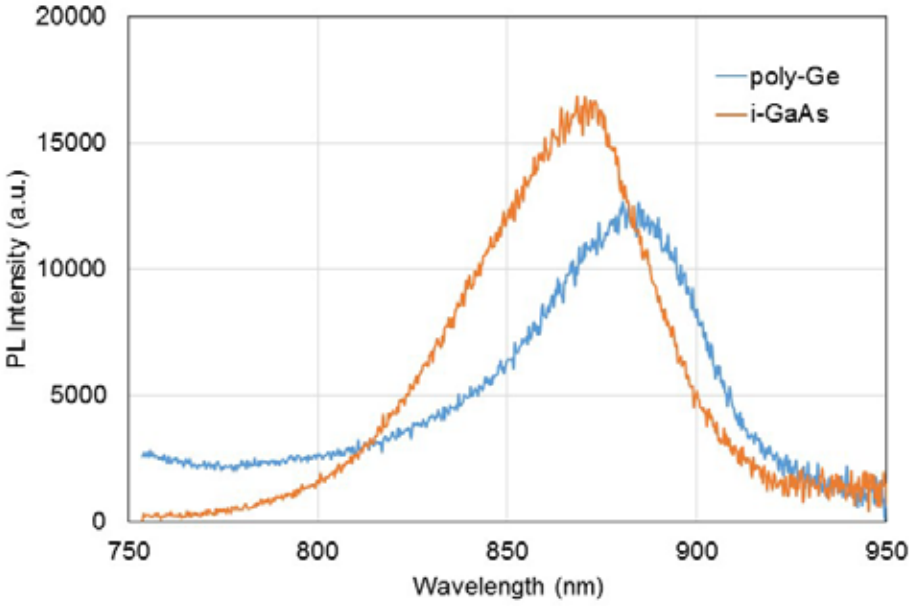

Figure 2 **Photoluminescence spectra of a poly-GaAs film grown on a poly-Ge template and a GaAs film grown on a single crystal i-GaAs substrate measured at room temperature with the same incident power.**

BAPVC Annual Project Report

Project Title: Improving the Long-Term Stability of Perovskite Solar Cells
PI: Michael McGehee, Paul McIntyre
E-mail: mmcgehee@stanford.edu, pcm1@stanford.edu

Summary:

We have been developing conformal, atomic layer deposited (ALD) titanium oxide (TiO_2) barrier layers to prevent volatile organic components of methylammonium lead iodide ($MAPbI_3$) from leaving perovskite solar cells to improve their thermal and long term stability. Conditions for low temperature ALD deposition of TiO_2 were determined in order to reduce damage to the perovskite during deposition. We have also deposited our first titanium oxide films on the perovskites and are working to further reduce damage to the perovskite during deposition.

Key Accomplishments:

We did preliminary research on ALD-TiO_2 protection of perovskite absorbers ($CH_3NH_3PbI_3$), which indicated that the perovskite material is not stable when the deposition temperature is above 100 °C. As typical ALD temperatures for TiO_2 are 150°C -170 °C, it was necessary to develop a low temperature ALD TiO_2 growth process for our project. To better understand the electronic and basic material properties of this material, we first studied low temperature ALD TiO_2 growth on crystalline silicon substrates. We used tetrakis(dimethylamino) titanium (TDMAT) as the titanium precursor and water as the oxygen source to try to deposit TiO_2 on silicon at 45 °C. We demonstrate that even at these low temperatures, the growth is quite linear, consistent with self-limiting precursor surface reactions (**Figure 1, left)**. X-ray photoelectron spectroscopy (XPS) measurements show a relatively small nitrogen concentration in the films, which indicates the organic component of the TDMAT leaves the film with little residue during deposition at 45°C. Electrical characterization (**Figure 1, right**) of this material shows that the leakage current decreases as the thickness increases. To test whether there are pin-holes in the film, we performed Auger analysis. The data shows that there is no signal present from the silicon substrate on which we deposit 10 nm TiO_2, which indicates good surface coverage for this film thickness. Further experiments are needed (e.g. conductive AFM) to test for pinholes in thinner low-temperature ALD-TiO_2 films.

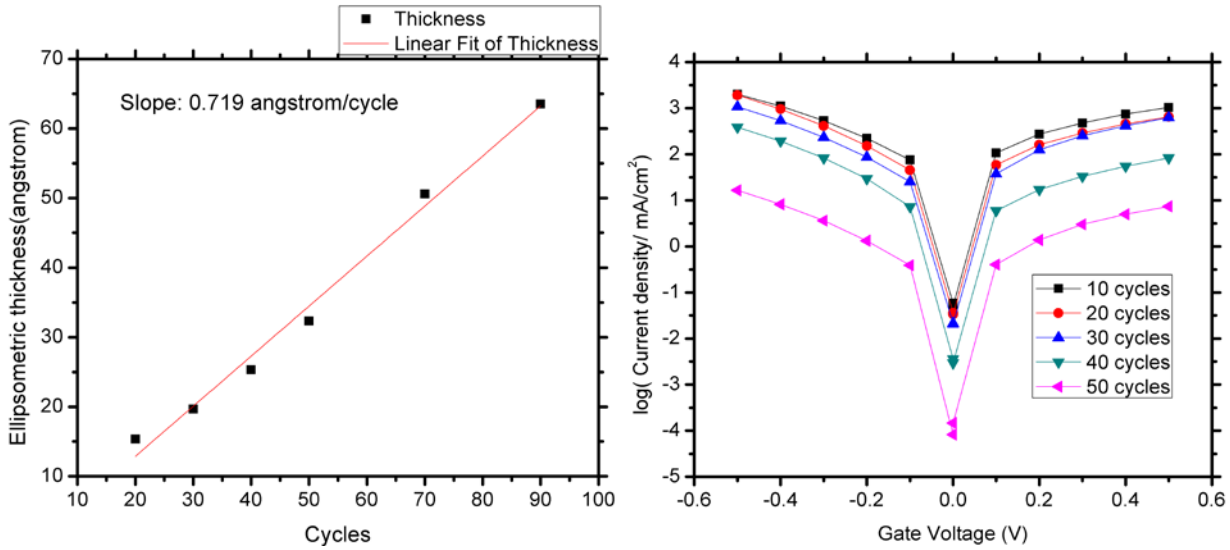

Figure 1. (left) Ellipsometric thickness of TiO_2 as a function of ALD cycles. **(right)** Current-voltage measurements of the silicon samples after ALD.

We have begun to deposit TiO_2 on top of perovskite films using this process. XPS measurements show the titanium signal increases roughly in proportion to the number of ALD cycles, indicating there is no problem initiating TiO_2 growth on top of the perovskite. However, X-ray diffraction (XRD) measurements show the presence of lead iodide (PbI_2), indicating that the perovskite is partially degraded after only 15 cycles of ALD. Optimization of the TiO_2 growth conditions is our current focus in order to develop conformal protective thin TiO_2 films which do not disrupt the quality of the underlying perovskite material and allow for efficient solar cell performance.

Future Work:

In the coming six months we will explore other TiO_2 ALD deposition conditions to minimize damage to the perovskite. In particular, we will try using other chemistries, such as ozone, that do not involve using water as the oxygen source, as water moisture is known to degrade the perovskite into lead iodide. Successful deposition will be determined by the lack of lead iodide peaks in the XRD pattern. We will also deposit C_{60} on top of the perovskite prior to titania deposition to try to protect the perovskite, as well as improve electron extraction in full solar cells. We may need to incorporate zinc nanoparticles into the C_{60} to help seed the titania growth to improve coverage. Additionally, we are beginning measurements using a residual gas analyzer (RGA) to identify the volatile compounds that leave perovskite films and solar cells when exposed to vacuum or heated. These studies will help inform the design of barrier materials and encapsulants to prevent the egress of these species.

BAPVC Annual Project Report

Project Title: Hybrid Tandem Photovoltaics Using Organometallic Perovskites on Top of Silicon and CIGS

PI: Michael McGehee
E-mail: mmcgehee@stanford.edu

Summary:

Hybrid tandem photovoltaics, two different semiconductor technologies used in a single tandem device, can improve the efficiency of solar modules without greatly increasing the module cost. They mechanically stack a semi-transparent perovskite device in a 4-terminal tandem configuration onto CIGS and Si solar cells and demonstrate net efficiency improvement. They monolithically integrate a perovskite solar cell with a silicon solar cell using a tunnel junction to make a 2-terminal tandem device.

Key Accomplishments:

In a continuation of the year one accomplishments, they have continued to improve the semi-transparent perovskite cell, achieving 12.7% efficiency with a peak transmission of 77% at 800nm. When paired with a 17.0% CIGS solar cell, they upgrade the cell to a tandem stack with 18.6% efficiency. They sent a separate semi-transparent perovskite cell to NREL for certification using a 17.0% silicon solar cell as the bottom cell, and certifying the tandem at 17.9% (Figure 1). These devices were reported in the journal *Energy and Environmental Science* (DOI: 10.1039/C4EE03322A) and a patent was sponsored by BAPVC and filed through Stanford concerning the method of depositing the transparent electrode. This work was featured by Science Magazine and Stanford News and subsequently reported by multiple news organizations.

As indicated in the future work section of last year's report, they designed and tested a monolithic 2-terminal tandem in collaboration with the Buonassisi group. Monolithically integrated tandems have design constraints that differ greatly from mechanically stacked tandems. The two most obvious design constraints are current density-matching of the subcells and the need for a transparent electrical connection between the subcells. For the electrical connection, they employ band-to-band tunneling on the top of the silicon wafer. They build the monolithically integrated tandem on an n-type silicon wafer, with a tunnel junction on the surface, a compact TiO_2 layer deposited by ALD, and the remainder of the perovskite cell deposited subsequently on top (Figure 2). Initial prototypes yielded respectable efficiencies, up to 13.7% at steady state. The V_{OC} of these tandems ranges from 1.55 to 1.65V. These devices were reported in the journal Applied Physics Letters (DOI: 10.1063/1.4914179) and a patent was sponsored by BAPVC and filed through Stanford concerning the method of electrically connecting the subcells with a silicon tunnel junction. This work was featured by *MIT News*, the American Institute of Physics, *The Conversation*, and *Scientific American*, and was subsequently reported by multiple news organizations including *The Economist*.

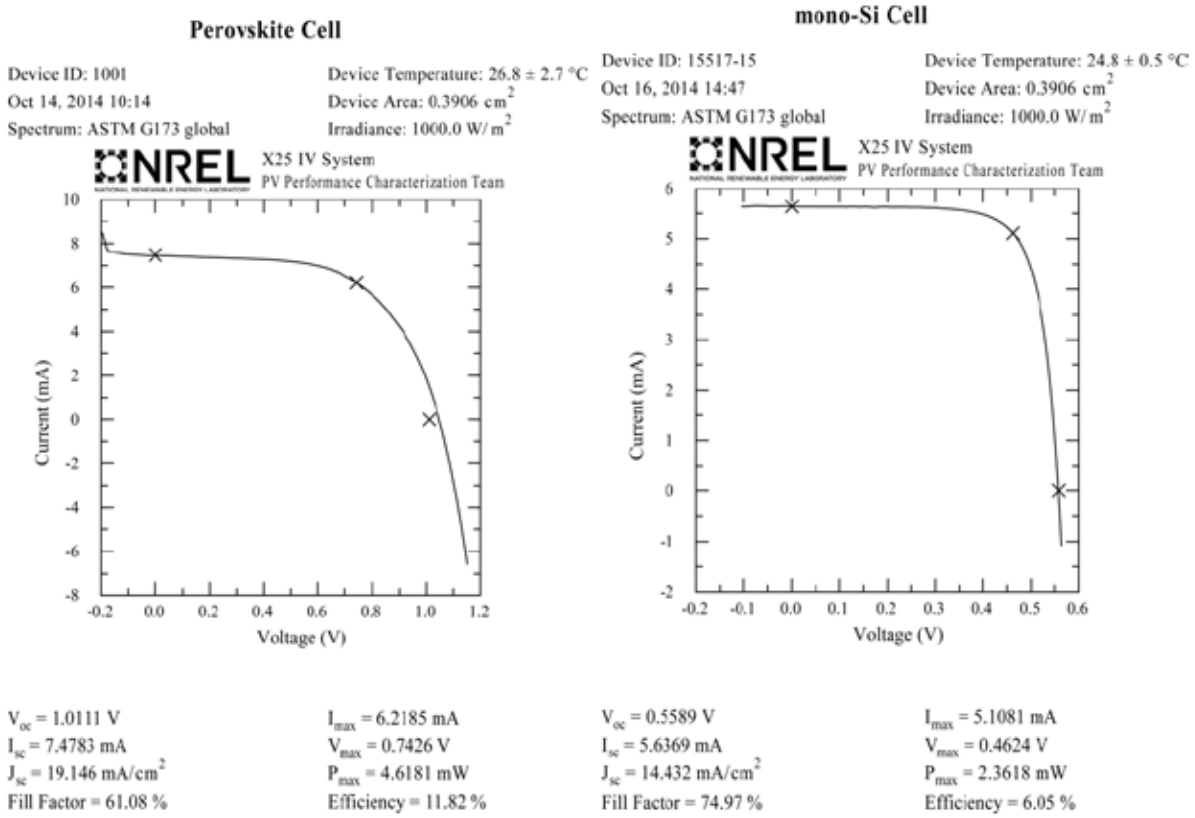

Figure 1. NREL certification of a mechanically-stacked tandem. The tandem efficiency is the sum of the individually measured cells, 17.9%.

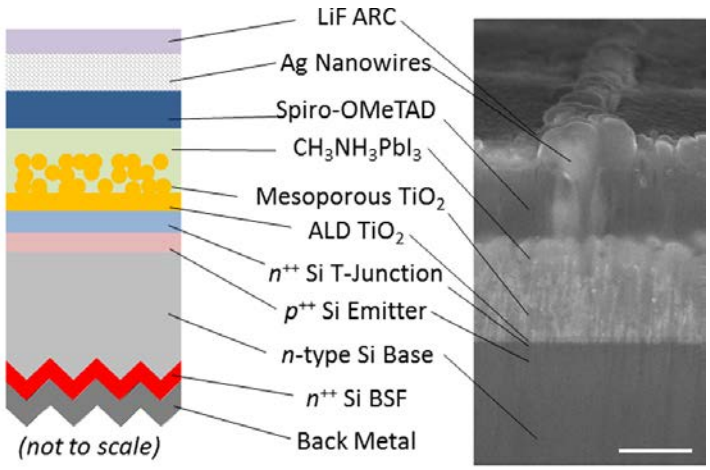

Figure 2. A schematic and SEM cross section image of a 1x1cm^2 monolithically integrated perovskite/silicon tandem achieving 13.7% efficiency.

Future Work:

They plan to certify the performance of the 2-terminal tandem and explore new 4- and 2-terminal tandem architectures including using inverted perovskite architectures and HIT silicon architectures. They will continue to work on cost modeling with Mike Woodhouse at NREL.

BAPVC Annual Project Report

Project Title: High V_{oc} Solar Absorbers; the Missing Link for High-Efficiency, Spectral-Splitting, Solar Cells
PI: Eli Yablonovitch; **Co-PIs:** Connie Chang-Hasnain and Ming Wu
E-mail: eliy@eecs.berkeley.edu

Summary:

High V_{oc} absorbers are required for future high-efficiency multi-junction cells, which could be grown as wide bandgap micro/nanopillars. The group investigated the characteristics of high bandgap micron-sized InGaP nanoneedles/pillars directly grown on lattice mismatched silicon substrates, and explored selective area growth for solar cell absorption enhancement. Single InP nanopillar solar cells with a conversion efficiency of 19.6 % and an open circuit voltage of 0.534 V under AM 1.5 G illumination were demonstrated by the group, both record for InP directly grown on Si.

Key Accomplishments:

One way of realizing low cost and high efficiency photovoltaics is to employ high quality III-V nanopillars synthesized on low cost substrates. The group demonstrated that a single InP nanopillar grown and fabricated on silicon substrate exhibits a record power conversion efficiency of 19.6% and an open circuit voltage (V_{oc}) of 0.534 V under AM 1.5 G illumination. This is the highest efficiency and V_{oc} ever achieved for an InP nanowire or nanopillar solar cell grown on a foreign substrate, which can be attributed to high-quality single-crystalline wurtzite-phased InP nanopillars grown using a novel regrowth technique to drastically reduce the dark current by three orders of magnitude. Taking advantage of dielectric antenna effect, external quantum efficiency is as high as 400% at 550nm and generally greater than 100% in the visible spectrum, beyond that predicted by Lambert-Beer law is achieved over a broad solar spectrum (Fig.1a). Specifically in the surface normal direction, the field enhancement compensates the reduced of surface exposure area, resulting in a relatively smooth I_{sc} (Fig. 1b). Similarly V_{oc} is relatively insensitive to angle (Fig. 1c) all under 1 sun illumination.

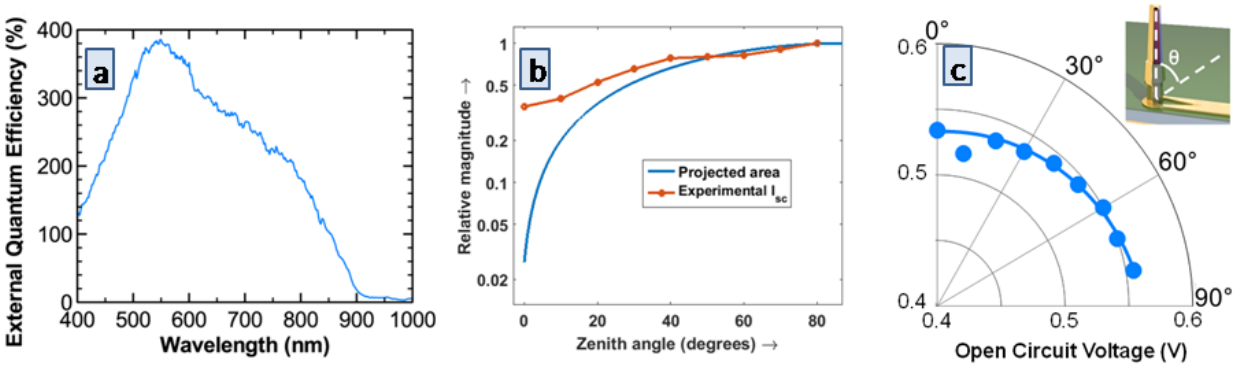

Figure 1. (a) Measured external quantum efficiency top-down illumination of a single InP nanopillar solar cell fabricated on silicon substrate. (b) I_{sc} as a function of incident angle under 1 sun (AM 1.5 G) IV characteristics of InP solar cell. (c) V_{oc} as a function of incidence angle.

It was also demonstrated, for the first time, single crystalline wurtzite InGaP nanoneedles with composition ordering directly grown on silicon substrate. Intense room temperature photoluminescence emission at 1.47 eV indicated the feasibility of employing InGaP needles as an efficient high-bandgap light emitter/absorber. By increasing Ga precursor flow it was possible to reach a wider bandgap of E_g~1.50 eV at room temperature and E_g~1.58 eV at low temperature, for $In_{0.82}Ga_{0.18}P$ intrinsic micropillars on a silicon substrate (Fig.2a-b), regardless of the lattice mismatch constraint, also presenting Fermi-level splitting values larger than 0.95 eV under 1 sun from equivalent V-I characteristic (Fig.2c). Selective area growth of micro/nanopillars on a patterned silicon substrate improved the density from 65% to 95% (Fig.2d), which can be used to enhance the absorption of the nanostructures and future device performances.

Spectral splitting PV, which laterally disperses the solar spectrum onto an array of PV materials with different bandgaps, can offer superior efficiency to tandem multi-junctions by eliminating the current and lattice matching constraints and improving robustness to spectrum variations. The spectral dispersion/splitting optics is realized using a low-cost thin-film diffractive optical element (Fig.3a), designed using computational optimization methods. A sample of the element was fabricated on photoresist, with experimental splitting efficiency shown in Fig. 3b.

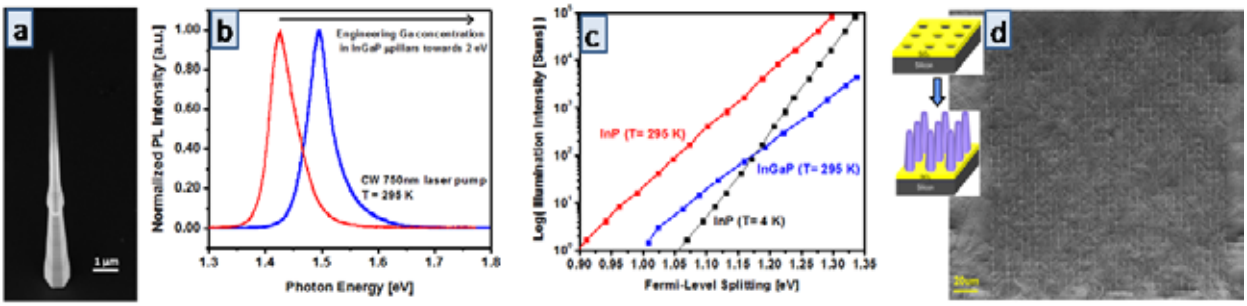

Figure 2. (a) Scanning electron micrograph of a micro-sized $In_{82}Ga_{18}P$ needle. (b) Ga content variation in InGaP towards 2 eV. (c) Comparison between Fermi level splitting from InGaP and InP micro/nanopillars. (d) High yield selective area growth of needles on a patterned silicon substrate.

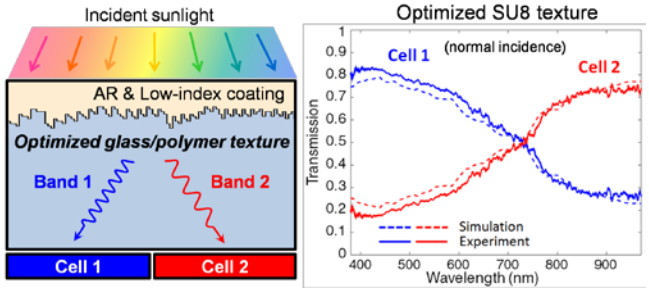

Figure 3. (a) Schematic of spectral splitting optics. (b) Optical efficiency of spectral splitting element fabricated on SU8 photoresist, showing experimental results and simulated performance of the fabricated structure. The transmission coefficient through each cell is normalized to the light passing through the sample.

Future Work:

Aspects to be taken into account in future works: (1) Continue to do growth development to increase Ga content towards 2 eV. (2) Optimize site controlled growth, supported by numerical simulations, to enhance the total absorption of ordered pillar arrays. (3) Study different device designs (p-i-n junctions, layer thicknesses, front-and back surface fields, etc.) (4) Develop high bandgap claddings materials for surface passivation and transparent metal. (5) Investigate spectral splitting designs for a larger cone of solar incidence angles for converting diffuse light. (6) Study higher resolution patterning techniques of dielectric thin films for spectral splitting.

BAPVC Annual Project Report

Project Title: High efficiency CdTe/MgCdTe double heterostructure solar cells
PI: Yong-Hang Zhang
E-mail: yhzhang@asu.edu

Summary:

The goal of this project is to demonstrate single-crystalline CdTe/MgCdTe double heterostructures (DH) and high efficiency solar cells on lattice-matched InSb substrates to better understand the systems material properties and device performance. The group has demonstrated a record-long minority carrier lifetime of 2.7 μs for CdTe/MgCdTe double heterostructures. In addition, the group demonstrated monocrystalline ZnTe/CdTe/MgCdTe double heterostructure solar cells with a maximum efficiency of 10.9 %, an open-circuit voltage (V_{OC}) of 759 mV, a short-circuit current density (J_{SC}) of 21.2 mA/cm^2 and a fill factor (FF) of 67.4 %.

Key Accomplishments:

High quality CdTe/MgCdTe double heterostructures (DH) are grown on lattice-matched InSb substrates using a dual chamber MBE system at ASU. The group has determined the interface recombination velocities for various CdTe/$Mg_xCd_{1-x}Te$ heterointerfaces with different Mg compositions. Fig.1 shows a significant reduction in the interface recombination velocity and Fig. 2 shows a greatly improved minority carrier lifetime. Using time-resolved photoluminescence, the interface recombination velocities for the CdTe/$Mg_{0.36}Cd_{0.64}Te$ and CdTe/$Mg_{0.46}Cd_{0.54}Te$ interfaces were found to be 66±17 cm/s and 47±20 cm/s, respectively. A record-long minority carrier lifetime of 2.7 μs is observed, showing the great potential of CdTe/MgCdTe double heterostructures in photovoltaic and other optoelectronic device applications. Experimental evidence indicates that single-crystalline CdTe is approaching the radiative-limited regime at room temperature. The recent results on high quality CdTe crystal growth on InSb and the critical role of CdTe surface recombination have already greatly helped First Solar to better understand their materials and device designs. This model material and resulting devices will help probe the fundamental physics of CdTe surfaces and interfaces, and eventually help improve the device performance of poly-crystalline CdTe cells at the manufacturing scale.

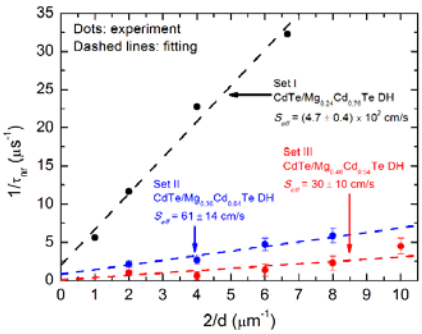

Fig. 1 Plots of $1/\tau_{nr}$ versus $2/d$ for CdTe/$Mg_{0.24}Cd_{0.76}Te$, CdTe/$Mg_{0.36}Cd_{0.64}Te$ and CdTe/$Mg_{0.46}Cd_{0.54}Te$ double heterostructures.

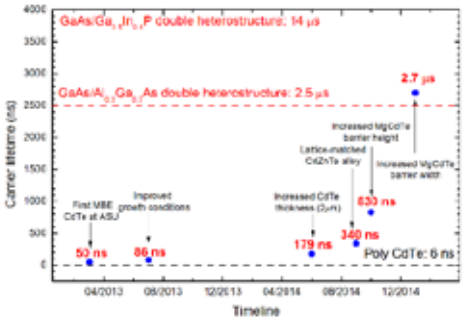

Fig. 2 The minority carrier lifetime progress of the CdTe/MgCdTe DHs.

The team designed and demonstrated monocrystalline p-ZnTe/p-CdTe/n-CdTe/n-MgCdTe double-heterostructure (DH) solar cells with a maximum efficiency of 10.9 %, an open-circuit voltage (V_{OC}) of 759 mV, a short-circuit current density (J_{SC}) of 21.2 mA/cm^2 and a fill factor (FF) of 67.4 %. The effective surface reflection from the hero sample is measured to be 7.7 % with 75 nm thick Al_2O_3 as the single layer AR coating, providing the light J-V curve and EQE curve in Fig. 3. The efficiency is lower than what simulations suggest mainly due to the combination of the low V_{OC} and FF, which are attributed to high interface recombination velocity at the p-CdTe/n-CdTe growth interruption interface. EQE and IQE measurements indicate low non-radiative recombination in the bulk CdTe region as well as at the CdTe/MgCdTe interface. However, a huge drop near, and above the ZnTe band gap is observed which can be attributed to absorption loss in the ZnTe layer, surface recombination loss and interface recombination loss at the p-ZnTe/p-CdTe and p-CdTe/n-CdTe interfaces. PC1D is used to fit several device variables to actual device performance. The results indicate that the surface recombination velocity is ~10^4 cm/s where the interface recombination velocity is ~10^5 cm/s at the p-ZnTe/p-CdTe or p-CdTe/n-CdTe interface.

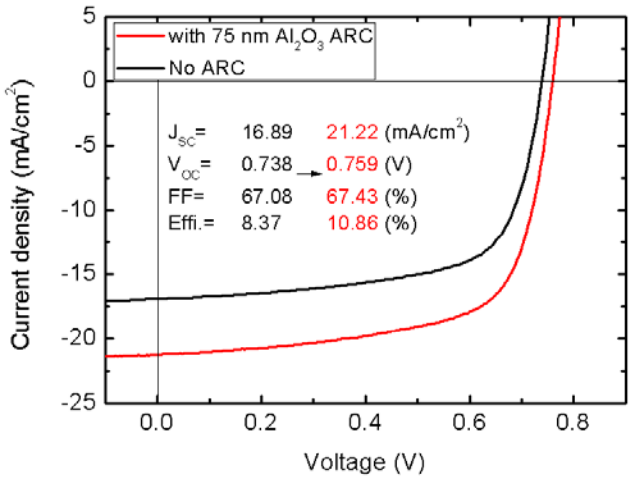

Fig. 3 (a) Light J-V curve of the ZnTe/CdTe/MgCdTe DH solar cell before and after ARC coating at room temperature under 1 sun illumination.

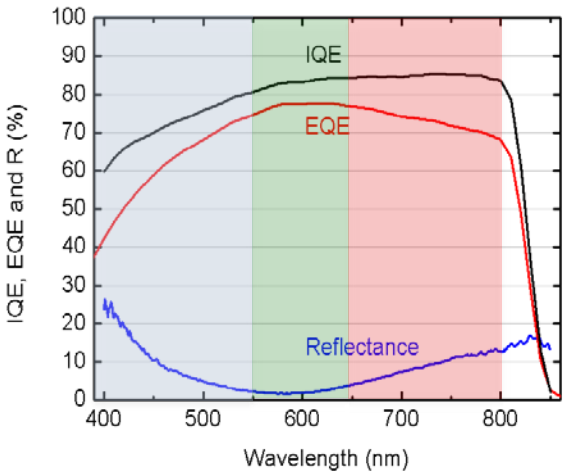

Fig. 3 (b) Measured EQE, reflectance, and IQE of the ZnTe/CdTe/MgCdTe DH solar cell under 1 sun illumination.

Future Work:

The group has identified two areas that are essential for the further improvement of the CdTe solar cells efficiency. The first is to successfully demonstrate p-type doping in CdTe, while the other is demonstration of higher V_{OC}. New device structure designs and p-type doping approaches are ongoing. Carrier transport across the CdTe/InSb hetrovalent interface will be investigated.

BAPVC Annual Project Report

Project Title: Low-cost and high-efficiency thin-film MgCdTe/Si tandem solar cells
PI: Yong-Hang Zhang
E-mail: yhzhang@asu.edu

Summary:

In this program, a new type of low-cost and high-efficiency solar cell is proposed by marrying two established solar cell technologies: polycrystalline II-VI MgCdTe thin-films and crystalline Si solar cells. The overall device structure has been augmented from the originally proposed HIT structure to the higher performance II-VI/Si tandem solar cell design. We demonstrated MgCdTe double heterostructures with excellent crystalline and interface qualities with a bandgap of 1.7 eV and lifetimes reaching up to 11.1 ns promising an effective material system for the upper II-VI subcell.

Key Accomplishments:

In recent years, the popular Si, GaAs, and CdTe single-junction solar cells are showing great progress, reaching 25.6%, 28.8%, and 21.5% efficiency, respectively. However, it is difficult to enhance the efficiency of single-junction solar cells beyond 30% due to fundamental limits, poor material quality, and/or high manufacturing cost. The proposed HIT solar cell design has been redesigned during the reporting period to incorporate a second, II-VI, upper subcell. It is believed that the 1.7 eV MgCdTe alloy is the most promising candidate for the top subcell because of the recent excellent achievements in high quality CdTe/MgCdTe double heterostructure growth [1-2]. The group demonstrated high-quality 1.7 eV $Mg_xCd_{1-x}Te$ epilayers grown on InSb (100) substrates using a dual chamber MBE system at Arizona State University. The structures are characterized by high-resolution X-ray diffraction (XRD), steady-state photoluminescence (PL), and time-resolved photoluminescence (TRPL).

To grow $Mg_yCd_{1-y}Te$ /$Mg_xCd_{1-x}Te$/$Mg_yCd_{1-y}Te$ double heterostructures with large band offsets to effectively confine carriers, growth conditions were tuned to approach a Mg composition *X* of approximately 0.13 and a composition *Y* of 0.50. XRD results show a Mg composition of 0.135 and Pendellösung fringes indicating excellent crystalline and interface qualities. Steady-state photoluminescence indicates that the 0.135 Mg composition result in a bandgap of 1.7 eV (≈730 nm), as shown in Fig. 1. Further time-resolved photoluminescence studies show carrier lifetimes reaching up to a current maximum of 11.1 ns as shown in Fig. 2.

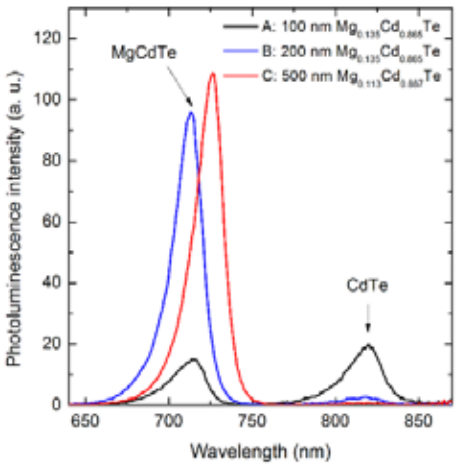

Fig. 1 Steady-state Photoluminescence results for various Mg compositions and absorber thicknesses.

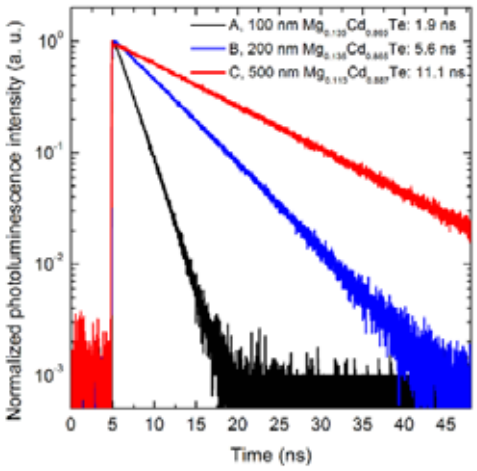

Fig. 2 Time-resolved Photoluminescence results and associated lifetimes for various Mg compositions and absorber thicknesses.

Future Work:

The fundamental research tasks are as follows: 1) demonstrate monocrystalline double-heterostructure $Mg_yCd_{1-y}Te/Mg_{0.15}Cd_{0.75}Te/Mg_yCd_{1-y}Te$ single junction solar cells, and 2) demonstrate polycrystalline CdS/ $Mg_{0.15}Cd_{0.75}Te/Mg_yCd_{1-y}Te$ single junction solar cells. Work within the group will focus on demonstrating a MgCdTe single-junction solar cell with a 1.7 eV bandgap on an InSb substrate; providing a foundation for future work on tandem systems.

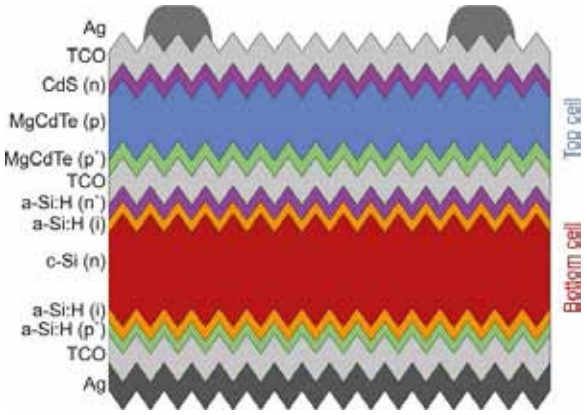

Fig. 3 Schematic of the proposed II-VI/silicon tandem solar cell.

Reference

[1] X.-H. Zhao, M. J. DiNezza, S. Liu, S. Lin, Y. Zhao, and Y.-H. Zhang, "Time-resolved and excitation-dependent photoluminescence study of CdTe/MgCdTe double heterostructures grown by molecular beam epitaxy," *Journal of Vacuum Science and Technology B*, vol. 32, p. 040601 (2014).

[2] X.-H. Zhao, M. J. DiNezza, S. Liu, C. M. Campbell, Y. Zhao, and Y.-H. Zhang, "Determination of CdTe bulk lifetime and interface recombination veocity of CdTe/MgCdTe double heterostructures grown by molecular beam epitaxy," *Applied Physics Letters,* vol. 105, p. 252101 (2014).

BAPVC Annual Project Report

Project Title: Design principles and defect tolerances of silicon / III-V multijunction interfaces
PI: Tonio Buonassisi
E-mail: buonassisi@mit.edu

Summary:

Atom Probe Tomography(APT) is a novel, high-resolution three-dimensional spatiochemical mapping technique capable of observing single atomic impurities at interfaces and in the bulk. Applying it to photovoltaic absorbers and devices allows the performance-limiting impurities and compositional inhomogeneities to be directly characterized. However, the technique is still in its adolescence, and truly quantitative measurement of semiconductors requires considerable care and material-specific technique development before reliable information can be acquired in wild-type specimens; to this end, custom specimens of Si and III/V materials have been fabricated and characterized, to measure interface compositions, bulk impurities, and compositional inhomogeneities and compare them to correlative measurements to ensure accuracy and precision of the Atom Probe technique.

Key Accomplishments:

Three separate avenues of investigation have been brought either to publication or to submission of the manuscript. The first has focused on using Atom Probe Tomography to investigate a series of carefully-prepared transition-metal contaminated Si specimens, with correlative SIMS, TEM, SEM, and diffraction measurements to establish the accuracy of the technique; see Fig 1 for an example. At the same time, this research has also investigated the dynamics of rapid solidification in supersaturated solutions of Si and a transition metal, in this case Co. The resulting manuscript has been published in Advanced Functional Materials, and can be found here: http://dx.doi.org/10.1002/adfm.201501450 . The main result of this work, in addition to establishing the accuracy of APT for measurement of some transition metals in Si, has been to greatly extend our knowledge of rapid solidification of alloys, cellular breakdown dynamics, filament formation and pinch-off in far-from-equilibrium systems, and impurity diffusion during solidification from the melt.

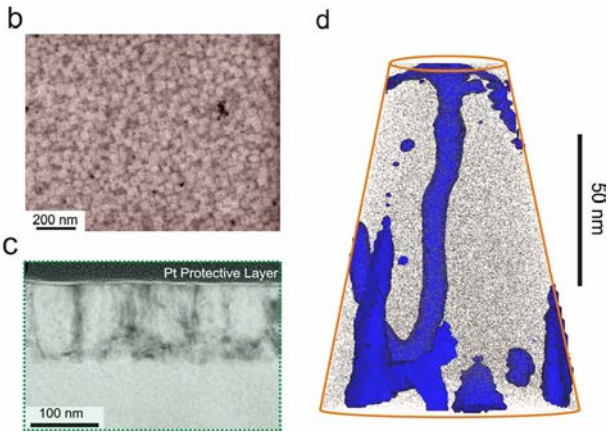

Fig 1. Taken from the linked AFM article. SEM (b), TEM (c), and APT (d) data showing the segregation of Co atoms into filamentary structures embedded within a Si matrix.

A second major direction has been the characterization of III/V-IV interface. Although Si-III/V interface specimens were not available, a series of Ge-InAlAs specimens have been acquired and characterized. These have been found to consist of impure Ge nanowires, ranging from 75 to 95 % atomic Ge with the balance As, embedded in an InAlAs matrix, seen in Fig 2. The interfaces between these materials are seen to be somewhat graded, with evidence of As segregation at the interface in addition to the As incorporation within the nanowires. The mechanism of formation has been modeled using a similar adatom-diffusion and phase separation model to the one mentioned above, and this work is currently being prepared for submission.

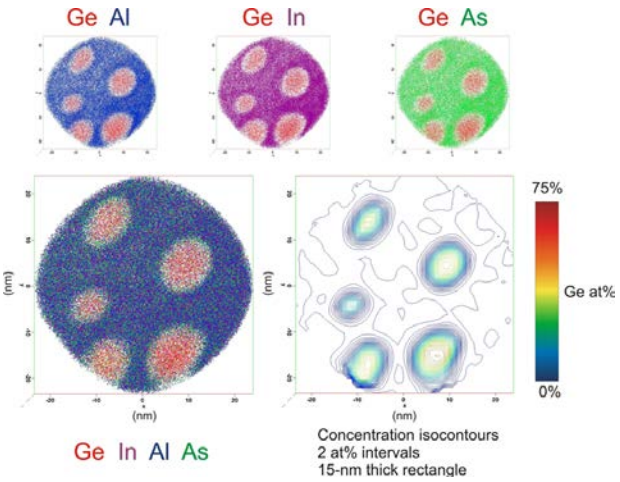

Fig 2. Cross-sectional views of APT dataset from InAlAs-Ge material, showing the distribution of the component atoms within the matrix and the embedded Ge nanostructures. A Ge concentration plot is also provided.

Finally, the third avenue of investigation has been characterization of the interface between Si and a transparent conductive oxide used as a contact material in some photovoltaic devices, in this case Aluminum-doped Zinc Oxide. This interface is known to exhibit Fermi-level pinning, with the mechanism of this pinning not being ully understood. Two separate types of AZO, one grown by pulsed-laser deposition and the other by sputtering, have been deposited on Si, and the interface composition has been investigated by APT. We have observed a layer of Al segregated within the AZO at the interface (seen in Fig 3), raising the local Al concentration to approximately the solubility limit in AZO, possibly leading to the formation of a degenerately-doped layer at the interface and leading to classic metal-on-semiconductor Fermi level pinning. This work is currently in preparation for submission as two manuscripts, one covering the mechanism of Al segregation, and the other the electronic effects of this Al-enriched layer.

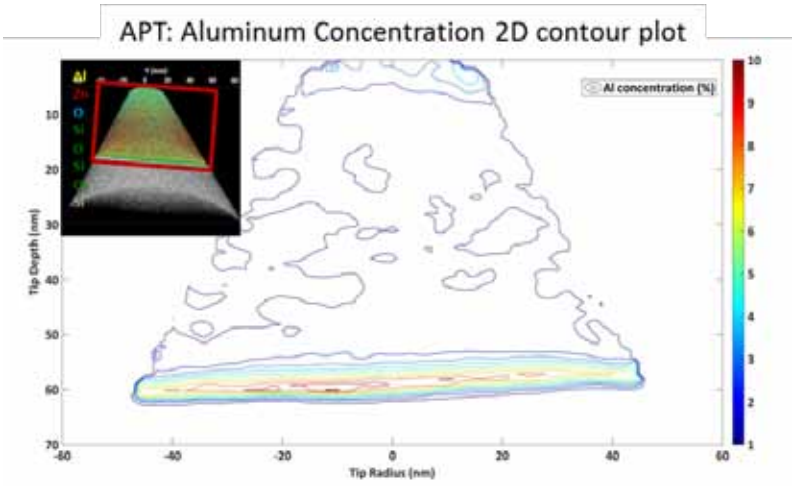

Fig 3. Al Composition profile of AZO on Si, showing Al enrichment at the AZO-Si interface (bottom of profile). Inset, a view of the full APT dataset, showing AZO on top of Si, with red box indicating the view window for the composition profile.

Future Work:

In addition to completing the above-mentioned work and submitting for publication, further efforts on III-V materials continue, as do efforts to verify APT's suitability for measurement of bulk impurities in Si. This last has proven surprisingly variable, as different

impurity elements have wildly varying behavior during the APT measurement. Fe and Cu, in particular, have demonstrated behaviors that necessitate in-depth investigation before APT measurements of these elements can be treated as trustworthy; work in this direction is underway. Several other impurities, including Au and Pd, have been found to be, at present, undetectable in Si by APT, even when the impurity atoms are present in tremendous excess of the solubility limit. This is believed to be the result of the difference in ionization energies between the impurities and the matrix atoms, so theoretical investigation of the local electronic environment around these atoms during APT measurement has begun. Lastly, we will commence measurement of III-V / Si interfaces.

BAPVC Annual Project Report

Project Title: Defect identification and mitigation in high-lifetime silicon materials: growth, processing, reliability
PI: Tonio Buonassisi
E-mail: Buonassisi@mit.edu

Summary:

High lifetimes in industrial silicon materials, in some cases exceeding 1 millisecond, can often be attributed to significant reductions in impurity concentrations. Research to support further lifetime improvements in high-performance materials demands measurement techniques capable of detecting low impurity concentrations, which can be below 10^{10} cm^{-3}. The Buonassisi group proposes measuring low concentrations of impurities in high-performance crystalline silicon with temperature- and injection-dependent lifetime spectroscopy (TIDLS) implemented with free carrier absorption, which promises a small spot size and full injection range. Initial temperature-dependent lifetime measurements have been collected and compared with room temperature QSSPC, highlighting the need for measurement calibration. As a next step, calibration experiments have been performed to isolate the temperature dependence of the free carrier absorption coefficient.

Key Accomplishments:

As exemplified in Fig. 1, the researchers integrate a temperature stage from Linkam Scientific Instruments, capable of controlling sample temperatures between 77K and 690K, with a free carrier absorption (FCA) lifetime measurement FCA is a transient lifetime measurement that tracks optical interactions of pump and probe light beams with the material. A neodymium-doped yttrium aluminum garnet (Nd:YAG) laser provides a 6 ns full-width half-maximum pump pulse at a variable wavelength, while a halogen lamp equipped with a monochromator emits a continuous wave probe beam at 1550 nm through the sample to an InGaAs probe detector (5 ns rise time). This approach offers several advantages, including high spatial resolution and flexibility in terms of thickness, passivation quality, impurity type, and impurity concentration.

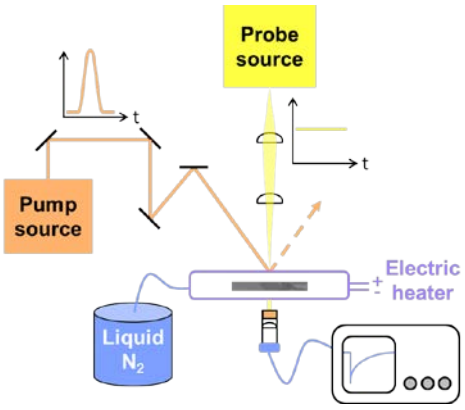

Figure 1: Schematic of free carrier absorption-based TIDLS setup, including an off-the-shelf temperature stage, a variable wavelength pump laser (1000-1300 nm), and a monochromatic probe beam (1550 nm).

Initial lifetime measurements have been made on a single-crystalline *p*-type Czochralski silicon sample. The passivation layer is 20 nm Al_2O_3 deposited by atomic layer deposition. The FCA measurements were conducted at 20°C, 75°C, and 125°C with a constant pump wavelength equal to 1050 nm.

Fig. 2 contains the measurement results, including detector voltage versus time (a), injection-dependent lifetime curves (b, c), and a photoluminescence image of the measurement sample (d). The resulting data displays a wide injection range, with the possibility to optimize the signal-to-noise ratio to achieve greater confidence in low injection ($< 5\times10^{14}$ cm^{-3}). There is agreement in the shape of the lifetime curve between QSSPC and FCA measurements; however, exact values

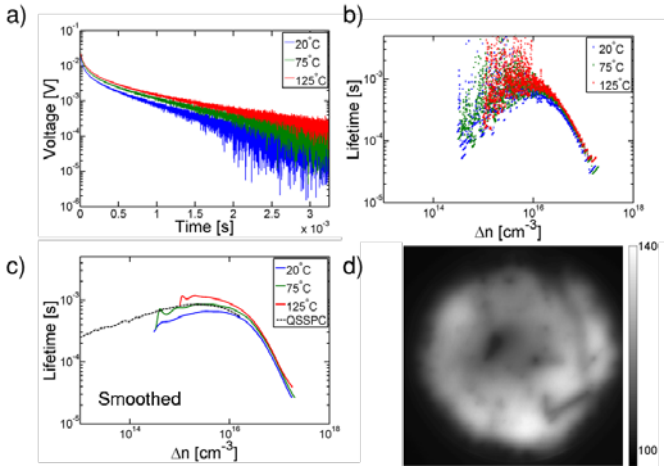

Figure 2: Free carrier absorption was used to measure the minority carrier lifetime of a *p*-type Czochralski sample between room temperature and 125°C.

are not reproduced. There are several possible explanations for this mismatch, including spatial inhomogeneity of the sample lifetime, misalignment of the pump and probe beams, and insufficient pump beam size compared to diffusion length. Calibration of the lifetime measurement as a function of temperature is required.

An important calibration step for this tool involves measurement of the temperature- and injection-dependent FCA coefficient (σ_{FCA}, units of cm^2). Previous studies have determined that σ_{FCA} is enhanced at injection levels greater than 3×10^{16} cm^{-3} and scales linearly with temperature; however, there is significant spread in the tabulated literature values (Fig. 3). Results from ongoing experiments to measure the temperature dependence of σ_{FCA} in low injection are also included in Fig. 3. To obtain these results, the injected carrier concentration is estimated using a large-area pyroelectric detector, while the detector response is determined from the voltage during the first 10 ns after the pulse (accounting for detector rise time).

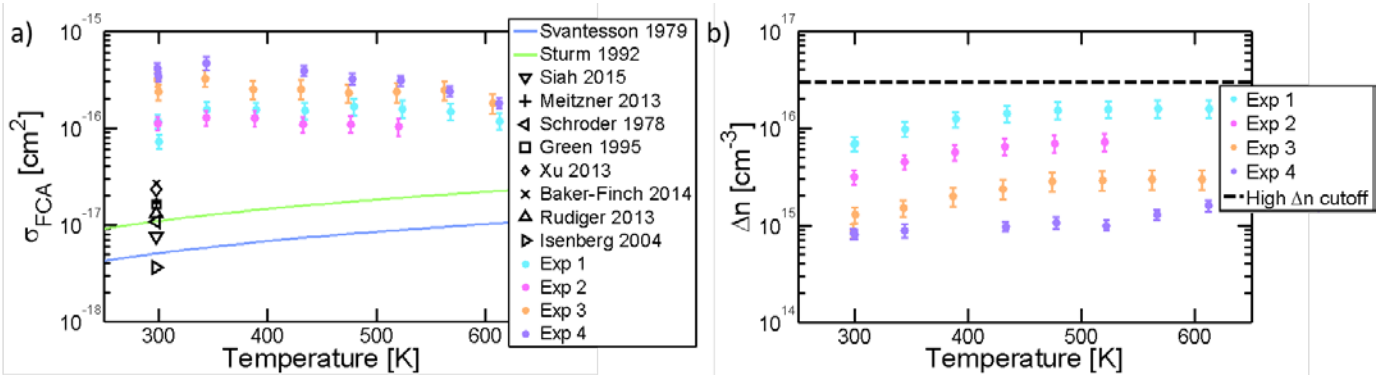

Figure 3: Reported values for the ambipolar free carrier absorption cross-section, plotted as a function of temperature.

Future Work:

To gain confidence in the lifetime measurement technique, researchers will seek to obtain agreement in lifetime measurements between QSSPC and FCA at room temperature. As part of this effort, discrepancies between measured and literature σ_{FCA} values will be investigated and resolved. TIDLS measurements will first be conducted on intentionally metal-contaminated samples. From the full temperature and injection-dependent spectra, defect parameters including defect level, ratio of capture cross-sections, and carrier capture time constant, will be extracted and compared to literature values. Finally, the technique will be applied to samples with suspected impurity contamination provided by industry collaborators.

BAPVC Annual Project Report

Project Title: Exploratory Photovoltaic Modeling and Simulation
PI: Peter Bermel (Purdue University)
Co-PIs: Mark Lundstrom, Ashraf Alam, Jeff Gray (Purdue University)
E-mail: pbermel@purdue.edu

Summary:
We have investigated the material properties of VLS-grown InP from BAPVC collaborators using a multi-probe method, and achieved a good fit with the best InP cells measured. Our hypothesis to explain the V_{oc} gap from typical InP cells is that material inhomogeneities observed in PL imaging give rise to low-V_{oc} areas that degrade the overall cell V_{oc}.

Key Accomplishments:
In the last year, we have explored the material properties of VLS-grown InP cells, supplied by BAPVC collaborators from Ali Javey's group at UC-Berkeley, through a multi-probe method. Four key types of experiments have been performed at multiple sites as part of our project: 1-photon time-resolved photoluminescence (TRPL), 2-photon TRPL, microwave photoconductance decay, and photoluminescent excitation (PLE). The raw data collected with typical best fit lines is shown in Fig. 1(a). We then combine these data sets into a single, consistent model for surface recombination velocity and SRH bulk recombination through least-squares fits to a detailed model of the material, developed in the Sentaurus TCAD simulation tool. The distribution of least-squares fits is provided in Fig. 1(b), which suggests InP thin-film samples have bulk lifetimes of 12 ns and surface recombination velocities of $3x10^4$ cm/s.

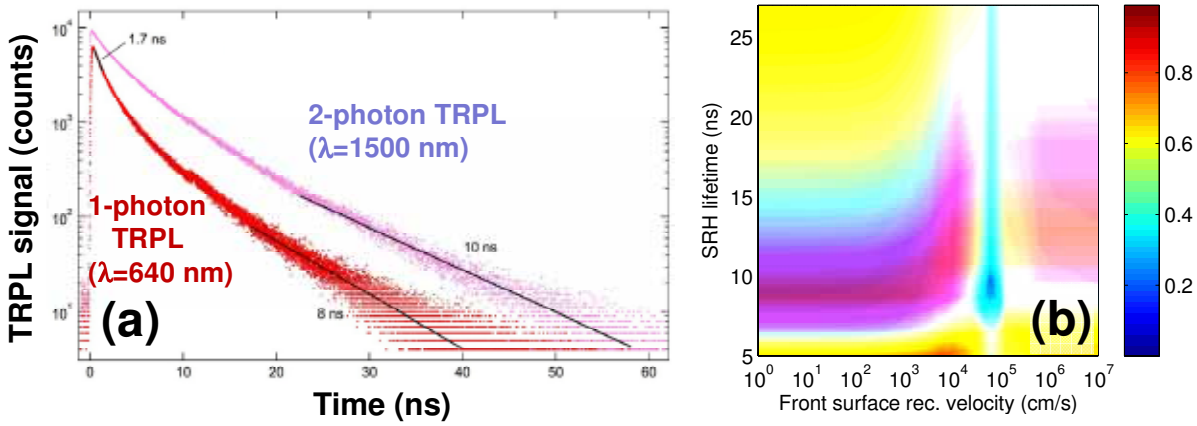

Figure 1. Multi-probe characterization of VLS-grown InP supplied by BAPVC collaborators (Javey group) (a) Time-resolved photoluminescence data from 1- and 2-photon probes at 640 nm and 1500 nm wavelengths; (b) Least-squared error from fitting TRPL and PLE data (not shown) to estimate surface and bulk recombination lifetimes.

This raw data is then used as input for a device-level model of an InP-based heterojunction solar cell, schematically depicted in Fig. 2(a). The results of this model are shown as a red solid line in Fig. 2(b). When comparing to InP experimental data, we find a close match with the best measured InP cells, but a substantial gap in Voc compared to a more typical large-area InP cell. Explaining the origin of this gap requires additional investigation.

As shown in Fig. 3, a photoluminescent image of the VLS-grown InP material reveals substantial variations in intensity, up to a factor of 50. This can be potentially explained as a variation in the bandgap of the underlying material (i.e., inhomogeneities), as shown by PL imaging in Fig. 3. This means that low-bandgap and thus low-V_{oc} regions limit the overall cell V_{oc}.

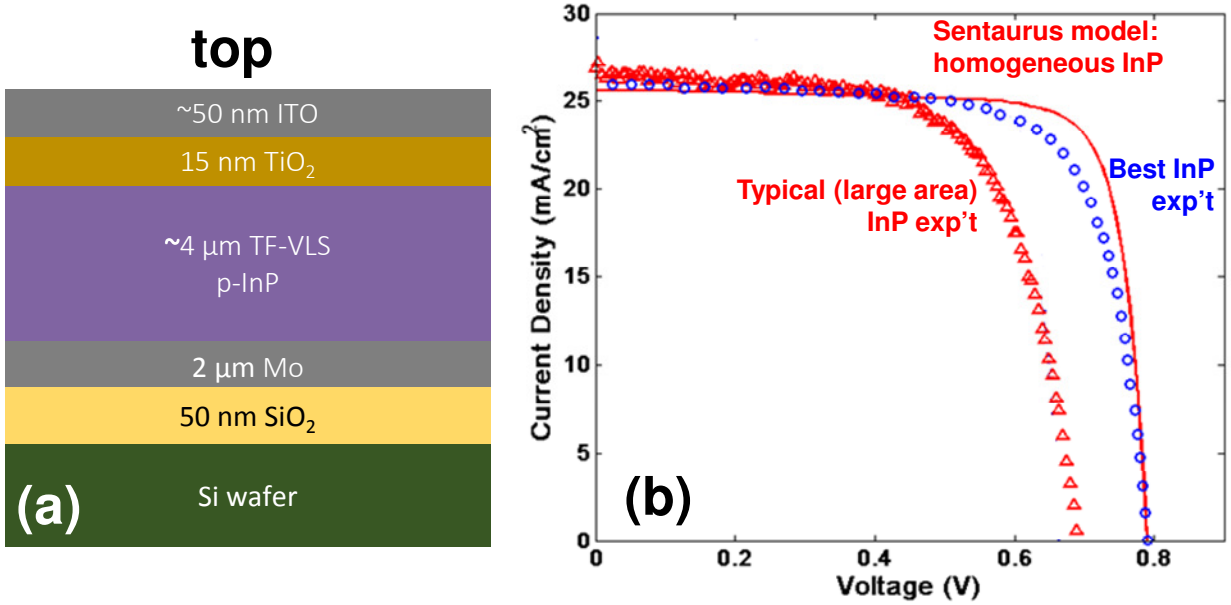

Figure 2. (a) Schematic of TiO_2/VLS-grown InP heterojunction solar cells; (b) Experimental data for best case and typical InP solar cells, along with model results utilizing input from Fig. 1. The match to the best cell shows that large-area InP cells suffer from significant degradation in V_{oc}, albeit with a slight boost in J_{sc}.

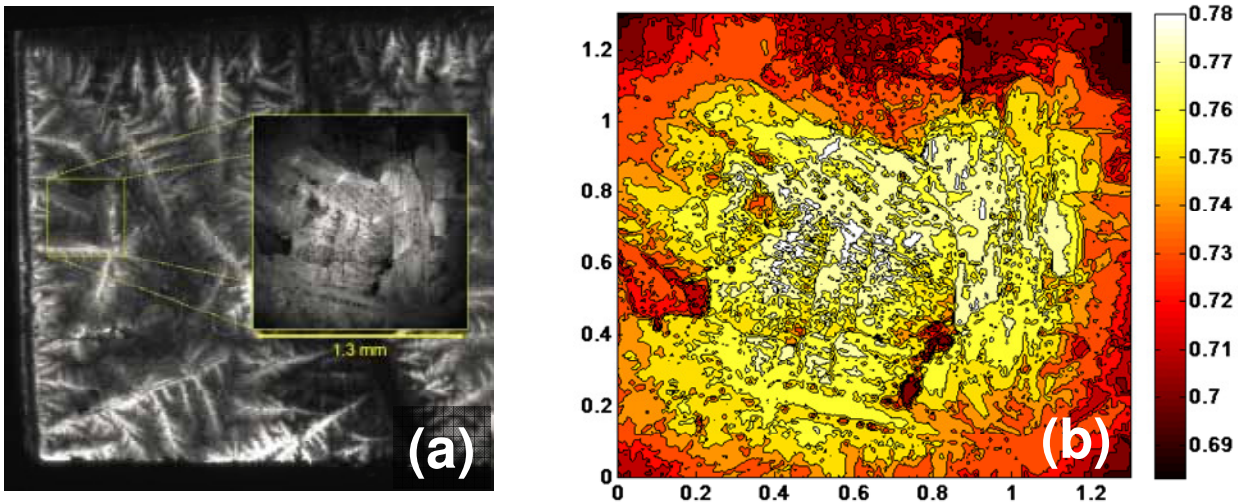

Figure 3. (a) Photoluminescence image of VLS-grown InP material taken at two magnifications; (b) Mapping of PL to V_{oc} distribution in 1.3 x 1.3 mm^2 region – this may explain the V_{oc} gap in Fig. 2.

Future Work:
The next steps here include: detailed modeling of observed large-area InP dark & light I-V curves, independent experimental confirmation of inhomogeneities, and designing mitigation strategies to improve large-area VLS-grown InP cell and module performance.

Thrust: Photon Management and Transparent Conductors

Key Challenges

The thrust spans two major areas: light management and transparent electrodes for solar cells. The key challenges are several folds:

1. Develop materials and structures to couple maximum sunlight into the solar cells and to achieve near-complete absorption of above bandgap photon with significantly reduced usage of absorber materials.
2. Develop low-cost highly transparent (~95%) and low sheet resistance electrodes (<5 ohm/sq) for solar cells with n- and p-type contact capability.
3. Develop process to implement the above materials and structures in practical scalable solar cell manufacturing.

Existing Projects in our Thrust

- *Theory and Simulation of Photon Management in Nanostructured Solar Cells*, Shanhui Fan (Stanford)
- *Solar Cell Efficiency Enhancement via Light Trapping in Resonant Dielectric Sphere Arrays*, Harry Atwater (Caltech)
- *Large-Area, Fast, and Electric-Field Assisted Continuous Coating for Nanostructured Photon Management*, Ning Wu (Colorado School of Mines)
- *Percolating Transparent Metallic Electrodes for Solar Cells*, Mark Brongersma (Stanford)
- *Ideal Transparent Conductors for Full Spectrum Photovoltaics*, Wladek Walukiewicz (LBNL)
- *New P-type Transparent Conductors*, Joel Ager (LBNL)
- *Graphene Electrode Eng. for Photovoltaic Application*, Kaustav Banerjee (UC Santa Barbara)

Potential New Areas of Interest

- *Extension.* Thus far, photon management is mainly aimed for enhancement of short circuit current. There are exciting opportunities to explore photon management to reduce photon entropy loss to increase open circuit voltage.
- *Integration.* Integrate photon management together with electrical transport to fully engineer the structure to enhance solar cell efficiency as a whole. In addition, there are significant opportunities to integrate the materials in the transparent conductor projects with the design and modeling efforts in the photon management projects. For example, transparent electrodes may be designed as an efficient structure for light management purposes. Alternatively, one may incorporate advanced optical design to reduce the loss in transparent electrode while maintaining its electrical properties.
- *Manufacturability.* Photon management will only be viable, if it can be implemented in a cost effective way. Study the integration of new photonic structures and transparent electrodes into practical scalable solar cell manufacturing.

BAPVC Annual Project Report

Project Title: Nanostructured metallic films as both broadband antireflective coatings and transparent electrodes for semiconductor devices

PI: Mark L Brongersma
E-mail: Brongersma@stanford.edu

Summary:
Nanostructured metallic films have emerged as potential replacement for metal oxide films as transparent electrodes in optoelectronic devices. An ideal transparent electrode should possess a high, broadband transmittance, regardless of the underlying semiconductor. Many metallic transparent electrodes are highly transmissive on glass, however, when integrated on a high index substrate, an additional anti-reflective (AR) layer such as silicon nitride is required to maintain high broadband transmissivity. Under the BAPVC program, the Brongersma group has demonstrated that optimized nanostructured metallic films with deep subwavelength structural features can behave as transparent dielectrics and thus be used as an AR coating (Fig. 1). In this role they feature a dual functionality both as an anti-reflective layer and a transparent electrode layer. Compared to previously proposed metallic electrodes, the demonstrated electrode feature a high broadband transmittance and low reflectance while preserving a high sheet conductivity (Fig. 2,3,4), a small dependence on incident angle (Fig. 5), and a design that can be easily tailored to the target low or high index semiconductor for optimal performance. This electrode technology eliminates the need for an additional dielectric anti-reflective layer reducing one material and one processing step.

Key Accomplishments:

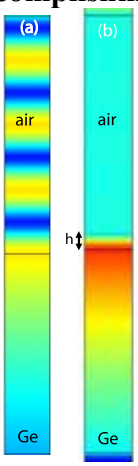

Figure. 1. **A nanostructured metallic electrode with deep subwavelength structural features resembles an artificial dielectric** (a) Magnetic field distribution shows high reflection of the incident light by a high index semiconductor such as Ge (λ = 1.3 μm). Reflection suppression and transmission enhancement (b) by a quarter wavelength thick dielectric layer (c) by an optimized deep subwavelength Ag grating (TM polarization).

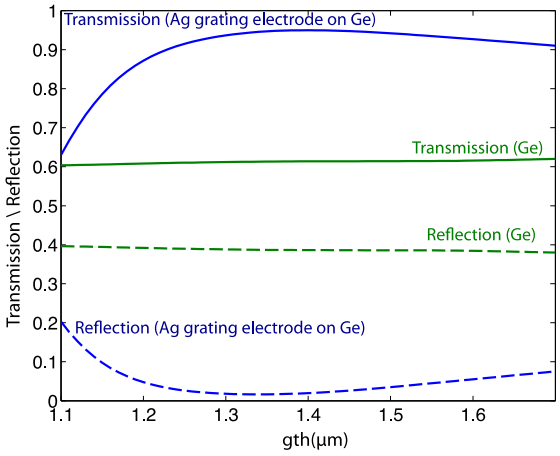

Figure. 2. **A subwavelength Ag grating electrode on Ge provides broadband transmission enhancement and reflection suppression while maintaining a high sheet conductivity.** The green and blue curves correspond to the geometries presented in Fig. 1 (a) and (c), respectively. Sheet resistivity of the Ag electrode is 0.12 Ω/sq.

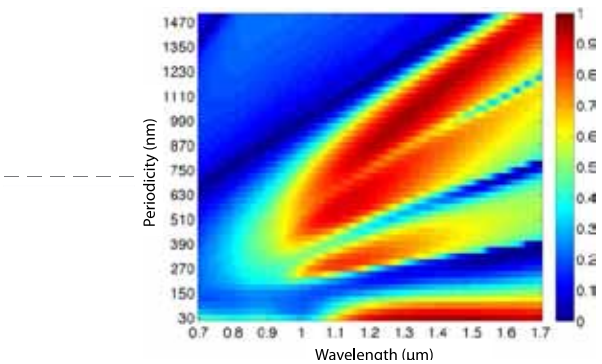

Figure. 3. **Transmission map for Ag grating electrodes with constant sheet conductivity on Ge shows electrodes with deep subwavelength structures provide the most broadband optical properties.** Sheet resistivity of all Ag gratings is 0.12 Ω/sq and Ag thickness is 193 nm.

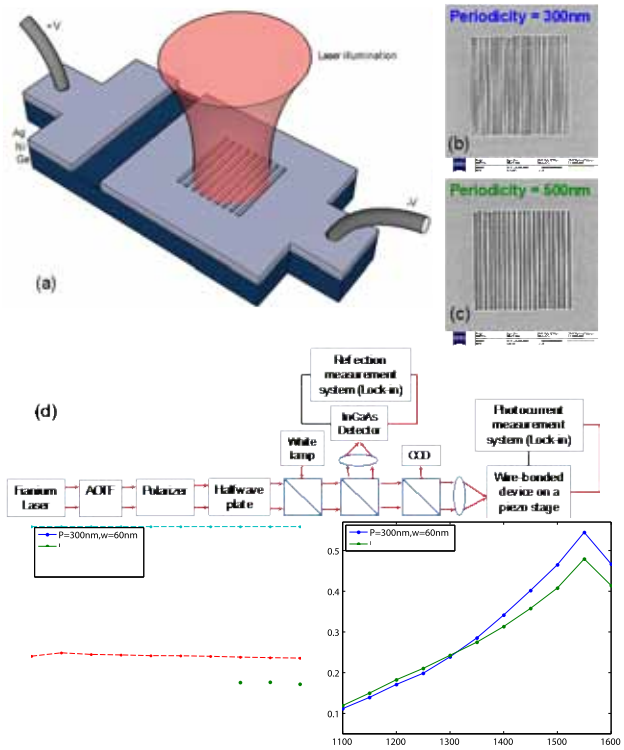

Figure. 4. **Optical reflection and photocurrent measurements confirm broadband high reflection suppression for nanostructured Ag electrodes.** (a) A schematic of the measurement platform where an electrode of a planar Ag-Ge-Ag Schottky detector is patterned with a grating geometry. The electrode transmits light into Ge where it generates electron-hole pairs that are extracted as photocurrent. (b, c) SEM images of Ag grating electrodes made with Neon ion beam milling with periodicity = 300 nm and periodicity = 500 nm (d) Photocurrent and reflection measurement setup for polarization and spectrally resolved measurements (e) Reflection measurements for Ag, Ge, and Ag grating electrodes with different periodicities on Ge (TM polarization) (e) Photocurrent measurements for Ag electrodes on Ge (TM polarization).

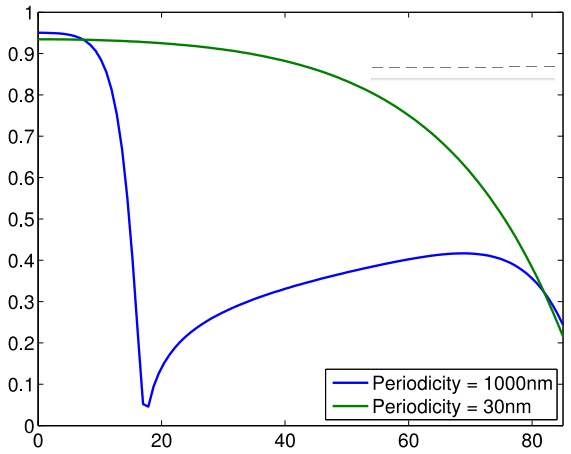

Figure. 5. **Transmission through a deep subwavelength Ag electrode has a small dependence on the incident angle.** The green and blue curves correspond to transmission of Ag gratings on Ge with periodicities of 30 nm and 1000nm. The sheet resistivity for both Ag electrodes is 0.12 Ω/sq.

Future Work:

The Brongersma group is currently developing polarization independent antireflective transparent electrodes over various semiconductor substrates. Althought a demonstration in the infrared spectral range was easiest, they are now also exploring the possibility to operate over the entire visible and infrared spectrum. If successful, this work will obviate the need for an additional dielectric antireflective layer. This work is expected to provide a significant cost reduction in the fabrication of conductive transparent electrodes based on the low cost of metals versus conventional transparent electrodes based on transparent oxides.

BAPVC Annual Project Report

Project Title: Optical metamaterials as antireflection coatings for solar cells
PI: Mark L Brongersma
E-mail: brongersma@stanford.edu

Summary:

Metamaterials are artificially engineered materials offering the unique opportunity to tailor their optical properties and functionalities. Under the BAPVC program, the Brongersma group has demonstrated that a traditional quarter wavelength-thick silicon nitride antireflection coating for silicon substrates can be replaced by a linear array of silicon nanowires having appropriate sizes and periodicity. The angular dependence and polarization-independence of the optical transmission were investigated. This project provides easy design guidelines for the fabrication of metamaterials capable of suppressing light reflection from silicon across a broad wavelength range, thus enhancing silicon-based solar cell efficiency. The averaged reflectivity in the visible spectrum of a substrate covered with a resonant metamaterial outperforms traditional antireflection coatings. An increase of 23% in the absorption efficiency by implementing optimized nanostructure arrays on a standard solar cell device structure is expected.

Key Accomplishments:
Every material reflects light, especially high refractive index substrates such as silicon. However, reflection represents an unwanted loss process in solar cells. Many different approaches to reduce reflection from flat substrates have been proposed: dielectric interference coatings, adiabatic index matching, surface texturing by chemical etching, optical scattering from plasmonic nanoparticles. Unfortunately, they present significant drawbacks. Our proposed approach takes advantage of the possibility to tailor the optical properties of effective materials composed by array of silicon nanowires (see the schematics picture on the left panels in Fig. 1). This project explored a broad parameter space with the goal of suppressing reflectivity from silicon in the visible wavelength range.

The effective medium approximation is often used to describe the optical permittivity of nanostructured layers. A metamaterial having the refractive index equal to the geometric mean between silicon and air indices can be realized under transverse electric (TE) polarization illumination by fabricating an array of silicon nanowire having filling fraction of 0.8. In Fig. 1(a) we show an SEM image of an array of 35 nm-large silicon nanowires fabricated on a silicon substrate using Focused Ion Beam. The calculated optical reflectivity at normal incidence is reported as a continuous line. Experimental reflectivity measured using an optical microscope is shown as scattered dots. Zero reflectivity around 550 nm has been achieved in this sample. However, larger nanowires are preferable because they are easier to fabricate on a large scale. On the other hand, as soon as the size of the nanowires is large enough to support structural optical (Mie) resonances, other effects must be taken into account and a deviation from the effective medium approximation is observed. We investigated the transition from the non-resonant to the resonant regime (while avoiding 1st order diffracted beams in the medium above the array). Deviation from the lowest-order effective medium approximation has been observed and a design guideline to achieve the same optical properties and spectral features for different

sizes of the wires has been provided. In Fig. 1(b) and (c) the optical reflectivity of silicon covered with arrays of nanowires having sizes of 65 nm and 75 nm are shown. The filling fraction of these arrays has been adjusted to 0.7 and 0.6 respectively in order to take into account the effect of optical resonances. A double layer silicon nanowire array has been proposed by the Brongersma group in order to obtain antireflection properties for unpolarized light. Fig. 1(d) shows a top-view SEM image of the fabricated sample. Calculated and experimental reflectivity are shown in Fig. 1(e). Very low reflection is obtained for both polarizations at around 550 nm.

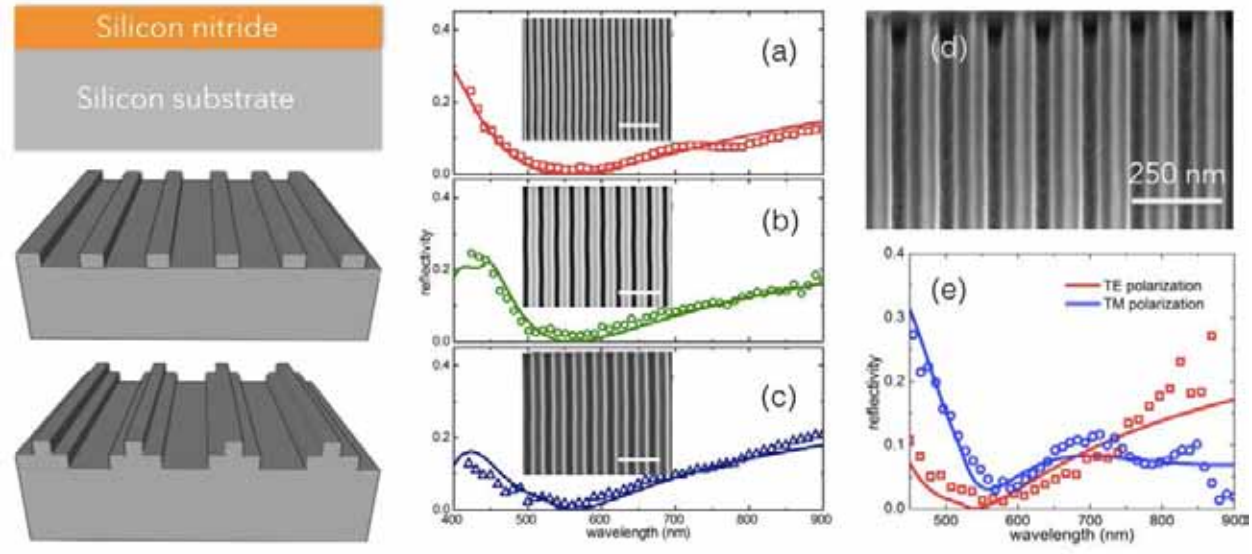

Figure 1. On the left, a schematic of Prof. Brongersma design of antireflection coatings. Traditional silicon nitride continuos layer (top) can be replaced by a linear array of nanowires (middle). A double layer structure (bottom) is proposed for polarization-independent response. Simulations and experimental data for different beam sizes are shown. Zero reflectivity near the peak of the solar spectrum can be achieved with nanowires of 35 nm, 65 nm, and 75 nm, respectively (a-c) under illumination with TE-polarized light. Scale bar is 200 nm. Panels (d-e) refer to unpolarized light instead. Low reflectivity can be achieved at both polarization using a double-layer linear array of nanowires.

Future Work:

The group is currently exploring new strategies that take advantage of optical resonances in silicon nanowires to further broaden the wavelength range in which reflection is negligible. In addition, the group aims to leverage on current result to design effective layers made of 3D silicon nanostructures. As such, this work is expected to provide a significant cost reduction in the solar panel antireflection coatings.

BAPVC Annual Project Report

Project Title: Theory and Simulation of Photon Management in Nanostructured Solar Cells

PI: **Shanhui Fan**
E-mail: Shanhui@stanford.edu

Summary:

This project aims to elucidate the fundamental physics that governs the current and voltage behaviors in nanostructured solar cells, and to develop strategy for enhancing solar cell efficiency thorough photon management. The key accomplishments in this period include a detailed balance analysis that elucidates the influence of optical physics on the voltage behavior of nanowire solar cells.

Key Accomplishments:

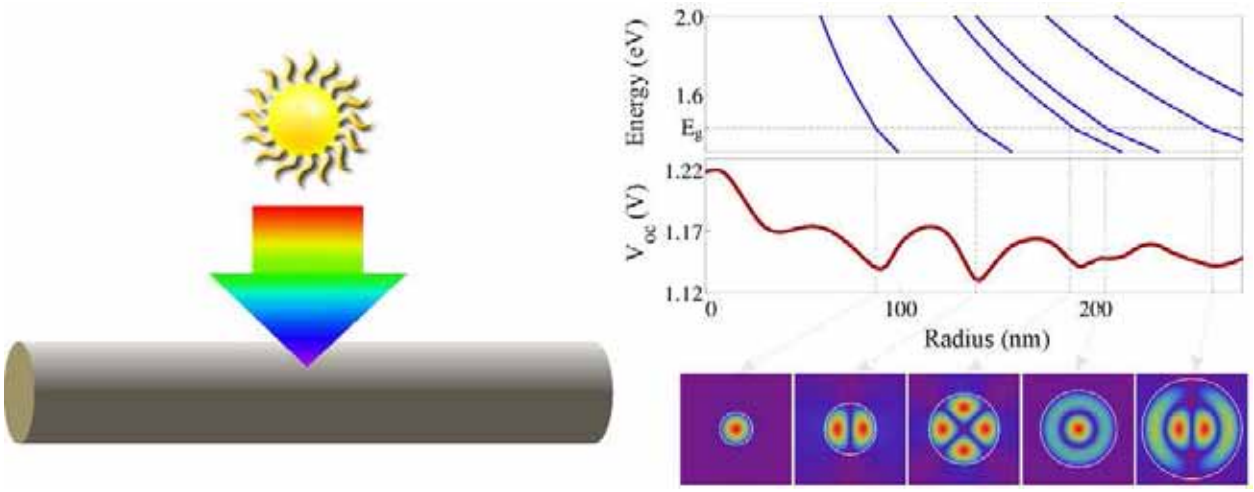

Figure 1. Left panel: Schematic of a GaAs nanowire solar cell. Right Panel: Top graph shows the resonance energy in the nanowire as a function of the radius, with the field patterm of these resonances exhibited in the botoom graph. The middle graph shows the open circuit voltage as a function of radius. The voltage drops each time the energy of the resonance cross the band gap of the semiconductor.

Semiconductor nanowire-based solar cells have been shown to be promising candidates for third-generation photovoltaics. Compared with traditional thin-film solar cells, the advantage of the nanowire cells include easily scalable manufacturing, lower cost, efficient charge separation, and tunable optical absorption. From the optical physics point of view, the nanowire geometry is interesting in that it supports a variety of optical resonances each with a spectral peak location that directly depends on the wire's diameter. In particular, a properly designed nanowire can support optical resonances with an absorption cross-section that is many times larger over the

nanowire's geometrical cross-section. Accordingly, there has been a strong interest in engineering the location of these optical resonances of the nanowire in order to enhance its optical absorption and therefore its short-circuit current performance. However, in order to understand the fundamental limiting performance of a nanowire solar cell, these studies on the nanowire's output current behavior need to be complemented with a better understanding of the nanowire's intrinsic voltage behavior.

We present a detailed balance analysis of current density−voltage modeling of a single-nanowire solar cell. Our analysis takes into account intrinsic material nonidealities in order to determine the theoretical efficiency limit of the single-nanowire solar cell. The analysis only requires the nanowire's absorption cross-section over all angles, which can be readily calculated analytically. We show that the behavior of both the current and voltage is due to coherent effects that arise from resonances of the nanowire. In addition, we elucidate the physics of open-circuit voltage enhancement over bulk cells in nanowires, by showing that the enhancement is related to the removal of resonances in the immediate spectral vicinity above the bandgap.

This work has been published in Nano Letters. (S. Sandhu, Z. Yu and S. Fan, Nano Letters 14, 1011, 2014).

Future Work:

We are in the process of extending the detailed-balance analysis, as described above, towards the understanding of nanophotonic silicon cells. Here, the efforts in particular will be focused on elucidating the impact of various intrinsic non-radiative recombination mechanisms, including the Auger recombination, and the surface recombination on the performance of nanophotonic silicon cells.

BAPVC Annual Project Report

Project Title: Optimal Integration of Transparent Electrodes and Photon Management
PI: **Shanhui Fan**
E-mail: Shanhui@stanford.edu

Summary:

The objective of the project is to continue to develop the understanding of the interplay of transparent electrodes and photon management, and to develop a pathway towards low-loss and light-trapping transparent electrodes for improved overall solar cell efficiency, while eliminating dedicated light-management layers.

Key Accomplishments:

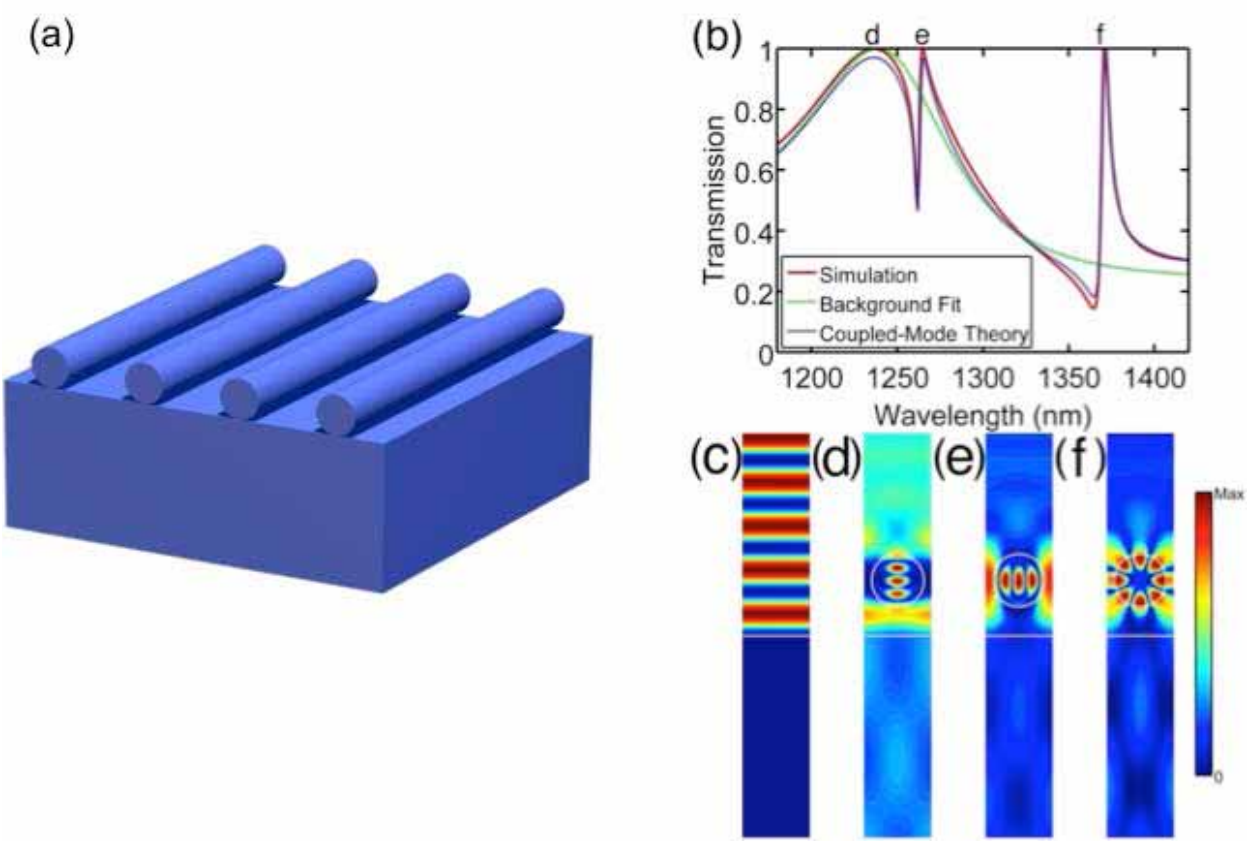

Figure 1. (a) Geometry consisting of resonant nanowires sitting on a substrate. (b) Transmission spectrum for the geometry in (a). (c) Various resonances in the geometry in (a).

Transparent conducting electrodes play critical roles in solar cell technologies . Traditionally, the performance of transparent electrodes is understood in terms of an optical-electrical trade-off in fundamental material properties ; for example increasing the carrier density improves the

electrical conductivity but decreases the optical transparency. We emphasize here, however, that in practical solar cells, the transparent electrode layer is placed in a complex electromagnetic environment involving other device layers. Thus the property of a transparent electrode needs to be understood taking into account the electromagnetic interaction between the electrode and the surrounding layers. This gives rise to a number of opportunities both in terms of loss reduction and in terms of light management capabilities for transparent electrodes.

In this period we undertake a study of the theoretical condition for optical resonances for anti-reflection. The initial study was carried out using dielectric nanowire, but the same physical principle can be generalized to metallic nanowire as well. We introduce the theoretical condition for complete reflection cancellation in this resonant antireflection scheme. Using both general theoretical arguments and analytical temporal coupled-mode theory formalisms, we show that in order to achieve perfect resonant antireflection, the periodicity of the array needs to be smaller than the free-space wavelength of the incident light for normal incidence, and also the resonances in the subwavelength objects need to radiate into air and the dielectric material in a balanced fashion. Our theory is validated using first-principles full-field electromagnetic simulations of structures operating in the infrared wavelength ranges. For solar cell or photodetector applications, resonant antireflection has the potential for providing a low-cost technique for antireflection that does not require nanofabrication into the absorber materials, which may introduce detrimental effects such as additional surface recombination. Our work here provides theoretical guidance for the practical design of such resonant antireflection schemes.

This work has been published in Optica. (K. X. Wang, Z. Yu, S. Sandhu, V. Liu and S. Fan, Optica 1, 388, 2014).

Future Work:

We are in the process of applying the same principle to the study of metallic nanowire as well, with the aim to designing metallic structures that can function as an anti-reflection layer.

BAPVC Annual Project Report

Project Title: Ideal transparent conductors for full spectrum photovoltaics

PI: Wladek Walukiewicz
E-mail: w_walukiewicz@lbl.gov

Summary:

The group has developed high quality Cadmium Oxide (CdO) based transparent conductors (TCO) thin films with excellent electrical and optical properties using radio frequency magnetron sputtering method. They demonstrated a significant improvement in the photon flux transmitted through CdO:In compared with commercial Fluorine doped Tin oxide (FTO) for PV technologies relying on the infrared part of the solar spectrum. They developed a low resistance ohmic contact between CdO and p-Si. The group has also discovered and optimized properties of CdNiO alloys for environmental protection of CdO TCOs.

Key Accomplishments:

Previously the group has developed a method to grow a high quality n-type Cadmium Oxide-based TCO thin films with excellent electrical and optical properties. In the past year, the group's research was focused on three areas:

(i) Evaluation of the advantages of CdO compared with standard, commercial TCOs;
(ii) Development of low resistance contacts to Si PVs;
(iii) Development of CdNiO protective layers;

(i) Fig. 1 shows the photon transmittance and accumulative photon count for solar spectrum passing through CdO:In and commercially available FTO of the same sheet resistance. A significant improvement in the transmission of NIR photons in CdO:In fully compensates for the small deficiency in UV transparency of this TCO. An accumulative photon count shows an advantage of the CdO based TCO for absorbers with λ_g>800 nm (E_g<1.6 eV). The superior NIR transparency demonstrates the feasibility of using CdO TCO in Si PV technology with λ_g=1130 nm.

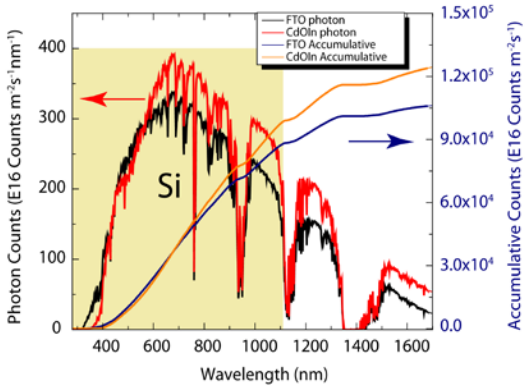

Fig. 1 Photon transmittance and accumulative photon count of commercial FTO and CdO:In films. Significant improvement in transmission of NIR photons (> λ=1130 nm) with CdO:In. More gain for longer wavelength absorbers.

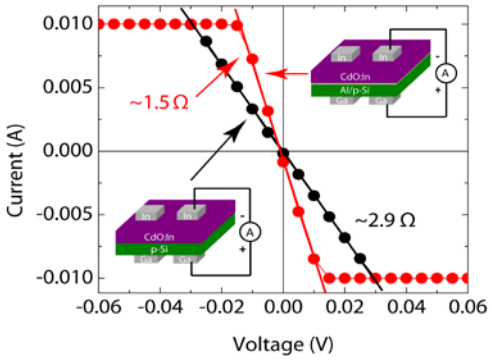

Fig. 2 Current-voltage curve of CdO:In/p-Si. Resistance of optimized p-Si/CdO:In interface does not contribute to the total series resistance.

(ii) Applications of CdO TCO to Si PV technology require low resistance ohmic

contacts between CdO TCO and Si. The group has developed a method to grow CdO:In films on p-type Si with very low contact resistance. Fig. 2 shows the current-voltage curve of CdO:In/p-Si heterostructure. The resistance of optimized p-Si/CdO:In interface does not contribute to the total series resistance of a standard Si solar cell. The contact resistance is further reduced by Al diffusion from Al interlayer at the interface.

(iii) An environmental stability is an important consideration for applications of CdO TCO.

The group has found that the decomposition of CdO-based TCOs under highly corrosive conditions is significantly reduced by alloying CdO with NiO. Fig. 3 displays the conductivity as a function of Cd content in the $Ni_xCd_{1-x}O$ films. The films exposed to a negative bias in an electrolyte become more conductive and less transparent (colored) due to loss of oxygen and material decomposition. The alloying of CdO with NiO reduces the decomposition. Coloration effect is decreasing with increasing Ni content and becomes negligible for Ni content larger than ~25%. The coloration effect has been attributed to the presence of the surface electron accumulation layer as the films show much larger stability for the positive bias (bleaching) conditions.

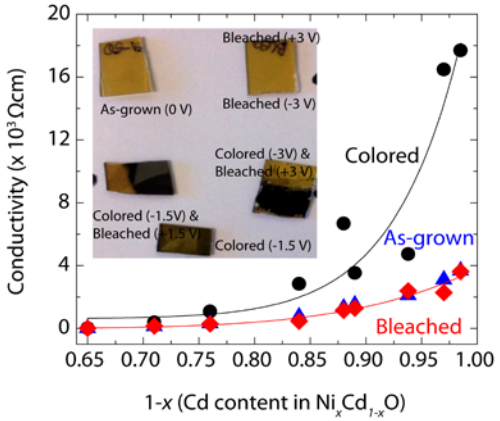

Fig. 3 Conductivity as a function of Cd content in the as-grown, colored, and bleached $Ni_xCd_{1-x}O$ films. Alloying of CdO with NiO reduces the decomposition. CdNiO with more than 25% Ni can be used as a protective coating.

Future Work:

The main focus of the group's future effort will be implementation of CdO-based TCOs for Si PVs technology. The performance of p/n and n/p Si solar cells with CdO-based transparent contacts will be compared with standard Si PVs using Ag grid. This work will be done in collaboration with Australian National University and a commercial Si PV company that have already provided Si p/n and n/p structures for CdO deposition to be compared with reference cells fabricated using standard Ag grid technology. The objective of this work will be to fabricate Si PVs with CdO contacts that are within 10% (relative) efficiency of the reference devices.

The detailed tasks are as follows:

1. Fabrication of n/p+ and p/n+ Si solar cells with CdO:In contacts (in collaboration with ANU and industrial partner).
2. Optimization of the CdO:In deposition conditions for low carrier recombination at Si/CdO:In interface.
3. Evaluation of CdO:In for use as anti-reflective coating on Si cells.
4. Comparison of the performance of Si cells with CdO:In TCO and with standard Ag grid.
5. Study of the effects of CdNiO protective layer on the cell performance.

BAPVC Annual Project Report

Project Title: Earth abundant p-type transparent conductors
PI: Joel W. Ager, Materials Sciences Division, Lawrence Berkeley Nat. Lab
E-mail: JWAger@lbl.gov

Summary:
P-type transparent conductors based on Cu-Zn-S alloys have been synthesized which have world record combinations of transparency and hole conductivity. A scalable process for the deposition of these materials has been developed. Successful device integration work has been performed with Si and III-V photovoltaic absorbers.

Key Accomplishments:
The conductivity, of p-type transparent materials (TCMs) has historically lagged behind that of well-known n-type transparent conductors such as indium tin oxide (ITO), Al-doped ZnO (AZO), and F-doped tin oxide (FTO). Moreover, most of the p-type TCMs reported thus far require processing temperatures in excess of 400 C, which will limit their applications in devices with limited thermal budgets such as many solar cell architectures.

Cu alloyed ZnS ($Cu_xZn_{1-x}S$) is an attractive materials system to overcome these limitations. Leveraging the group's prior work on elevated temperature deposition,[1] the entire composition range from ZnS to CuS/Cu_2S was synthesized by pulsed laser deposition. As shown in Fig. 1, there is a "window" of p-type conductivity and excellent optical transmission for Cu contents in the range of 9-40%. For optimal films, the combination of optical transparency and p-type conductivity is the highest achieved for a transparent hole-conducting material deposited at room temperature and rivals that achieved for higher growth temperatures (Fig. 2).[2]

To increase the industrial relevance of the material, an inexpensive chemical bath deposition procedure was developed using mild conditions and earth-abundant precursors. Measurements performed within the BAPVC with M. Toney's group at SSRL were critical for determining the film microstructure and maximizing film conductivity and transparency. The transparency can be as high at 80% at 550 nm, with corresponding sheet resistivities of 400 Ω/sq; these values both meet project performance goals and represent state of the art performance for a p-type transparent conductor.

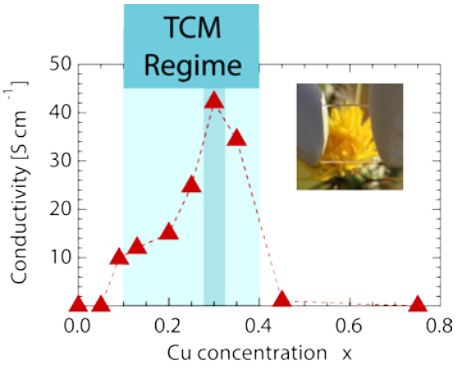

Fig. 1. Measurements of conductivity for transparent $Cu_xZn_{1-x}S$ films ($0 \leq x \leq 0.75$). The maximum hole conductivity, 42 S cm^{-1}, is observed at $x = 0.30$.

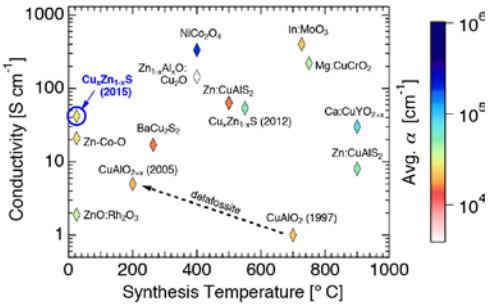

Fig. 2. Conductivity plotted against maximum processing temperature for the highest performing CuxZn1-xS films of this study (x = 0.30, circled in blue) and for a group of the highest performing p-type TCM films in the literature. The color scale represents increasing absorption coefficient (averaged over 400 – 800 nm), with white the lowest (most transparent) and blue the highest (least transparent).

An efficient PV device using a p-type TCM had not been reported in the literature, in particular with a low temperature process. In collaboration with BAPVC researcher Ali Javey's group, solar cell integration was performed by fabricating n-Si/p-CuZnS and np^+-Si/p-CuZnS structures. Excellent hole collection was found in the n-Si/p-CuZnS cells with 1 sun open circuit voltages exceeding 400 mV. Figure 3 shows current-voltage data from a np^+-Si/p-CuZnS structure, with the >30 mA cm^{-2} short circuit current, achieved without an anti-reflection layer, attesting to the transparency of the p-type contact.

The developments in this project eliminate the main barriers preventing the use of p-TCMs in device applications and thus will enable new applications such as thin film tandem solar cells based on abundant elements and, potentially, other applications, such as "invisible" electronics on flexible substrates.

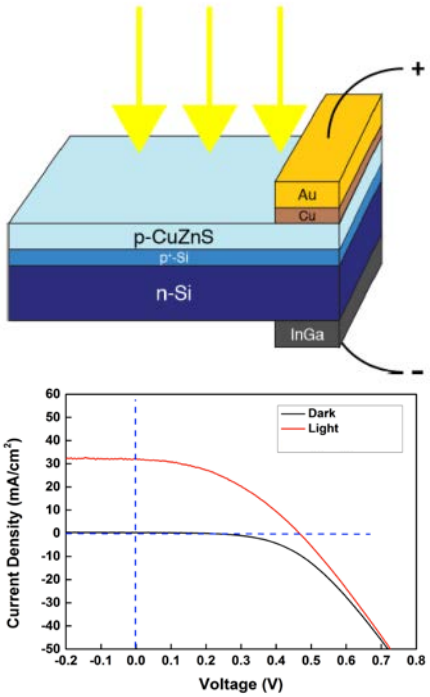

Fig. 3. Current-voltage data from a np^+-Si/p-CuZnS device. The p-type transparent contact was made by chemical bath deposition. Device size 1 cm x 1 cm, simulated AM1.5G illumination.

Future Work:

The focus of the future work will be further optimization of the chemical bath deposition process aiming at higher transparency while retaining the world-record level hole conductivity. The PV device integration work will focus on improving the fill factor for the Si-based devices. Also, the use of p-CuZnS as an ohmic (also electron-blocking) back contact to earth-abundant absorbers such CZTS will be explored. Ultimately, replacement of the Mo now used for this purpose may enable new types of thin film tandem architectures to be developed.

[1] A.M. Diamond, L. Corbellini, K.R. Balasubramaniam, S. Chen, S. Wang, T.S. Matthews, L.-W. Wang, R. Ramesh, and J.W. Ager, Phys. Status Solidi **209**, 2101 (2012).
[2] R. Woods-Robinson, J. K. Cooper, A. Faghaninia, L. T. Schelhas, V. L. Pool, M. T. Toney, C. Lo, I. D. Sharp, and J. W. Ager, ms. under review.

BAPVC Annual Project Report

Project Title: Thin Si HIT Cells With High Performance Metasurfaces Light Trapping and Passivation
PI: Harry A. Atwater
E-mail: haa@caltech.edu

Summary of Key Accomplishments:

To realize the ambitious goal of superior HIT cell performance in thin (< 50 micron) cells relative to conventional HIT cells, advanced light trapping and state-of-the-art passivation are required of high lifetime materials. To this end, we have in the last year characterized 1) reflectance of high aspect ratio, high lifetime Si structures defined by dry etching, and report what is to our knowledge a **new world-record low angle/spectrum averaged reflectance for Si of R = 0.45 %** from λ = 400-950 nm and 0-50 degree incidence angle 2) and bulk recombination lifetime in the few-100s microsecond range for dry etched and passivated surfaces and passivated 15 micron tall wires and 3) few-microsecond range bulk recombination lifetime for high-aspect ratio (70 micron tall) passivated wires fully removed from their substrate, under peel-off conditions representative of a Si cell mechanical liftoff process.

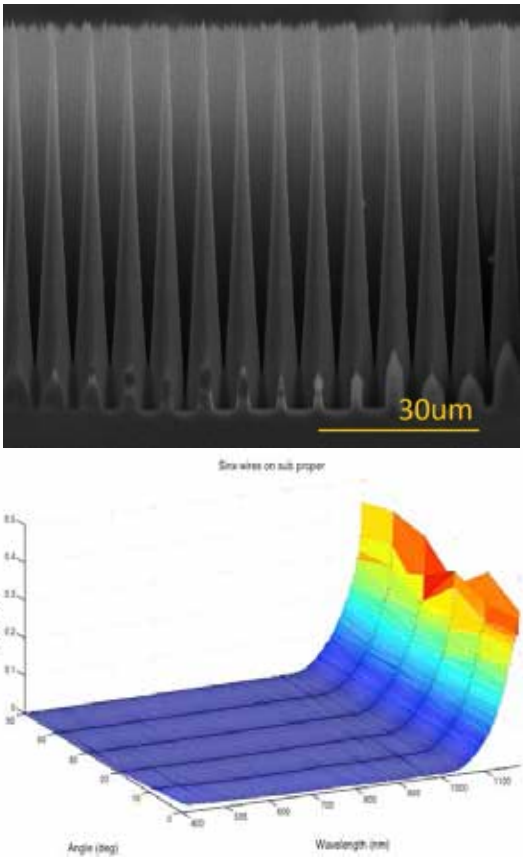

Fig. 1. High aspect ratio crystalline Si microwires fabricated by inductively couple reactive ion etching (above) and reflectance (below). These structures exhibited a world record low spectrum and angle integrated reflectance of 0.45% (400-950 nm wavelength; 0-50 degrees.)

Crystalline silicon is the predominant photovoltaic cell technology and HIT cells hold the current Si record cell efficiency of 25.6% under non concentrating conditions. The maximum efficiency for Si cells is ~29% given by Shockley–Queisser limit, implying there is still room for improvement in efficiency. To approach this limit, we need to achieve 1) extremely low surface reflectivity 2) light trapping at or near the ray-optic limit in Si absorbers with planar equivalent thickness <40 microns 3) very high bulk minority carrier lifetime and very low surface recombination velocity at surfaces. We report here results for a high bulk lifetime microwire absorber morphology, and discuss surface reflectance, bulk lifetime and surface passivation.

Silicon microwire arrays are highly efficient light absorbers with an enhanced near infrared absorption allowing their overall sunlight absorption to approach the ray optic light trapping absorption limit with low areal packing fractions. Previously we have synthesized silicon microwires via vapor-liquid-solid CVD processes employing metal catalysts, and found that the metal catalyst contaminates crystalline silicon absorber and limiting the lifetime in these microwires (~20ns).

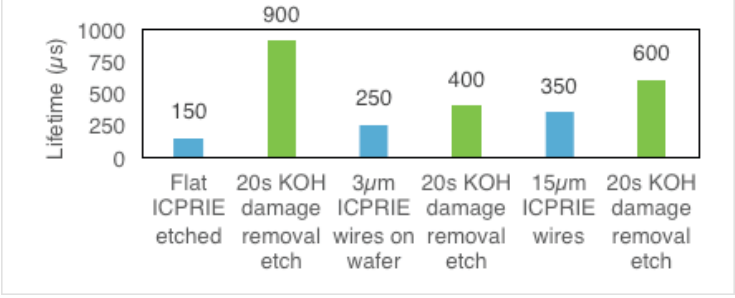

Fig. 2 Minority carrier lifetime inferred from microwave photoconductive decay measurement for dry etching and subsequent chemical etching of Si with 1 msec as-received wafer bulk lifetime. KOH etching recovers the measured lifetime of flat and 15 micron tall wires to 900 and 600 microseconds, respectively.

In our current work we have explored microwire synthesis via dry etching. Specifically we have used cryogenic inductively coupled plasma reactive ion etching of high (>1 msec) bulk lifetime wafers as an alternative process for making silicon microwires. By choosing the dry etching conditions to be primarily chemical, the surface damage can be minimized. Chemical etching following the dry etching for ~20s in 30% KOH at 80°C has been demonstrated to remove the surface damage and aid in recovering the lifetime as illustrated in Fig. 2.

Higher aspect ratio (70 micron tall) microwires defined on ICPRIE-etched Si wafers were fabricated in other experiments, and then removed from the substrate, and subsequently passivated by several types of chemical treatments. These included passivation of substrate-removed wires in iodine/ethanol, 2% HF/water, 49% HF/water and 1:1: HCl/water. The lifetimes of etched wafers and microwires collected separately in a vial under various passivation ambients as given in Fig. 3 below. A maximum lifetime of 1.9 microseconds is observed in Silicon microwires (15 μm diameter, 70 μm tall) passivated in 1:1 HCl solution after damage removal on front and back surfaces. This corresponds to a diffusion length of ~75 micron in the microwires.

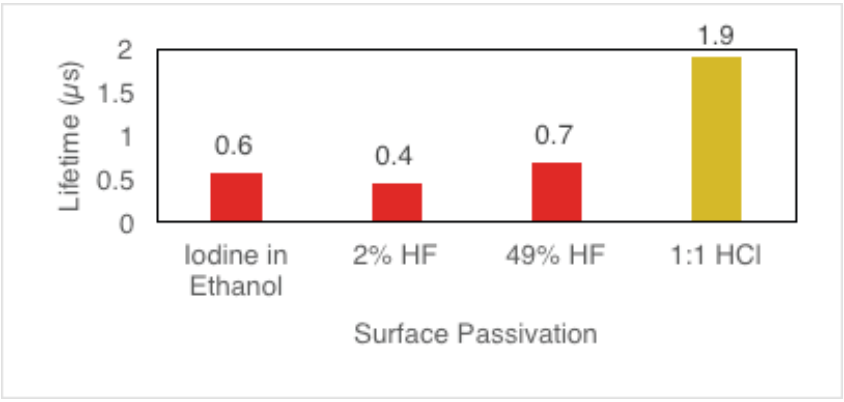

Fig. 3 Minority carrier lifetime inferred from microwave photoconductive decay measurement for dry etching and subsequent chemical passivation of Si removed from bulk wafer substrate. Passivation in 1:1: HCl/water afer KOH etching recovers the measured lifetime of 70 micron tall wires to 1.9 microseconds, corresponding to a 75 micron diffusion length.

Future Work:

We plan to integrate the findings with results of the work from Brongersma and Bowden to develop a process for a thin light-trapping HIT cell with record photocurrent density for absorber layer equivalent thicknesses less than 50 microns. Specifically we will characterize

quantitatively the spectral absorption and photocurrent spectral response (preliminary measurements already completed), and will work to 1) integrate our microwire absorber layer structures with the Arizona State a-Si:H growth process and 2) combine insights with the Stanford group about metasurface light trapping for chemically passivated Si structures.

BAPVC Annual Project Report

Project Title: Graphene Electrode Engineering for Photovoltaic Applications
PI: Kaustav Banerjee
E-mail: kaustav@ece.ucsb.edu

Summary:
The UCSB group has been developing a graphene synthesis process, which can significantly reduce the cost of high-volume graphene production, during the past year. They found it is possible to achieve 90% transmittance and small sheet resistance of 10 Ω/□ by engineering the number of graphene layer as well as the grid density. Using electrochemical transfer method, the fabrication cost of graphene was significantly reduced to $7.5/m^2, which is close to the cost of ITO ($6/m^2).

Key Accomplishments:

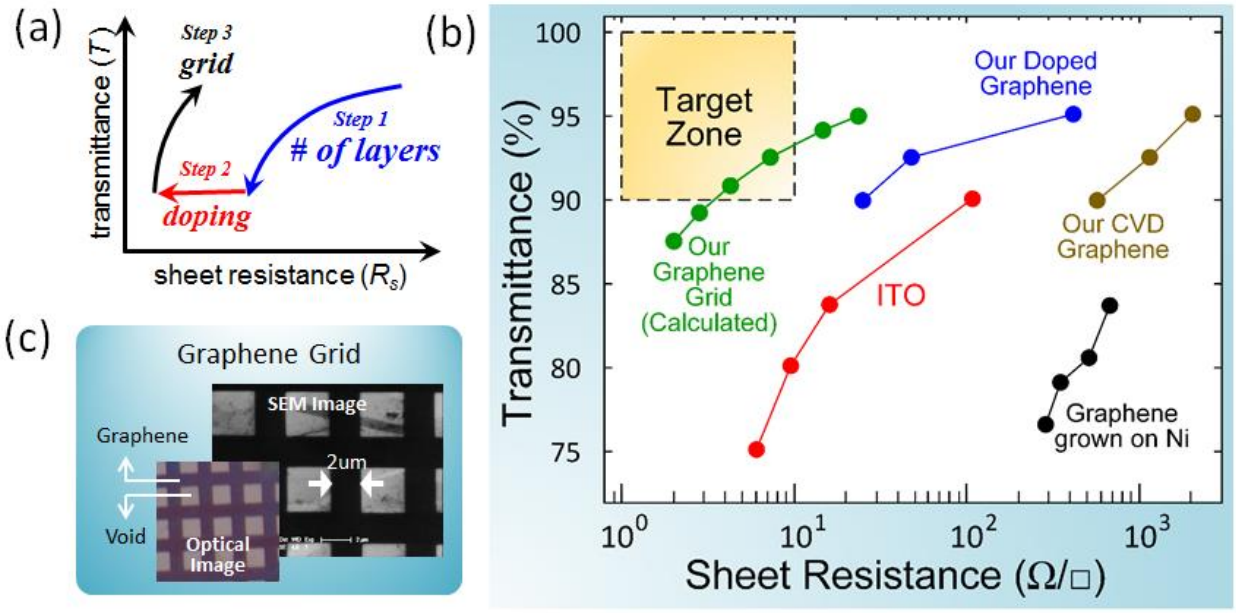

Figure 1. Graphene-based gird. (a) The principle of transmittance and sheet resistance engineering of graphene grid. (b) Comparison of sheet resistance and transmittance from the work at UCSB and other results from the literature. (c) Optical image of the fabricated graphene grid.

The UCSB group has theoretically and experimentally studied surface charge transfer doping[1], substrate doping[2] and intercalation doping of FLG. In the second year of the BAPVC project, their study revealed that intercalation doping is an efficient and stable doping method. By using intercalation doping, 4 layer graphene can attain small sheet resistance of 20 Ω/□, which is the smallest value reported compared with any reported values to date. However, this method requires long process time (12 hours), which in turn increases the fabrication cost. Hence, it is highly desirable to explore a new method to reduce the sheet resistance of graphene, while keeping the high transmittance of graphene film. Recently, they found that it is possible to achieve the 90% transmittance and small sheet resistance of 10 Ω/□ by engineering the number

of graphene layers as well as the grid density (Fig.1a). The sheet resistance and transmmittance of graphene grid is even better than that of intercalation doped few layer graphene (Fig.1b).

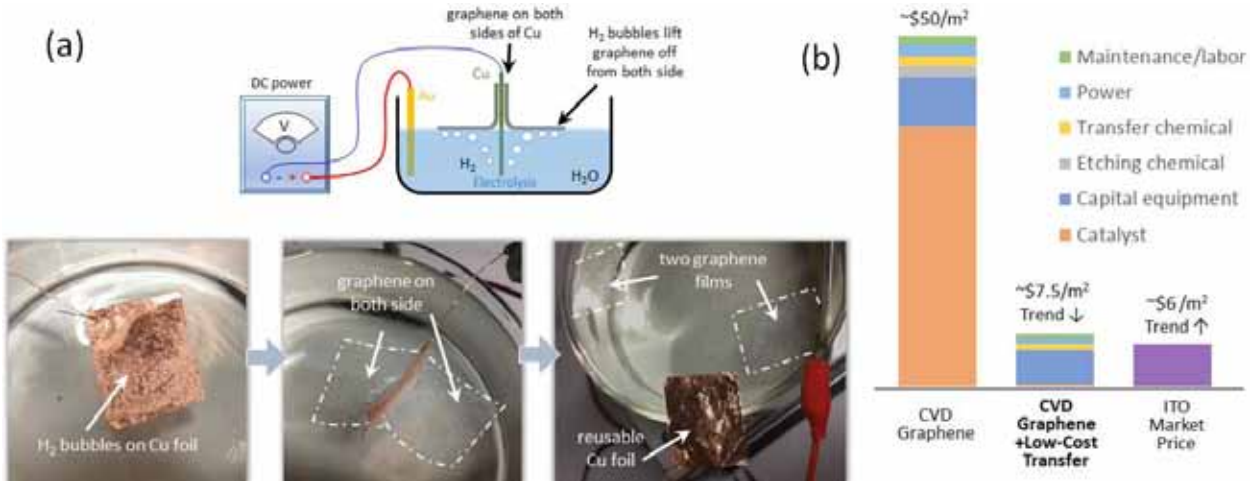

Figure 2. (a) The schematic (upper) and optical images (lower) of bubble transfer method. (b) The cost analysis of graphene growth compared with the current cost of ITO.

The bottleneck of the application of graphene in industry-scale is the high fabrication cost of graphene film, which is also the major concern from the industry members of BAPVC. UCSB group conducted a comprehensive cost analysis of graphene synthesis. From the analysis results (Fig.2b) it was concluded that the consumption of catalyst leads to the high cost because the catalyst has to be etched away to separate the graphene from the catalyst film. In addition, this etching process requires use of etcher and solvent to remove the supporting PMMA layer on top of the graphene. These chemicals will also increase the cost. UCSB group developed a bubble method (Fig.2a) which can separate graphene films from the two sides of the catalyst without the catalyst etching process. Hence, the catalyst film can be reused many times (100 times for 25 μm film). In addition, the etcher is not necessary for the transfer. This method is totally green compared with the normal etching transfer method. More importantly, the cost of the UCSB graphene film is around $\$7.5/m^2$ which is close to the ITO market price ($\$6/m^2$), but predicted to continue increasing in the future. It is worth noting that the UCSB graphene process is still lab-scale and the cost will reduce when produced in high-volume. Additionally, this price ($\$7.5/m^2$) can be further reduced by using non-PMMA supporting layer, which does not require the solvent remover in the near future.

Future Work:
A new supporting material should be developed to replace PMMA. Using this new chemical, the usage of solvent such as acetone can be avoided to further reduce the cost.

1. Khatami, Y.; Liu, W.; Kang, J.; Banerjee, K. *Proc. SPIE 8824*, *Next Generation (Nano) Photonic and Cell Technologies for Solar Energy Conversion IV*, 88240T, September 25, 2013.
2. Khatami, Y.; Li, H.; Liu, W.; Banerjee, K., *IEEE Transactions on Nanotechnology*, Vol. 13, No. 1, pp. 94-100, 2014.

BAPVC Annual Project Report

Project Title: Large-Area, Fast, and Electric-Field Assisted Continuous Coating for Nanostructured Photon Management

PI: Ning Wu, the Department of Chemical and Biological Engineering, Colorado School of Mines
E-mail: ningwu@mines.edu

Summary:
The CSM group has achieved the fabrication of non-close packed colloidal patterns on conducting substrates with the assistance of both AC and DC electric fields. They have demonstrated the potential to fabricate uniform photonic/plasmonic structures for photon management. We have also observed the fabrication of chiral colloidal structures which have potentials for unique and novel light-matter interactions.

Key Accomplishments:

1. Electric-field assisted coating of non-close packed pattern

We employ a low-power alternating current (AC) electric field to manipulate a number of attractive and repulsive forces between colloidal particles, which generate non-close packed hexagonal particle arrays in solution. We then apply direct current (DC) pulses to induce an electrophoretic force that points towards the bottom substrate. The particles are permanently fixed on the substrate when the DC current is larger than a critical value. The periodic structures can be maintained even after solvent evaporation. The experiment setup that combines both AC and DC fields is shown in **Fig.**1. The strength of the DC electric field is critical. **Fig.** 2 demonstrates that a low DC current does not disturb the pattern formed in solution but could not fix the particles permanently. A high DC current introduces significant lateral movement of individual particles. Although it can fix the particles, the ordered pattern cannot be maintained. With an intermediate DC current, we can fix the particles while maintaining the ordered array. Moreover, we have demonstrated that this method is based on physical principles that can be applied to a variety of particles with different materials properties. A manuscript is in preparation.

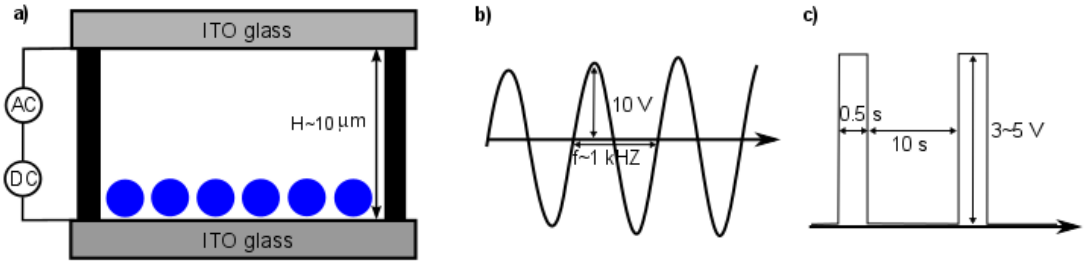

Fig. 1 a) a cross-section view of the experimental setup. b) AC electrical field employed to form non-close packed particle pattern. c) DC pulses employed to fix the particles on the bottom substrate.

2. The formation of chiral colloidal clusters

Shown in **Fig. 3**, two to four dielectric dimers are assembled into compact clusters that exhibit left and right handedness in configuration. Similarly, the metallodielectric Janus spheres can also orient their metallic parts into chiral clusters. The cluster configuration is primarily determined

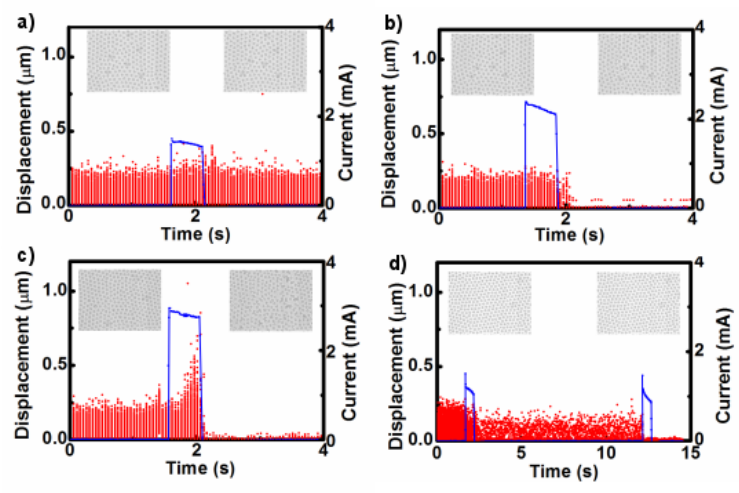

Fig. 2 Particle displacement (red dots) under different DC voltage pulse (blue curves). a) 3V DC pulse cannot fix the particles. b) 3.5V DC pulse can fix the particle while maintain the pattern c) 4V DC pulse can fix the particle but would destroy the pattern. d) Multi rounds of 3V DC pulse can fix the particle while maintain the pattern.

by the induced dipolar interactions between constituent dimers. Our theoretical model reveals that in-plane dipolar repulsion between petals in the cluster favor the achiral configuration, while out-of-plane attraction between the central dimer and surrounding petals favor a chiral arrangement. It is the competition between these two interactions that dictates the final configuration. The structures shown in **Fig. 3** could be excellent candidates for studying unique optical response of individual clusters, as well as periodic arrays of them.

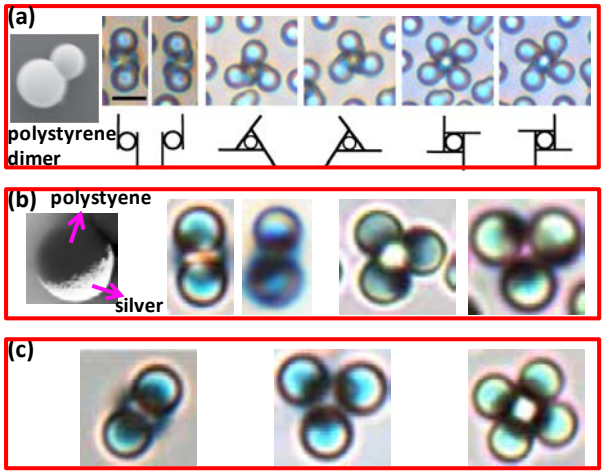

Fig. 3 Chiral and achiral structures formed by the self-assembly of dielectric and metallodielectric building blocks under AC electric fields. (a) Left- and right-handed chiral clusters formed by an increasing number of dielectric dimers. (b) Chiral clusters formed by silver-polystyrene metallodielectric spheres. (c) Achiral clusters for comparison.

Future Work:

We will keep investigating the flow-coating method, with the goal to increase the coating speed and reducing the density of defects. We will also continue the study that combines the electric-field assembly with the flow coating technology. Our final goal is to fabricate the non-close packed particle arrays that can be applied to both dielectric and metallic particles on conducting substrates.

References

1. Fuduo Ma, Sijia Wang, David T. Wu, Ning Wu, "Electric-field–induced assembly and propulsion of chiral colloidal clusters", *Proceedings of the National Academy of Sciences* **112**, 6307–6312, 2015.

Thrust: Silicon Absorbers and Cells

Key Challenges

Silicon-based solar cells are the dominant PV technology today with more than 80% market share. The research infrastructure is equally strong. This thrust must focus on those challenges with the greatest opportunities for successful university research. The key challenges which are being addressed to enable high volume manufacturing of high efficiency Si cells are listed below:

1. Commercially viable manufacturing of thin crystalline Si solar cells below 50um
2. Fundamental science of crystal growth and bulk defects for low-cost, high-quality ingots
3. Passivation of thin crystalline Si to meet the high efficiency targets
4. Absorption of all available light within a reduced absorber volume
5. Metallization and packaging of thin Si cells into lightweight modules

Existing Projects in our Thrust

- *High Efficiency Ultrathin Silicon Solar Cells*, Yi Cui (Stanford)
- *Thin Crystalline RPCVD Back Contact Cells*, Sanjay Banerjee (Texas)
- *Laser Wafering*, Stuart Bowden (Arizona State)
- *Module Interconnects and Crystalline Film Silicon by Atmospheric Pressure Processing*, van Hest (NREL)
- *High-resolution, High-speed Printing of PV Contacts*, Vivek Subramanian (Berkeley)

Potential New Areas of Interest

- Processes for thin Si absorber preparation, such as spalling, epi-lift-off, templated growth, etc.
- Fundamental science of crystal growth and bulk defects for low-cost, high-quality ingots
- Methods for nano-texturing on thin Si surfaces, such as colloidal lithography, nano-imprint, etc.
- Improved passivation of thin crystalline Si foils including passivation of nano-textured surfaces
- Printing contacts on thin Si foils, including liquid precursor development

BAPVC Annual Project Report

Project Title: High Efficiency Ultrathin Silicon Solar Cells

PI: Yi Cui

E-mail: yicui@stanford.edu

Summary:

The goal is to generate high efficiency ultrathin silicon solar cells with an understanding of their device physics and developing manufacturing process. The Cui group at Stanford University has reported progress in the production of < 10μm monocrystalline silicon at a wafer scale with regular fabrication processability and experimentally demonstrated that with novel nanoscale photon management structures, 3μm-thick Si can absorb 58% of the above bandgap sunlight and 7μm of 86%. They studied the balance between excellent photon absorption and efficient electrical collection in ultrathin monocrystalline-Si solar cells, and demonstrated >80% EQEs at wavelengths from 400 to 800 nm in a sub-10- μm -thick Si solar cell, resulting in 13.7% power conversion efficiency. Furthermore, a thin Si manufacturing technique is explored with metal-assisted chemical etching (MACE).

Key Accomplishments:

Ultrathin monocrystalline Si cells offer the potential of saving materials, increasing manufacturing throughput, and enabling easy low-weight installation. The Cui group developed wafer-scale free-standing ultrathin monocrystalline Si fabrication with uniform thickness from 10 to sub-2μm by KOH chemical etching (see Fig1 (a,b)). These ultrathin Si exhibits excellent mechanical flexibility and bendability, as shown in Figure.1(d,e). Unexpectedly, these ultrathin Si materials can be cut with scissors like a piece of paper, and they are robust during various regular fabrication processing. To demonstrate their processability, the Cui group fabricated planar and double-sided nanotextured solar cells on these free-standing ultrathin Si films. Furthermore, they also experimentally demonstrated a large light absorption enhancement by a double-sided surface nanotexture design on the free-standing ultrathin Si films. Light absorption in 3μm thick Si film is largely enhanced with a130% increase in Jsc, achieving 58% absorption of the above bandgap sunlight. 7μm thick Si can absorb 86% of the above bandgap sunlight.

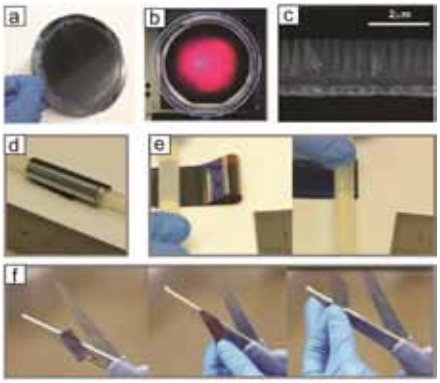

Fig. 1, (a) and (b) 4-in. wafer-size ultrathin Si films illuminated by the white light from the backside. (c) SEM image of the cross sections of a double- sided patterned films.(d) A 3μm thick Si film was wrapped around a plastic rod with diameter of 7 mm. (e) The Si film was folded and then pressed by the plastic rod. The minimum folding radius is around 1 mm. (f) Si cutting process using scissors. Ref[1]

Despite the exciting success of nanoscale texturing in light trapping, the power conversion efficiencies of nanostructured Si solar cells, however, remain below 19% for thick devices and below 11% for thin devices. The Cui group fabricated a sub-10-μm-thick Si solar cell with a 13.7% power conversion efficiency which utilizes all-back-contact design to overcome the critical problems of nanostructured devices: Auger and surface recombination. In general, nanostructured solar cells have a highly doped emitter layer at the front, fabricated by high-temperature diffusion processes. Because the diffusion profile of the dopants is dependent on the surface morphology, a nanostructured device tends to have a much deeper junction depth with a higher concentration compared with a planar device. It leads to severe Auger and surface recombination of charge carriers. Another problem of nanostructured Si solar cells is the increased surface area. Considering the fact that the surface recombination becomes more critical to device performance as the absorber becomes thinner, the increased surface area in a thin Si solar cell can lead to a severe decrease of efficiency. The Cui group designed devices with two main advantages: the all-back contact design and the nanocones. Its all-back-contact design prevented Auger recombination loss near the front (see Fig.2), and its nanocone structure minimized the increase in surface area while enhancing the light absorption significantly.

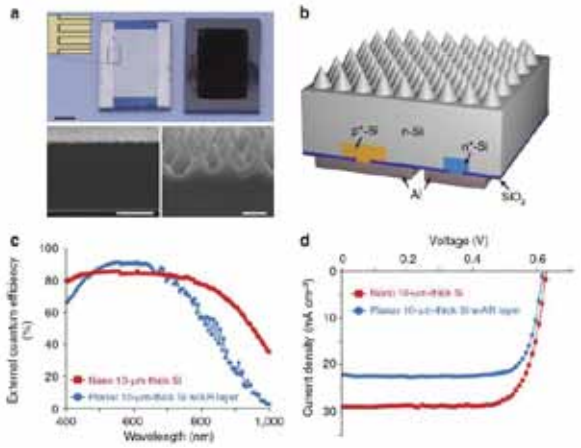

Figure 2. Ultra-thin Si nanocone solar cell. (a) Optical image and SEM cross-sectional views of the 10-μm-thick Si solar cell. (b) Schematic illustration of the device. (c) EQE data of the device and a planar control. (d) J – V characteristics of two devices in c. Ref [2]

MACE is explored as a method of scalable production for thin Si because it is an easily scalable, low-cost selective wet etching technique. The final goal is to simultaneously etch thin Si wafers of arbitrary thickness directly from an ingot with little raw Si material loss. Thus far, the Cui group has demonstrated slicing vertically through a wafer of over 300 μm thick to produce long silicon slivers, as shown in Fig.3. Upon noticing that some of the etched Si looked very dark to the eye, the group further explored and developed a hybrid metal-semiconductor nanostructured interface, producing a structure that absorbs an average 97% of the visible spectrum with a sheet resistance of 16 Ω/□ while 60% of the top-down surface is covered with metal. The group continues to explore the applications of ultra high-aspect ratio MACE and this nanostructured interface.

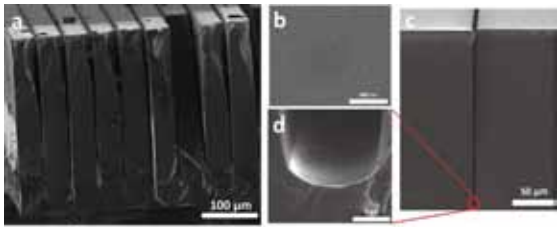

Figure 3. Metal-assisted chemical etching of Si. (a) SEM cross section of 5 μm wide lines etching over 300 μm down. (b) Nanostructure of evaporated metal layer. (c) MACE trench. (d) Zoomed in bottom of trench

Reference:

1. S. Wang, B. Weil, Y. Li, K. X. Wang, E. Garnett, S. Fan, and Y. Cui, "Large-Area Free-Standing Ultrathin Single-Crystal Silicon as Processable Materials," Nano Letters 13(4393)(2013).

2. S. Jeong, M. D. McGehee, and Y. Cui, "All-back-contact ultra-thin silicon nanocone solar cells with 13.7% power conversion efficiency," Nature Communications 4(2950) (2013).

3. V. Narasimhan, T. M. Hymel, R. A. Lai, and Y. Cui, "A hybrid metal-semiconductor nanostructure for ultrahigh optical absorption and low electrical resistance at optoelectronic interfaces," ACS Nano (under review)

Future Work:

Future work focuses on the push for higher efficiencies in the 10-20μm Si solar cell. This goal can be accomplished via two methods: 1) producing a heterostructured intrinsic thin-layer (HIT) solar cells; 2) good passivation with an oxide layer and careful surface preparation of ultrathin Si solar cells. The goal is to improve the 13.7% efficiency to 17.5%, and then further to over 20%. 3) Develop scalable and low-cost manufacturable process to generate thin Si with low material loss.

BAPVC Annual Project Report

Project Title: High efficiency a-Si:H /c-Si/a-Si:H dual heterojunction solar cells on exfoliated ~ 25 µm monocrystalline silicon substrates by improved surface treatment and passivation

PI: Sanjay K. Banerjee
E-mail: banerjee@ece.utexas.edu

Summary:

Dual heterojunction (DHJ) solar cells consisted of a-Si:H/c-Si/a-Si:H architecture can obtain excellent passivation qualities at low deposition temperatures. Together with the low cost, kerf-less mechanical exfoliation method, 12.4 % efficient monocrystalline DHJ silicon solar cells of ~ 25 µm thickness are demonstrated. Improvements of the surface cleanness after front side texturing and passivation film quality were successfully conducted.

Key Accomplishments:

The Banerjee group at UT-Austin has demonstrated low cost, kerf-less mechanical exfoliation of 25 µm thick monocrystalline silicon foils, up to 8 inch in diameter, in which the parent wafer can be re-used for subsequent exfoliation. They have previously demonstrated a-Si:H/c-Si/a-Si:H dual heterojunction (DHJ) solar cells on thin silicon foils with 11 % efficiency. They have increased the overall efficiency of the cells by improving the surface cleanness after front side texturing. Auger Electron Spectroscopy (AES) measurement revealed that a combination of SC-15 solution (Surface Chemistry Discoveries, Inc) treatment followed by piranha clean resulted in the least amount of potassium and carbon contaminants at the textured surface as described in Table 1 and Fig 1.

Sample#	Treatment after KOH texturing	Carbon (Atomic %)	Potassium (Atomic %)
1	None	2.84	1.11
2	Piranha	2.32	0.88
3	SC-15	2.11	0.25
4	SC-15+Piranha	1.63	0.22

Table 1. Treatment splits after front side texturing of exfoliated samples and their calculated atomic percentage of C & K contaminants using AES

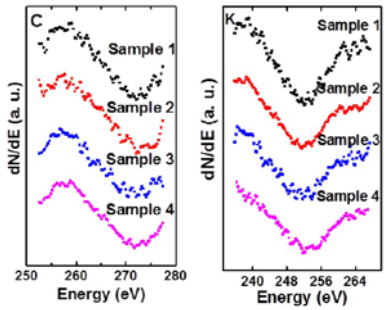

Fig 1. AES spectra with differentiated peaks of C & K

Along with the improved surface cleanness, they have also increased the a-Si:H passivation film quality. By increasing the deposition temperature of a-Si film from 150 ˚C to 200 ˚C followed by post deposition annealing (PDA) at 260 ˚C for 60 minutes, the minority carrier effective lifetime (τ_{eff}) increased from 16 µs to 1.5 ms as shown in Fig 2 (a).

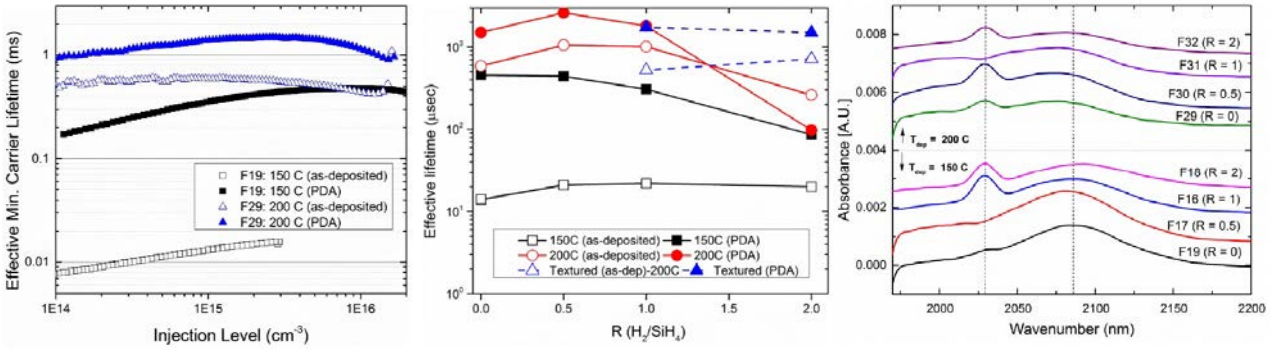

Fig 2. (a) τ_{eff} of a-Si passivated silicon substrate (FZ, n-type, <100>, 2 Ω·cm) for 150 ˚C and 200 ˚C deposition temperature with PDA

(b) τ_{eff} of a-Si:H passivated silicon substrate for different H_2/SiH_4 (R) ratio for textured and non-textured surfaces

(c) FTIR absorption spectra for various a-Si:H deposition conditions

Also, introducing hydrogen dilution during a-Si film deposition proved additional increase in τ_{eff} for both textured and non-textured surfaces which is presented in Fig 2 (b). Fig 2 (c) represents the fourier transform infrared spectroscopy (FTIR) measurement of various a-Si:H films with different deposition conditions. An optimal range of R exists for maximum τ_{eff} where both mono- and di-hydride bonding co-exist inside the film. Incorporating the improved surface cleaning method along with high quality a-Si:H passivation film deposition resulted in efficiency of 12.4 % as described in Fig 3.

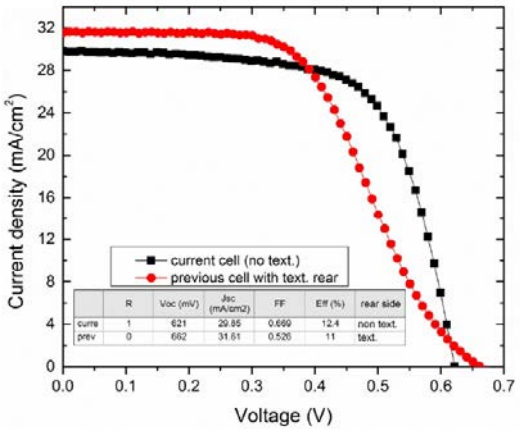

Fig 3. J-V characteristics of DHJ cells on exfoliated ~25 µm substrates

Future Work:

Future work will be focused on two major aspects; increasing the overall efficiency of a-Si:H based heterojunction solar cells and further reducing the cell thickness. The approach will be to optimize the n+/p+ doped a-Si:H and anti-reflective coating (ARC) layer as well as to explore helium based plasma deposition of a-Si:H. Mechanically exfoliated silicon films of < 15 µm will developed. Finally, metal-thin insulator-semiconductor (MIS) architecture solar cells on exfoliated substrate using large area 2-D materials such as graphene and h-BN will be studied for flexible photovoltaic applications.

BAPVC Annual Project Report

Project Title: Laser Wafering
PI: Stuart Bowden
E-mail: sgbowden@asu.edu

Summary:

The focus of this work is the design and understanding of a novel semiconductor wafering technique that utilizes the nonlinear absorption properties of band-gapped materials to achieve bulk (subsurface) morphological changes in matter using highly focused laser light. A method and tool was designed and developed to form controlled damage regions in the bulk of a crystalline sapphire wafer leaving the surfaces unaltered. The controllability of the subsurface damage geometry was investigated, and the effect of numerical aperture of the focusing optic, energy per pulse, wavelength, and number of pulses was characterized for a nanosecond variable wavelength laser.

Key Accomplishments:

The researchers developed a model to for the subsurface laser ablation in sapphire as shown in Figure 1. The combination of a ray-optics and electron plasma accurately predicted the shape, size, and location of permanently modified material in the bulk of sapphire for multiple focusing optics, laser wavelengths, number of pulses, and a wide range of beam power.

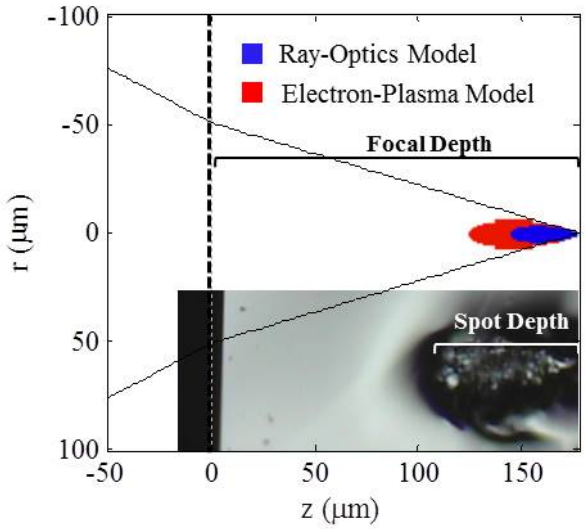

Figure 1: Ray-optics and electron-plasma bulk laser damage models compared to optical microscope image of bulk damage region. Damage spot formed from a single laser pulse at 315 µJ energy per pulse, 667 µm wavelength, focused 100µm beneath the surface with NA=0.50 reflective objective.

Lastly, having characterized the parameters controlling subsurface damage spot formation, arrays of damage were formed in the bulk of a crystalline sapphire wafers to attempt layer liftoff. Multiple samples of varying spot size, depth, spacing, and array area were prepared as well as some additional laser machining processes like outline surface ablation and corner drilling to allow preferential etch penetration. A plane of subsurface damage was

demonstrated. However, complete layer liftoff was not achieved to date. In order to fully define a laser wafering process, other methods of damage layer preparation and/or material liftoff should be attempted.

Future Work:

Other techniques for mechanically assisted layer liftoff after subsurface laser damage plane formation will be attempted. A layer of subsurface damage was demonstrated but the liftoff has not yet been achieved. Etches for the layer of damage are being investigated to further weaken the damage plane so that subsequent thermal or mechanical stress can achieve the final goal of lift off.

BAPVC Annual Project Report

Project Title: Novel Interconnects
PI: Maikel van Hest & Talysa Stockert
Email: maikel.van.hest@nrel.gov & talysa.stockert@nrel.gov

Summary:

The goal of developing novel interconnects is to monolithically interconnect PV cells in modules employing a single pass process after the deposition of all layers while simultaneously reducing dead zone area. Printed interconnects have been made for CIGS and CdTe using aerosol jet printing of dielectric and metal inks in conjunction with laser and mechanical scribing. Architectures using a 3-scribe and 2-scribe method were developed with best results obtained using PMMA (dielectric) and NovaCentrix Silver Nano-crystalline (metal) Inks.

Key Accomplishments:

The monolithic interconnect architecture serves to electronically isolate the top and bottom electrodes in the P1 scribe, as shown in Fig. 1. Fig. 1(b) and Fig. 1(c) show the alternative architectures of the 3-scribe and 2-scribe methods, respectively. Each method was constructed using laser-scribing via pulsed YAG at 1064 nm for P1 scribes and mechanical-scribing with a tungsten-carbide tip on an actuated scriber for P2 and optional P3 scribe through the full solar cell stack. Dielectric material, poly(methyl methacrylate) (PMMA), and metallization with NovaCentrix silver nano-crystalline ink were deposited using an aerosol jet system with a substrate temperature of 100°C and 150°C, respectively. An actuated mechanical scribing station was added to the printing station, eliminating the need for alignment between scribing and printing.

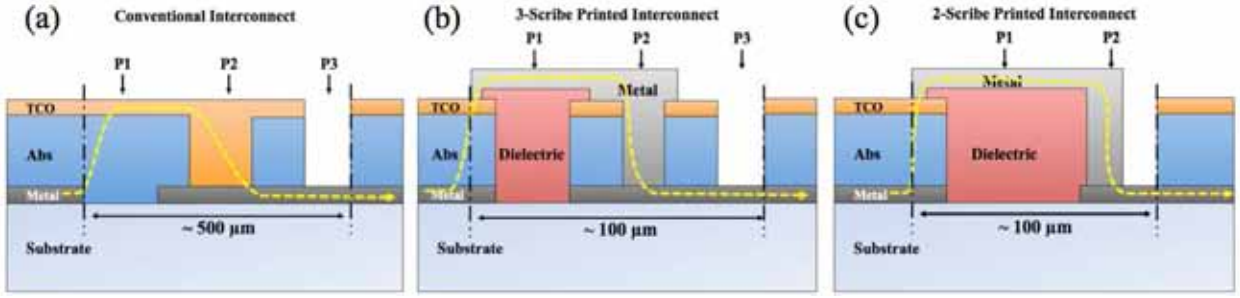

Figure 1: (a) Conventional, (b) 3-scribe printed, and (c) 2-scribe printed interconnect architectures. Cross-sections are labeled with the scribe numbers of P1, P2, and P3 for separation of bottom electrode, top electrode, and next cell, respectively. Areas between the black vertical bars represent the dead zones, which do not contribute to the power production of the cell. The yellow path represents current flow needed for voltage addition.

The 3-scribe printed interconnects were demonstrated for CIGS and CdTe mini-modules. CIGS 3-scribe mini-module J-V traces, shown in Fig. 2 (a), produced near perfect voltage addition for five cells, with minimal current loss or degradation of fill factor. Similarly Fig. 2 (b) presents the

CdTe 3-scribe mini-module where three out of four cells have voltage addition with steady current and fill factors. With the demonstration of proof of concept and identification of compatible materials for printed interconnects, focus shifted to the 2-scribe method in order to minimize the dead zone area. CIGS 2-scribe mini-modules demonstrate good voltage addition of seven out of the ten cells connected, with each drop in current and fill factor corresponding to an addition of a shorted cell. Printed interconnects using the 2-scribe method produce interconnects with widths smaller than 250 µm. With additional optimization 100 µm widths using current equipment is feasible. Cost modeling of the novel printed interconnect shows that the manufacturing costs of a 14% CIGS module can be reduced by 3 cents/W_p.

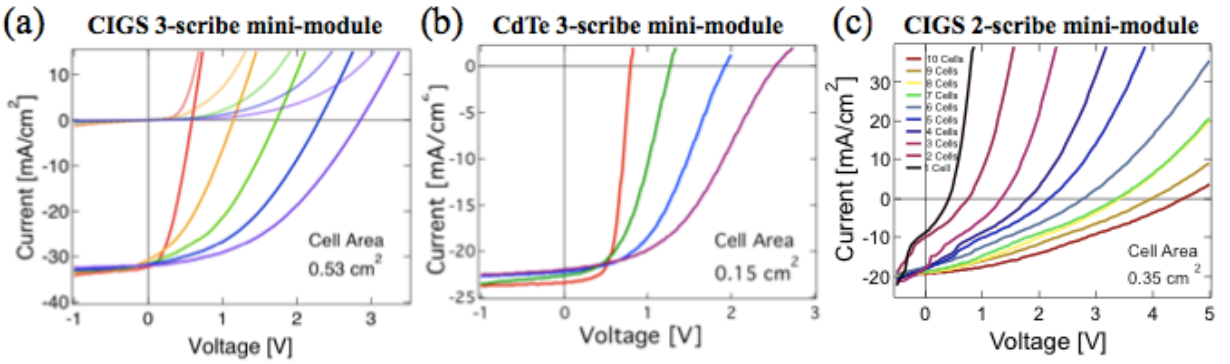

Cells	Voc		Jsc	FF	PCE
#	V	ΔV	mA/cm2	%	%
1	0.59	0.59	32.3	38.8	8.70
2	1.15	0.56	30.8	35.8	7.45
3	1.73	0.58	31.7	39.1	8.40
4	2.30	0.57	31.7	41.6	8.93
5	2.86	0.56	32.0	42.9	9.24

Cells	Voc		Jsc	FF	PCE
#	V	ΔV	mA/cm2	%	%
1	0.80	0.80	23.4	61.1	11.50
2	1.28	0.48	22.6	48.3	6.70
3	1.93	0.65	22.2	44.5	6.37
4	2.53	0.60	22.0	43.3	6.03

Cells	Voc		Jsc	FF	PCE
#	V	ΔV	mA/cm2	%	%
1	0.42	0.42	8.80	32.6	1.20
2	0.77	0.35	5.00	31.3	1.20
3	1.35	0.58	5.93	25.8	2.07
4	1.82	0.47	4.46	27.3	2.22
5	2.19	0.37	3.64	27.1	2.16
6	2.79	0.60	2.95	29.0	2.38
7	3.39	0.60	2.69	28.4	2.59
8	3.43	0.05	2.39	30.9	2.53
9	3.99	0.56	2.10	23.4	2.60
10	4.56	0.56	1.94	33.1	2.93

Figure 2: J-V traces showing voltage addition from (a) CIGS 3-scribed, (b) CdTe 3-scribed, and (c) CIGS 2-scribe printed interconnects with corresponding open circuit voltage, short-circuit current density, fill factor, and efficiency. CIGS 3-scribed interconnects demonstration successful connection of 5 cells with perfect voltage addition. Four cells on CdTe were connected using the 3-scribed method. CIGS 2-scribe interconnects demonstrated 10 cells connected in series with clear voltage addition.

Future Work:

For the remainder of the project, work focuses on identifying causes for shorts that are formed during the printing of monolithic interconnects. This information will improved the yield and enable the reduction of the interconnect width (<100 µm). To identify causes of shorts and other defects, DLIT, EL, and PL are used throughout the full process of printing the interconnects. Once the printing conditions are optimized, the monolithic interconnect will be applied to CIGS materials with high efficiency (>15%). Finally the work will be summarized in a manuscript that will be submitted for publication in a peer reviewed journal. Continued effort is made to acquire additional funding for this project.

BAPVC Annual Project Report

Project Title: Materials and Processes for High-Resolution Printed Bus Bars
PI: Vivek Subramanian
E-mail: viveks@eecs.berkeley.edu

Summary:

In this project, researchers are developing materials and processes for high-resolution bus bars through a combination of development of high-resolution gravure printing and development of advanced nanoparticle conductor inks. In the last year, substantial progress has been made on improving the resolution of gravure printing. Sub-2µm features have been realized, printed at printing speeds of ~1m/s. This represents a world-record achievement for gravure. Additionally, we have shown that gravure can be used to print on flexible and rigid glass substrates.

Key Accomplishments:

In the area of high-resolution printing, significant progress has been made, going beyond even our previous world record achievements. Sub-2µm features have been realized using our previously reported custom gravure printing tool. Features sizes as small as 2µm have been realized with good line edge roughness and pattern fidelity, while maintaining high printing speeds of ~1m/s, as shown in figure 1. Good conductivity has been obtained using commercial nanoparticle inks.

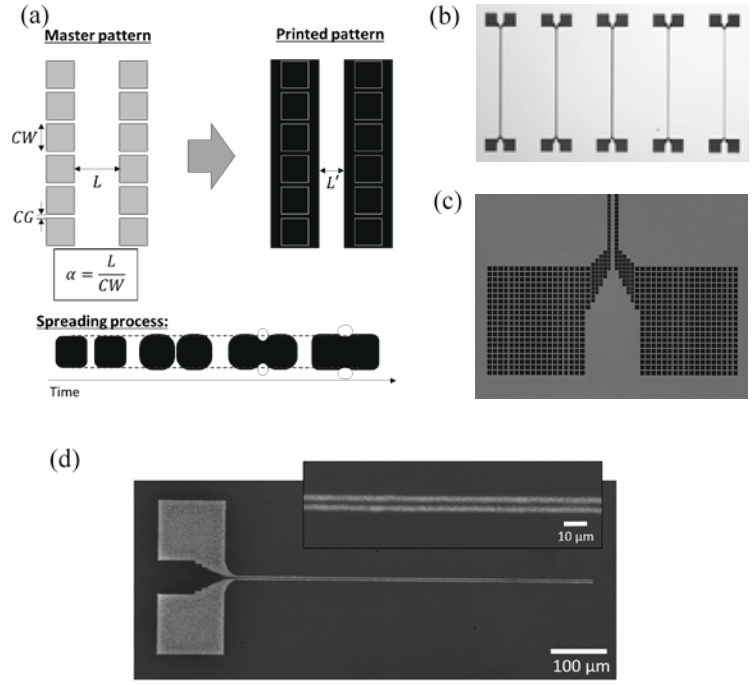

Figure 1: (a) Definitions of highly-scaled gravure patterns. Cell width and gap length are defined as width of square cells and spacing between cell edges, respectively. Printed gap length, L′, is smaller than defined gap length, L, due to the spreading process. (b) electrode patterns on a printing plate. Cell widths in lines are 6 to 2 µm from the left to right. (c) a close-up image highlighting cell arrangement of lines, contacts and taper joints. Cell widths in lines and contacts

are 5 and 4 μm, respectively. (d) A representative electrode pair after sintering of the smallest line width (2.38 μm) and gap length (1.7 μm).

Additionally, we have shown that gravure can be used to print on rigid and flexible glass. Specifically, as a demonstration, we have shown that sol-gel-derived transparent conductors can be printed on Corning Willow Glass (Figure 2) and on rigid glass slides.

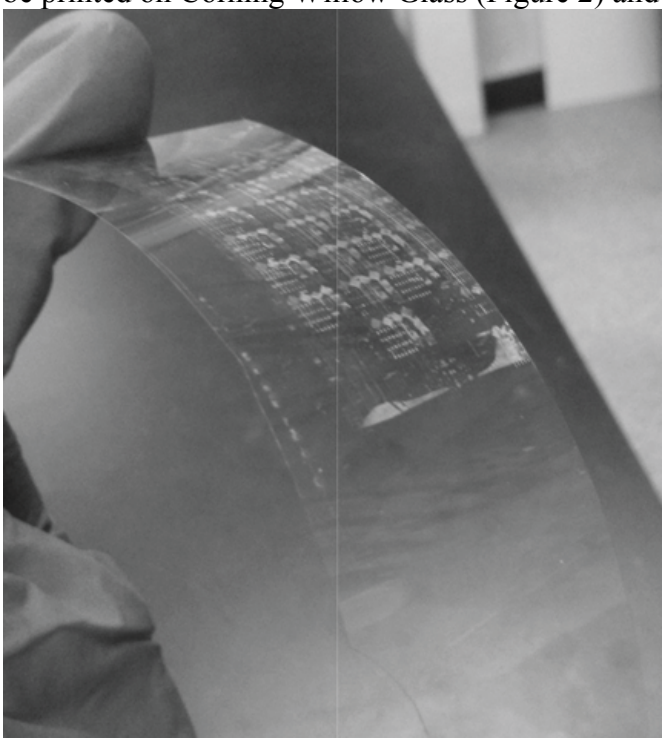

Figure 2: Gravure printing on Willow Glass

Future Work:

We are continuing to work on copper / silver alloys for low-cost conductor inks. In the future, we will integrate these alloyed particles into our printing processes to demonstrate the integration of all aspects of this work.

Thrust: Thin-Film PV

Key Challenges

Thin-film solutions faces four significant challenges: (1) increasing efficiency of modules (particularly decreasing the gap between lab scale champion cells and production modules), (2) reducing direct materials costs, (3) reducing capital intensity of manufacturing, and (4) design and validation for long-term field reliability.

Existing Projects in our Thrust

- *Bandgap Grading in CZTSSe Solar Cells and SnS*, Bruce Clemens and Stacey Bent (Stanford)
- *Fundamental Modeling of Chalcopyrite Solar Cells*, Scott Dunham (UW)
- *Laser Processing of CdTe Solar Cells*, Chris Ferekides and Mike Scarpulla (USF/Utah)
- *Advanced Evaporation Source Design*, Greg Hanket (IEC)
- *Development of Multicolor Lock-in PL Methods*, Hugh Hillhouse (UW)
- *Identifying Problem Areas in CIGSe and CdTe Based PV Devices*, Mark Lonergan (UO)
- *In Situ Characterization of Grain Growth in Thin Film Semiconductors*, Delia Milliron and Paul Alivisatos (UT/LBNL)
- *Advanced Materials Characterization*, Mike Toney and Alberto Salleo (SLAC/Stanford)
- *Non-Equilibrium Processing of CdTe Absorbers*, Colin Wolden (CSM)
- *Applying Cation-Exchange Chemistry to Nanowire Array PV*, Peidong Yang (Berkeley)

Potential New Areas of Interest

- *Theory and Modeling*. Improved collaborative device-modeling resources that, in coordination with materials and device characterization, will inform and guide materials and device development.
- *Materials Chemistry of absorbers*. Improved understanding of defects and grain growth, and their role in metastability, composition, morphology and heterogeneities present both intra-grain and at interfaces and grain boundaries, is critical to advancing device design, process optimization, and performance.
- *Thin Film Device Architecture*. Efforts to optimize heterojunctions, interfaces, transparent conducting layers, carrier-selective contacts, and interconnects are desired. Efforts are also needed to explore means of de-coupling processes, e.g. separating of the "activation" of the absorber layer from intermixing at the CdS/CdTe interface which currently occur simultaneously during the $CdCl_2$ treatment.
- *Device and Materials Stability*. Collaborative research is needed to proactively test innovative device and materials stability under operating conditions (temperature, bias, and light) in order to screen for commercial viability.
- *Device Reliability*. Evaluation of packaged device reliability under combined thermo-mechanical, electro-chemical, and photo-chemical stresses in combination with commercial or BAPVC-developed encapsulants is needed to quickly identify interface adhesion issues and screen for commercial viability.
- *Low Capital Cost Manufacturing*. An expanded focus on developing new low capital cost processing routes to CdTe and CIGS would help thin film technologies compete with crystalline silicon.

BAPVC Annual Project Report

Project Title: Copper nitride (Cu_3N) and indium nitride (InN) thin films for photovoltaic applications

PI: Bruce M. Clemens
E-mail: bmc@stanford.edu

Summary:

For copper nitride (Cu_3N), Density Functional Theory (DFT) calculations show that the intrinsic point defects give shallow defect transition levels in the bandgap. Experimentally, Cu_3N thin films have been demonstrated with high minority carrier lifetime. For indium nitride (InN), the group has successfully deposited epitaxial, high quality InN thin films on sapphire substrates using radiofrequency (RF) magnetron sputtering (low-cost, high throughput deposition method).

Key Accomplishments:

Density Functional Theory (DFT) calculations indicate shallow defect transition levels in the bandgap for copper nitride (Cu_3N), with the dominant point defects being the copper vacancy (V_{Cu}) and the nitrogen vacancy (V_N). Hall-effect measurements show that the Cu_3N film is p-type, with hole density of 1.3 x 10^{17} cm^{-3} and hole mobility of 2.9 $cm^2/V.s$. Time-resolved photoluminescence (TRPL) indicate that the minority carrier lifetime is very high (close to 35 nanoseconds). Photoluminescence measurements reveal an optical transition at 1.7 eV, which corresponds to the direct bandgap value of Cu_3N. X-Ray diffraction measurements show films that are highly (00L) oriented out-of-plane, and with complete random orientation in-plane. Lastly, current-voltage measurements of the Cu_3N / ZnS heterojunction show good diode rectification behavior, making Cu_3N a promising non-toxic, earth-abundant material for photovoltaic applications.

The group has also recently embarked on a new project that involves deposition of high-quality epitaxial indium nitride (InN) thin films for optoelectronic device applications. Thus far, they have successfully demonstrated epitaxial growth of high-quality indium nitride (InN) thin films on c-axis oriented sapphire substrates. X-Ray Diffraction (XRD) rocking curve measurements of the InN (002) reflection indicate an impressive full-width-half-maximum (FWHM) of only 0.003°, speaking to the high quality of the crystal orientation in these films.

Future Work:

Future work on the indium nitride project includes incorporating Ga into InN to synthesize indium-gallium-nitride (InGaN) alloys. This allows tuning of the semiconductor bandgap between 0.7 eV (InN) and 3.4 eV (GaN), enabling the ideal bandgap for solar cells based on the Shockley-Queisser limit.

BAPVC Annual Project Report

Project Title: Laser lift-off of GaAs thin-films
PI: Bruce M. Clemens
E-mail: bmc@stanford.edu

Summary:

Continuing from previous work, we successfully used a 1064 nm Q-switched laser to heat and ablate a buried InGaAsN layer grown epitaxially on a GaAs substrate, thus enabling lift-off of thin (~1μm) GaAs films. We have since upgraded to a more powerful laser, capable of irradiating and causing lift-off in GaAs wafer pieces as large as 50 mm^2. As part of demonstrating wafer re-usability, we have made significant progress towards using a fast planar etch to remove melt debris without damaging the substrate.

Key Accomplishments:

We obtained and restored a Quanta Ray Pro 350 laser, which outputs up to ~2 J per pulse, and has a beam profile as show in Figure 1. This allows for irradiating larger areas above the threshold fluence for lift-off. However, so far these larger films so removed have had cracks, and ongoing work will focus on getting crack-free films.

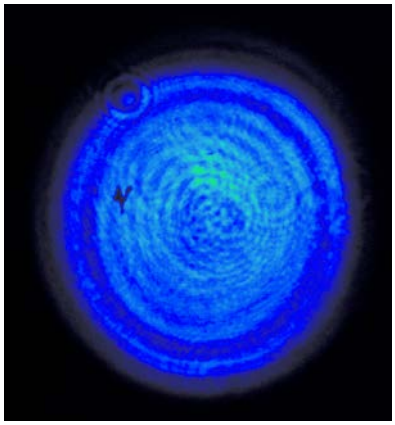

Figure 1: Beam profile of Quanta Ray Pro 350

A second prong of the work is to demonstrate that the GaAs wafer can, after liftoff, be reused as a growth substrate. This requires removing the melt debris that is left behind after laser lift-off. We determined that the InGaAsN layer is etched by solutions of $NH_4OH:H_2O_2:H_2O$. Thus with this ammonium etch we can remove the InGaAsN melt debris; however, the GaAs substrate will also be etched since it has similar composition to the dilute nitride. We found that an epitaxially-grown InGaP layer between InGaAsN and the GaAs substrate protects the latter during the ammonium etch. A subsequent HCl dip selectively removes the InGaP from the GaAs. Finally, we found that after irradiation the InGaAsN and InGaP layers can intermix to form InGaAsP, as shown in Figure 2. InGaAsP is no longer an effective etch stop for the ammonium etch, so future device stacks will incorporate a thicker InGaP layer, or a GaAs buffer layer to separate the InGaP from the nitride.

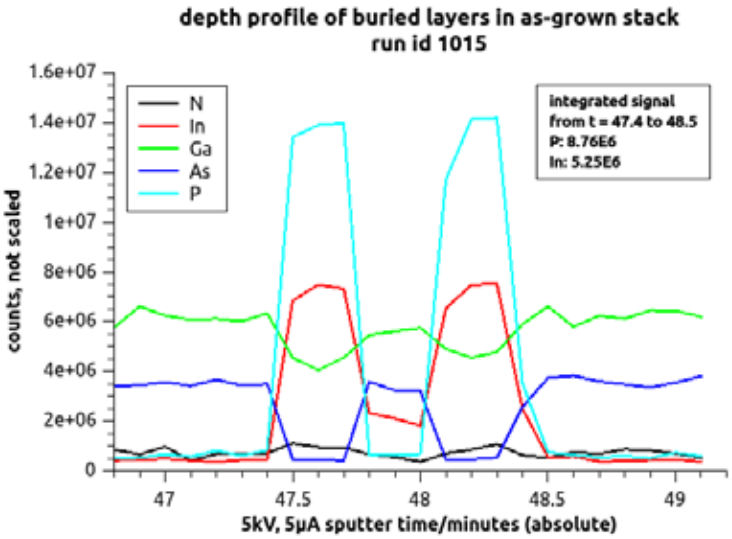

Figure 2:

a. Auger depth profile of as-grown etch-stop stack (from left to right: GaAs film / InGaP / InGaAsN / InGaP / GaAs substrate)

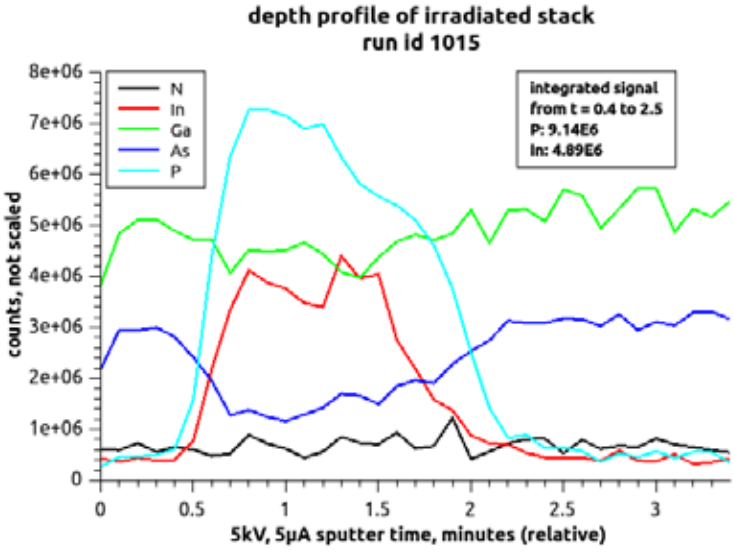

b. Auger depth profile of etch-stop stack irradiated below critical fluence for lift-off. Laser pulse is from substrate side (incident on InGaAsN layer from right side in plot).
Note the integrated signals for P and In closely match that in as-grown stack.

Future Work:

In the future we will grow a double heterojunction of InGaP/GaAs/InGaP, and measure the carrier lifetime in this layer before and after lift-off, since high carrier lifetime is critical for good GaAs solar cell performance.
Then, we will etch the melt debris from the substrate and regrow another double heterojunction. Measuring and comparing carrier lifetimes in subsequent film growths will be our metric for characterize re-usability of the substrate.

BAPVC Annual Project Report

Project Title: SnS based photovoltaics
PI: Stacey F. Bent
E-mail: sbent@stanford.edu

Summary:

Polysulfide ligand exchange on zinc sulfide nanocrystal surfaces was investigated as a method for improved film formation using metal chalcogenide inks. Native ligands on surfaces of colloidal ZnS nanocrystals were efficiently exchanged with polysulfides. Ligand exchange was shown to improve crystallinity and composition in annealed ZnS thin films.

Key Accomplishments:

Nanocrystal inks have been explored as a low-cost, solution-based method for forming thin metal chalcogenide films for use in photovoltaics. The physical and chemical properties of nanocrystals can be modified by changing the ligands attached at their surfaces. A ligand exchange procedure with ammonium polysulfides was developed to replace the native ligands on cubic zinc sulfide nanocrystals, as a model system for nanocrystal inks used in the deposition of metal chalcogenide thin films. Several mixtures of polysulfides in various solvents were prepared with different average chain lengths and used to achieve high yield ligand exchange, as confirmed by several spectroscopies, including x-ray photoelectron spectroscopy (Figure 1). The results also showed that polysulfide content can be increased with longer surface ligands, and that the exchange process yields compositionally pure surfaces before and after high temperature anneals.

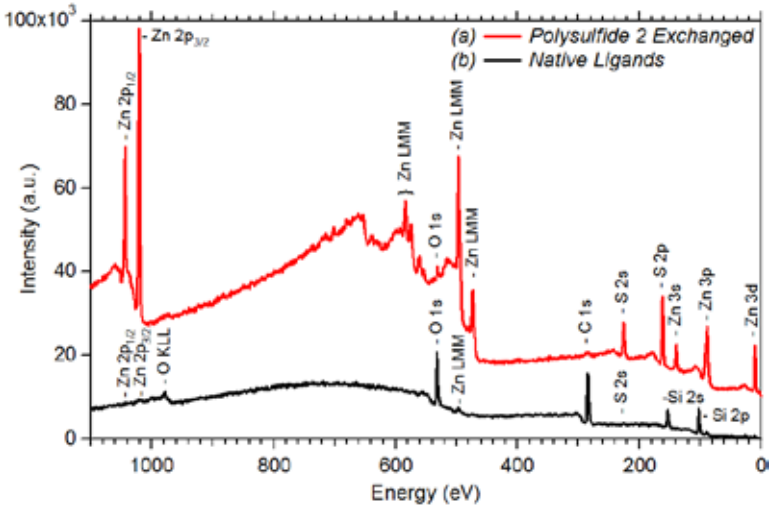

Figure 1: X-ray photoelectron spectra of dried ZnS nanocrystal films with (a) polysulfide ligands and (b) native ligands.

The effect of the polysulfide-terminated ZnS nanocrystals on subsequent film formation was also studied. X-ray diffraction and scanning electron microscopy showed that, when annealed in nitrogen at 525°C, polysulfide ligands lead to average crystal sizes 2-3 times larger than in the

un-exchanged control sample. The ligand exchange procedure itself did not alter nanocrystal size. Nanocrystal inks prepared from the exchanged samples formed thin films that exhibited exhibit superior grain growth, morphology, and composition compared to the un-exchanged material. Overall, polysulfide species were demonstrated as alternative ligands for the surfaces of metal chalcogenide nanocrystals, which when incorporated in an efficient ligand-exchange procedure can improve the quality of nanocrystal inks.

BAPVC Annual Project Report
Project Title: Advanced Materials Characterization
PI: Mike Toney & Alberto Salleo
E-mail: mftoney@slac.stanford.edu, asalleo@stanford.edu

Summary:

The Toney Group at SSRL characterizes photovoltaic materials with X-ray techniques. SSRL has developed several in-situ thermal processing chambers that have been utilized on projects with members of the BAPVC. The rapid thermal processing (RTP) chamber has been utilized by the Milliron group to characterize CZTS and CIGS nanoparticles as they transition to sintered films. The in-situ annealing chamber and in-situ Se annealing chamber have been utilized by several projects in the Bent group. An investigation has also been done into the chemical character of the Cl remaining in Cl derived perovskites both in-situ and ex-situ X-ray absorption spectroscopy (XAS). Diffraction and XAS has been utilized to better understand the CuZnS TCOs developed by the Ager group. The work of the Salleo group within BAPVC focuses on using sensitive sub-gap measurements to characterize optical absorption and defects in photovoltaic materials and entire PV stacks.

Key Accomplishments:

The RTP chamber developed under a Bridge proposal can heat samples at a rate of 100°C/s to a temperature of 1200°C taking XRD every 100ms and is a powerful tool for measuring PV materials under industry relevant conditions. The Milliron group has used this to study the kinetics of their CZTS and CIGS nanoparticles sintering into films during annealing. With the RTP, the phase transition from Wurtzite to Kesterite can be seen as a function of temperature Fig1.

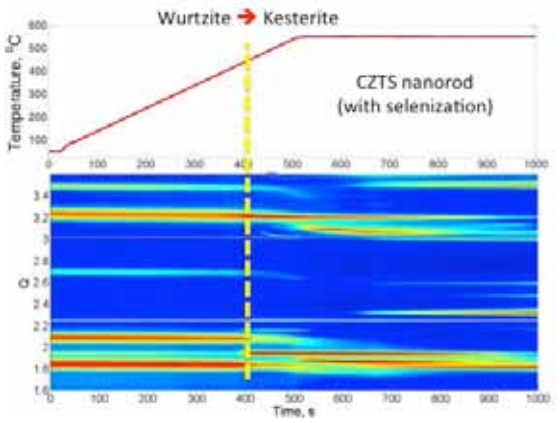

Figure1: In-situ annealing of CZTS nanoparicles shows the Wurtzite to Kesterite transition.

The Ager group at LBL is developing $Cu_xZn_{1-x}S$ alloys as a promising p-type transparent conductor. Initial studies by the Ager group suggested that their films were amorphous; however, the Toney group has been able to determine that the films are nanocrystalline and to determine the crystalline structure of these films. X-ray diffraction patterns of $Cu_xZn_{1-x}S$ films are shown in Fig. 2. The XRD shows that the films contain both sphalerite and wurtzite ZnS phases with predominantly wurtzite at x=0.30, which corresponds to a peak in conductivity.

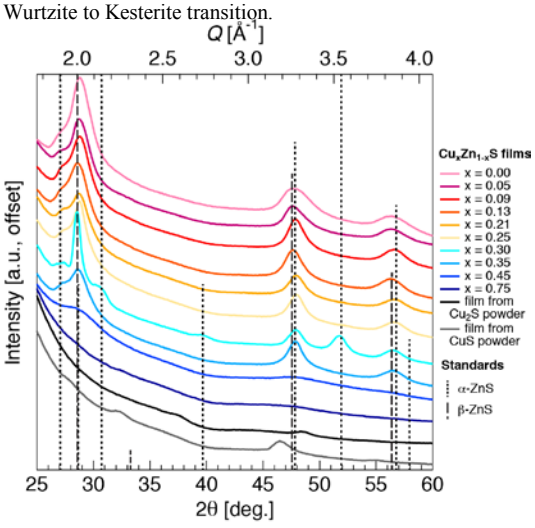

Figure 2. XRD of $Cu_xZn_{1-x}S$ films deposited on quartz at room temperature for $0 \le x \le 0.75$. Films contain a mix of sphalerite (β) and wurtzite (α) ZnS, with wurtzite dominant in the $x = 0.30$ film.

Work has been done on hybrid perovskite solar cell absorbers to understand the role that Cl plays in improving the performance of Cl derived $MAPbI_{3-x}Cl_x$ (MA = methyl ammonium) solar absorbers. XAS has verified that Cl remains in the films after typical annealing. Comparing the spectra of Cl of fully converted (to $MAPbI_{3-x}Cl_x$) films to

XAS of MACl and $PbCl_2$ standards, we showed that the remaining Cl is not the precursors remaining in the film. Further work is needed to understand where in the film the Cl is incorporating.

Measurements implemented by the Salleo group include: below-gap photocurrent measurements (FTPS) in photovoltaic stacks to characterize defects and locate whether they are found in the active layer or in other regions of the stack; true absorption (i.e. excluding scattering) above gap using photothermal deflection spectroscopy (PDS) in thin and thick layers; and absorption below-gap in active layers using PDS to characterize defects. In 2014 through the spring of 2015, Salleo group collaborations with BAPVC members on FTPS measurements increased significantly, including ones with GE/First Solar, the University of Oregon (Mark Lonergan's group), the Colorado School of Mines (CSM - Colin Wolden), and 3-Sun.

In cadmium telluride cells, the appearance of defects in the sub-gap region of the semiconductor can be related back to variations in processing. Thus, FTPS is an important characterization tool to understand the changing materials properties with processing. The EQE over 7-8 orders of magnitude was measured for several sets of GE cells. These cells showed substantial variation in both height and width of the sub-gap absorption region, as well as substantial variation in PCE. Correlation of the sub-gap absorption to changes in PCE is ongoing. The Salleo group also characterized cadmium telluride cells made at CSM as part of a round-robin comparison effort to measurements done at the U. of Oregon.

3Sun operates an a-Si:H/ micromorph tandem facility. As an extension of work from the previous year, measurements have begun on the tandem cells in order to identify defects that occur when the entire stack is deposited. The Salleo group has developed a biased-light FTPS measurement, the results of which are shown in Fig. 3. The biased-FTPS measurement mirrors the monochromatic EQE of the individual cells, but can measure many more orders of magnitude.

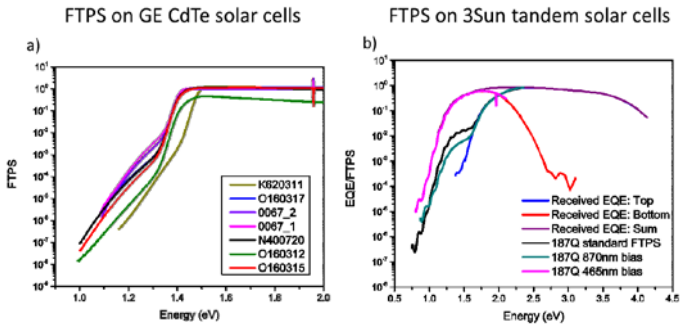

Figure 3. a) FTPS on several CdTe cells from GE of varying efficiency and sub-gap absorption. b) FTPS on tandem cells. The black line indicates the FTPS measurement with no bias light. The IR-biased and blue-biased spectra are overlaid with the monochromatic EQE measured by 3Sun for the top and bottom cells respectively.

Future Work:

The Toney group will continue collaborating with members of the BAPVC in order to better understand PV materials structure-function relationships and processing routes to formation. Work is ongoing with the Milliron group using the RTP and the Bent group using the in-situ Se annealing chamber. Future work will be done with the Ager group to determine the location of the Cu atoms by utilizing resonant x-ray diffraction (REXD). This will allow determination of whether the Cu atoms in the samples are substituted for the Zn atoms in the ZnS lattice or are a disordered component of the film. Work is just starting up with the Wladek group investigating the $(SnTe)_x(CdO)_{1-x}$ alloy systems. These films appeared to be amorphous at approximately x = 0.35 to x = 0.69; however, initial XRD studies at SSRL suggest there may be a nanocrystalline component of these films. Future work will include XAS and small angle x-ray scattering (SAXS). In the Salleo group work is ongoing to use biased-FTPS to identify subgap states in the higher-band gap cell.

BAPVC Annual Project Report

Project Title: Advanced Evaporation Source Design
PI: Gregory M. Hanket
E-mail: hanket@udel.edu

Summary:

The past year has focused on the demonstration of stable Cu effusion rates for various levels of melt depletion. The system has been converted to the evaporation of mixed Ga-In vapor, which will now be the full focus of the program until temporally stable vapor composition has been demonstrated. An invention disclosure has been submitted describing the incorporation of an internal centrifugal separator at the entrance to the effusion nozzle as an additional layer of redundancy against spitting. The insulation in the vicinity of the nozzle has been identified as a likely source of condensation and subsequent spits observed on the substrate – this aspect of the source design will be revisited if time permits after demonstration of a stable Ga-In mixed vapor.

Key Accomplishments:

The evaporation rates and deposition profiles for Cu evaporated at varying melt depletion levels have been characterized and have met the program goal of less than 50% variation in effusion rate. Results are shown in Figure 1.

Consideration of the evaporation and flow processes within the source have identified possible mechanisms for the production of spits within the source: 1) melt boiling since the vapor pressure above the melt must necessarily be less than the saturation pressure (this is a necessary but not necessarily sufficient condition for boiling) for any net evaporation to occur and; 2) wall cooling due to gas expansion as the vapor flows through various internal rate restricting orifices. While theoretical analysis is ongoing to further clarify whether either of these mechanisms may be occurring, the possibility of these mechanisms led to a fundamental change in source design approach: instead designing with the goal of preventing spit formation, a more robust approach is to assume the presence of droplets in the flowing vapor, and then to remove these droplets. This motivation let to the concept of incorporating centrifugal separation into the design. The design concept and predicted spit trajectories are shown in Figure 2.

Future Work:

The system has been reconfigured for the evaporation of a mixed Ga-In vapor, which was delayed due to the onset of Cu spitting (see the following paragraph). The demonstration of a stable Ga-In vapor composition for progressive melt depletion will be the primary focus for the remainder of the program.

The issue with Cu spitting is most likely due to condensation on the felt insulation about the nozzle due to vapor backscattering. This issue will most likely be addressed in the short term by the use of replaceable shielding around the nozzle to prevent run-to-run accumulation of condensation. In the longer term, however, the issue of vapor backscattering, particularly when

considering real world operation in the presence of an ambient Se pressure which will further amplify backscattering, may require more careful design of the nozzle exit or may prove to be a fundamental limit on effusion rate.

Modeling efforts are ongoing regarding temperature and pressure profiles within the source, as well as calculations of droplet drag in a flowing vapor. These modeling efforts will be consolidated into a comprehensive design approach.

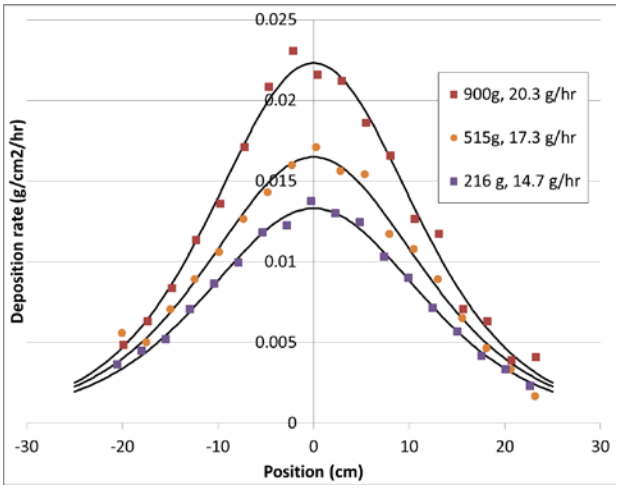

Figure 1. Cu deposition profiles for varying melt depletion levels. The design volume of the crucible accommodates 1 kg of Cu.

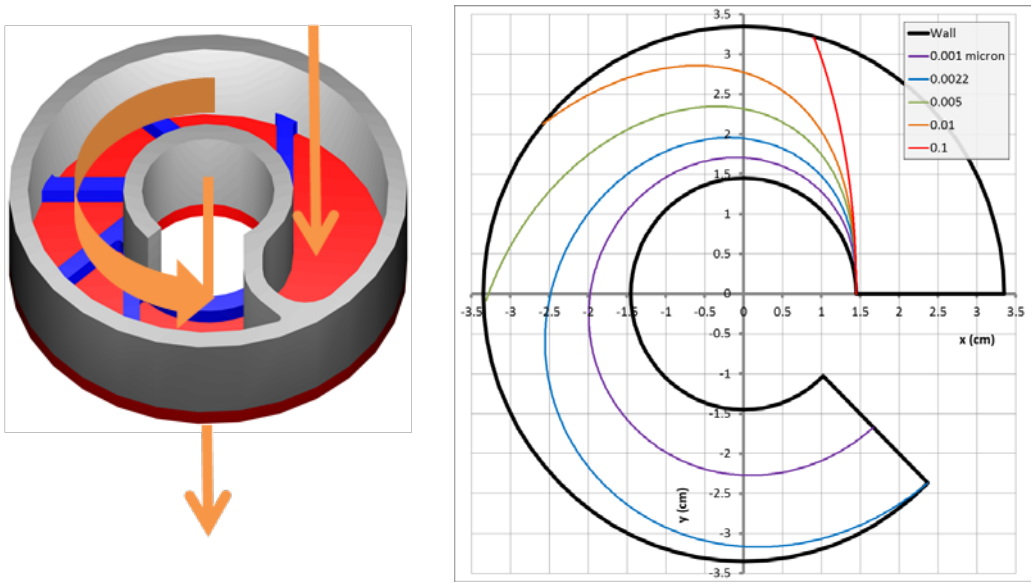

Figure 2. (Left) Conceptual design of a centrifugal separator for incorporation into vacuum evaporation sources. (Right) Predicted trajectories of Cu droplets from 1 nm up to 0.1 micron diameter for a vapor flow rate of 15 g/hr through the separator.

BAPVC Annual Project Report

Project Title: Development of Multicolor Lock-in Photoluminescence Methods for In-Situ Process Monitoring and Ex-Situ Mapping of Solar Cell Absorber and Interface Quality
PI: Hugh W. Hillhouse
E-mail: h2@uw.edu

Summary:
The goal of the project is to develop a new photoluminescence technique to interrogate surfaces and buried interfaces that is robust in a manufacturing environment and will generate easily interpretable output so that it can be correlated to product quality or even integrated into a process control scheme. We have completed a prototype of the instrument and collected data sets on various semiconductors including GaAs, InP, and CdTe. The difference PL spectra show that the surface of InP is high quality (as expected) while GaAs and CdTe have high surface recombination.

Key Accomplishments:
We have completed a prototype instrument. The schematic of the full instrument set-up is shown in Figure 1. The current prototype uses two laser beams (640 nm and 514 nm) that are pulsed and interlaced before illuminating the sample. The time-modulated steady state PL is collected, passed through a monochromator, detected, and demodulated.

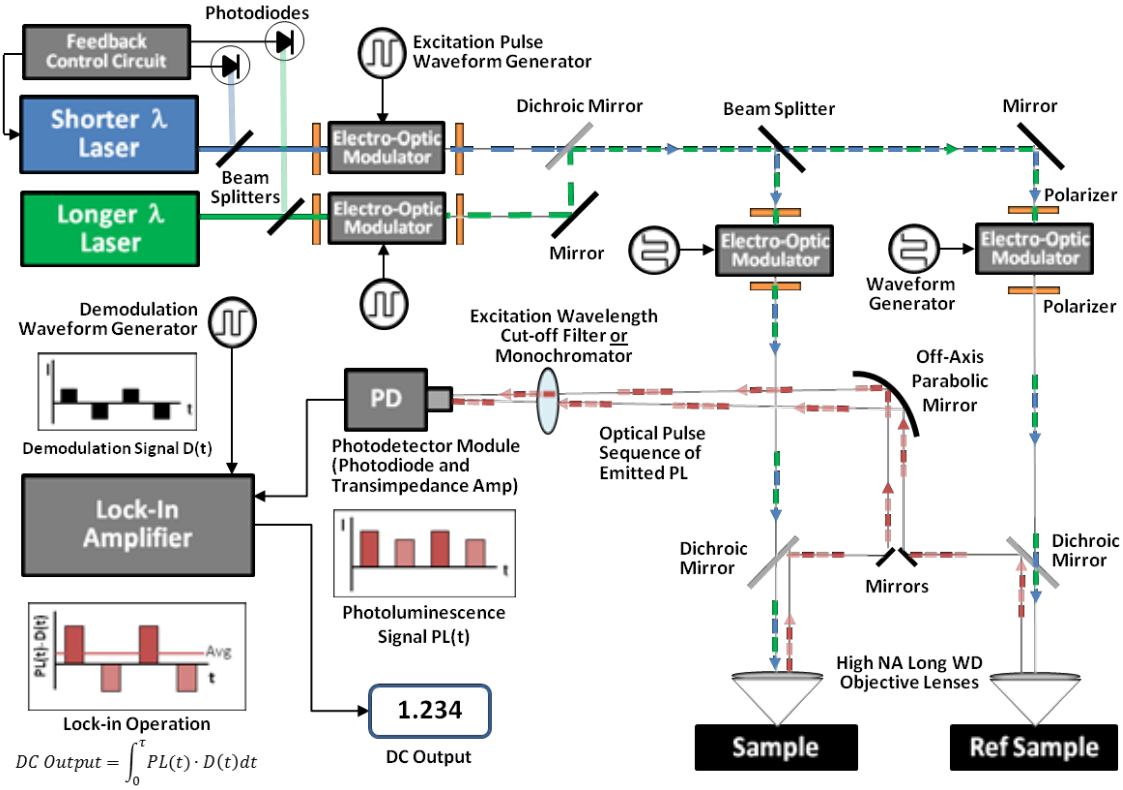

Figure 1. Schematic of a standalone modulated Multicolor Lock-in PL instrument that is robust to drift, fouling, and noise. The optical path from the exit of the last electro-optical modulator to the sample to the detector may be fiber coupled to avoid alignment issues.

The instrument is calibrated such that the number of photons in the 640 nm pulse is the same as the number of photons in the 514 nm pulse. Since the penetration depth is larger for the 640 nm light, the photoexcited carriers are spread out over a larger area and the injection level is lower. If the effective rate of recombination at the surface is the same as the bulk, the PL intensity from the 514 excitation should be higher. However, if the surface recombination is high then the PL intensity from the 640 should be higher. For both the GaAs and CdTe, then difference in PL intensity (614 nm excitation minus 514 nm excitation) is positive, indicating high surface recombination. However, for InP the opposite is observed. This is commensurate with expectations for InP (see Figure 2).

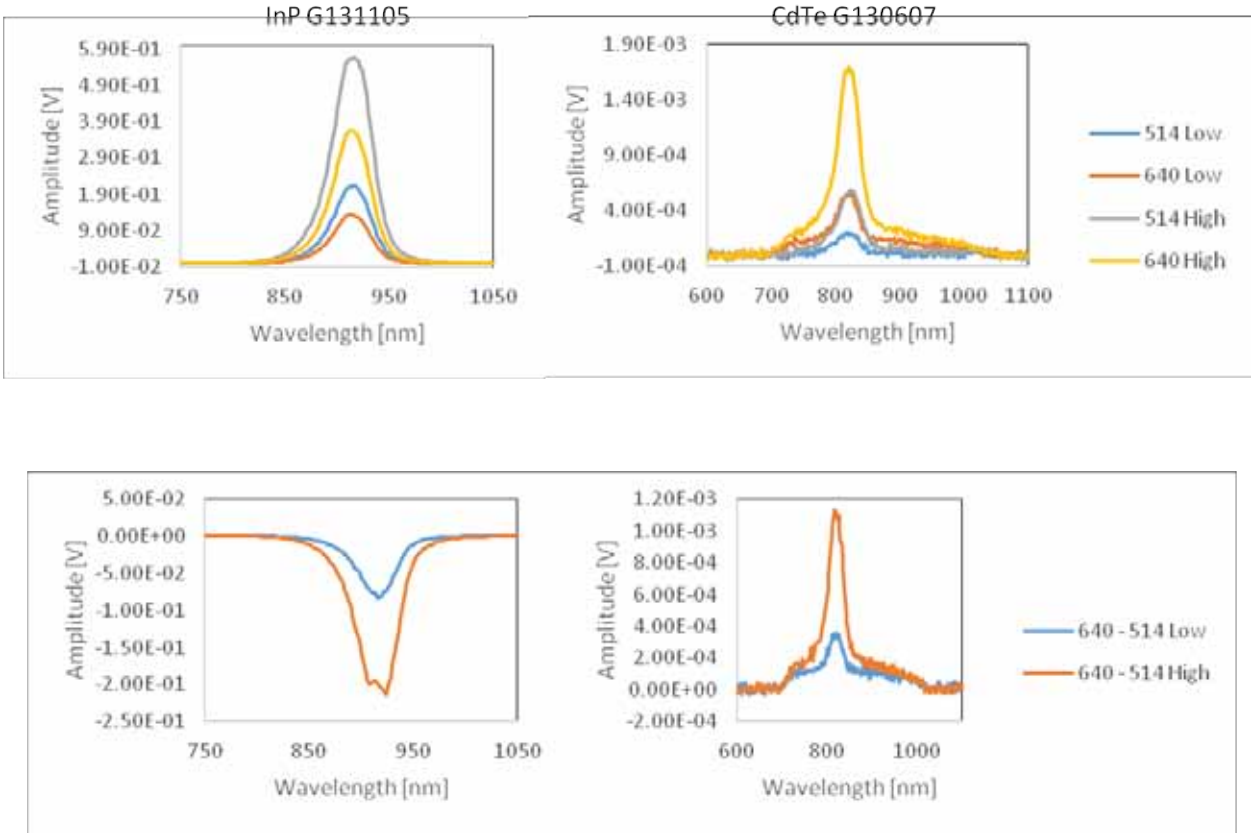

Figure 2. Demodulated PL signals from InP (left column) and CdTe (right column). The top row shows the PL spectra for both 640 and 514 excitation for two different excitation intensities. The bottom row shows the demodulated difference spectra. ***NOTE: All these data are extracted in tens of milliseconds from the modulated beam arriving at the detector***. The data show that the InP surface is passive while the CdTe surface has high surface recombination velocity.

Future Work:
We are now collecting data from different materials (GaAs, CdTe and CIGS) and conducting surface treatments to illustrate the capability of the tool. In addition, we are working towards adding a reference sample.

BAPVC Annual Project Report

Project Title: Fundamental Modeling of Chalcopyrite Solar Cells
PI: Scott T. Dunham, University of Washington, Seattle
E-mail: dunham@ee.washington.edu

Summary:

This project deals with theoretical modeling and calculation of the properties of defects in CIGS and CZTS absorber materials. The long term goal is predictive models for defect evolution, impurity kinetics and phase transformation in these materials to enable optimization of fabrication processes for maximum cell efficiency and reliability. A tool for calculation of the concentrations of dominant defects has been developed based on ab initio calculations combined with stoichiometric input data, while calculation of barrier heights leads to estimation of diffusivities. Monte Carlo simulations are used to connect these results to nanoscale ordering and impurity redistribution, with results connected to device simulation to predict impact on performance.

Key Accomplishments:

Fundamental understanding of the complex behavior of impurities and point defects in CIGS ($CuIn_xGa_{1-x}Se_2$) and CZTSSe ($Cu_2ZnSnS_xSe_{4-x}$) under realistic processing conditions is essential for effective applications in thin film solar cell devices. Last year, the group developed a tool for calculation of the concentrations of intrinsic lattice defects at given CZTS and CIGS stoichio-metries. A method was developed that makes use of defect formation energies from ab initio calculations combined with mass action relations between the defects to enable calculation of concentrations of defects in all accessible charge states under a given set of stoichiometric constraints and processing temperature. This year, that method was extended to allow for use of an arbitrary combination of stoichiometric constraints and chemical potentials in the presence of impurities such as sodium, potassium, and cadmium and associated extrinsic defect complexes. In addition, migration barrier heights calculated with the nudged elastic band method provide insight into the effect of the local lattice structure on the diffusion of dominant point defects. Figures 1 and 2 illustrate typical results. Figure 1 shows the behavior of dominant defect concentrations in $Na+CuIn_xGa_{1-x}Se_2$ for x = 0.9 under varying anion/cation ratio ω for Cu-poor conditions and a typical sodium concentration of 0.1%. In this case, the defect concentrations summed over all charged states are shown, and the material transitions from n-type to p-type at ω=1.024. Figure 2 compares the energy barriers for nearest-neighbor copper vacancy-mediated diffusion of Cu, Na_{Cu}, and K_{Cu} computed with density function theory and the nudged elastic band method. Our results for various CIGS compositions within the stable range of chemical potentials suggest that the formation of Na_{III}^{2-} and K_{III}^{2-} donors (where III = In or Ga) either dominates or directly competes with the formation of neutral Na_{Cu}^{0} and K_{Cu}^{0} substitutionals, respectively. Moreover, the low barrier for diffusion of sodium and potassium via hopping on the copper sublattice may provide an energetically favorable pathway through which the local valence structure is repaired.

One of the major goals of this project is to understand ordering and phase separation in CIGS. Determination of phases in CIGS can be attained by canonical Monte Carlo simulations. The group has performed a comparative analysis of a wide range of functional forms to approximate

the energy of arbitrary CIGS configurations. These configurations include those with intrinsic defect clusters such as the complex containing two copper vacancies and a group-III-on-Cu antisite, which may be responsible for the existence of ordered defect phases. These energy functional models are used as the basis for the canonical Monte Carlo simulation. The results of these simulations have been used to generate classes of stable CIGS configurations at various temperatures, revealing the formation of indium/vacancy-rich regions as illustrated in Fig. 3.

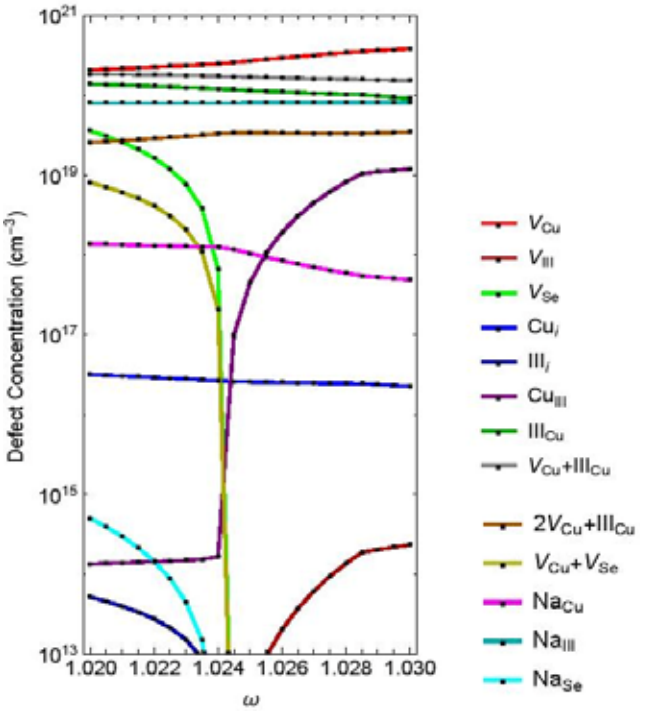

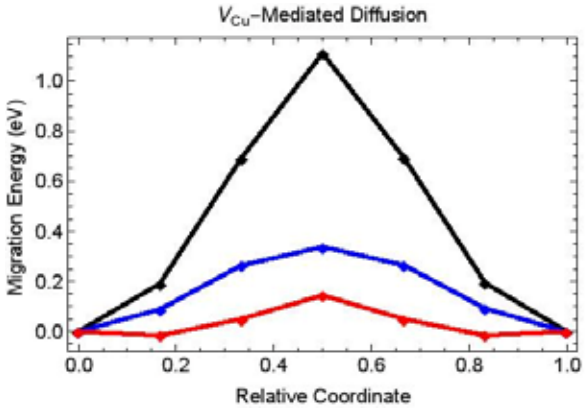

Fig. 1 (left): Dominant defect concentrations in Na+CIGS under Cu-poor conditions with In/Ga = 0.9 and T = 973K.

Fig 2 (above): Migration barriers for Cu vacancy mediated diffusion of Cu and Na_{Cu}, K_{Cu} substitutionals.

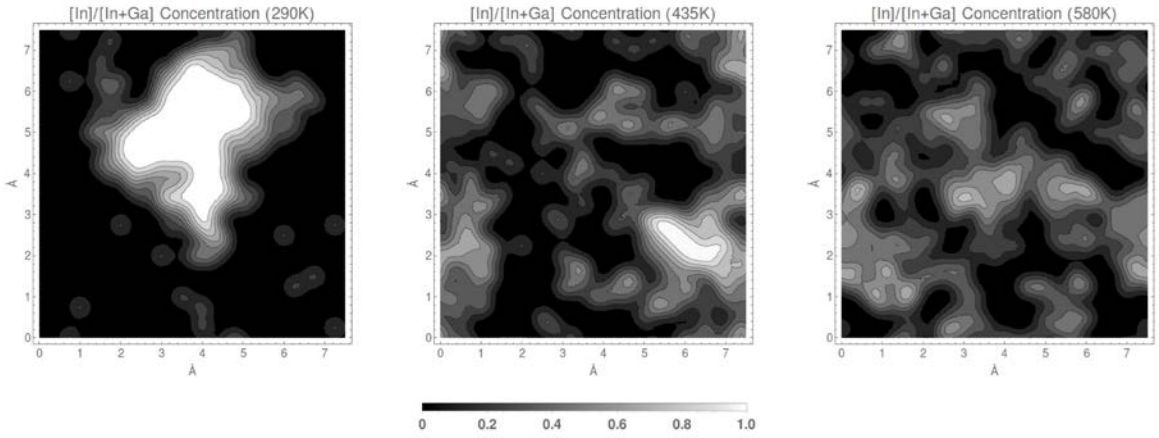

Fig. 3. Contour plot of In fraction after MC simulation at 290K, 435K and 560K for systems with 1800 cation sites (3600 total sites), an average [In]/[In+Ga] fraction of 25%, and an average vacancy concentration of 2.5% of cation sites.

Future Work:

The plan for the coming year is to extend the analysis to a broader range of impurities and explore the impact of impurity diffusion and phase separation on CIGS device performance.

BAPVC Annual Project Report

Project Title: Identifying Problem Areas in CIGS and CdTe Based Photovoltaic Devices
PI: Mark C. Lonergan
E-mail: lonergan@uoregon.edu

Summary:

CdTe, InP, and CIGS devices were characterized using a variety of junction capacitance techniques, which elucidate the spatial, electronic, and chemical properties of defects present in the absorber material. Because these measurements were performed on complete devices, they enable a direct examination of the relationship between device performance, fundamental absorber properties and growth conditions. In CdTe and InP, growth conditions were directly linked to observation of particular defects and associated impacts on device performance. In CIGS a new, metastable, optical transition was observed whose impact on performance is not yet understood.

Key Accomplishments:

Building on previous work by this group [1], transient photocapacitance (TPC) and transient photocurrent (TPI) were used to study the sub-bandgap absorption in CdTe thin-film solar cells jointly fabricated by the Colin Wolden's group at the Colorado School of Mines, and by Teresa Barnes at the National Renewable Energy Laboratory. These measurements identified defect levels at E_V + 1.2 eV and E_V + 0.9 eV (Fig. 1). Using rapid thermal processing (RTP) to precisely control copper content in the devices studied (verified using ToF-SIMS) [2], the defect at E_V + 0.9 eV was associated with the presence of copper in the absorber layer [3]. The energetic depth of the copper-associated defect suggests that it could be responsible copper's detrimental effect on the minority carrier lifetime in CdTe devices.

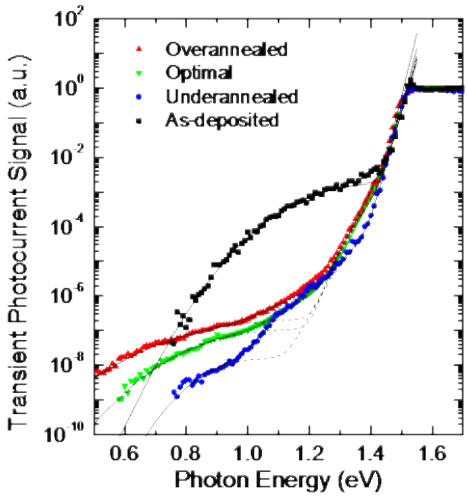

FIG. 1. TPI spectra for CdTe absorbers with Cu content varied using rapid thermal processing. Note that the 1.2 eV feature is greatly reduced by annealing while the 0.9eV feature is enhanced by RTP anneals that incorporate more copper in the absorber.

In collaboration with the Javey group at UC Berkeley we examined a set of vapor-liquid-solid grown InP samples in which a H_2 plasma treatment is associated with an increase in V_{oc} from about 500 to 600 mV. Comparison of TPI spectra from these films shows a corresponding

reduction in a defect signal centered at about 1.07 eV, suggesting this defect may play a role in limiting V_{oc} (Fig 2). This is in reasonably close agreement with photoluminescence spectra obtained by the Javey group which show a similar magnitude reduction in a defect centered at ~1.12 eV.

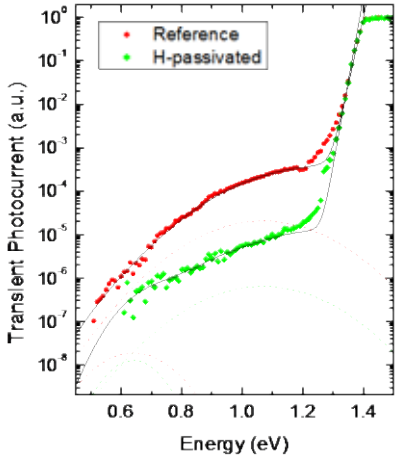

FIG. 2. TPI spectra for VLS-InP absorbers with and without H_2 plasma treatment. While the reference cell's subgap response is dominated by a single defect at ~1.07 eV, two defects are required to obtain good fits to the cell treated with H_2. By fixing the energy and FWHM of the 1.07 eV defect to be the same as in the reference cell, but allowing the magnitude to decrease, the H-passivated spectrum is well fit with the addition of a second defect at 0.64eV. The 1.07eV defect transition is reduced by a factor of 30.

Future Work:

In the case of CdTe, it would be desirable to compare the results so far obtained for polycrystalline devices to truly Cu free single crystalline samples. It remains to be seen whether challenges obtaining good contact to CdTe crystals can be overcome in a way that allows TPC and TPI spectra to be taken. In the case of InP the sample set is being expanded to follow up on these results and TPC spectra will indicate whether a minority or majority carrier transition is associated with the 1.07 eV defect. We are also following up what appears to be a strong temperature dependence of minority carrier collection from the space charge region in these devices. In CIGS we have observed, for the first time, a metastable optical transition in TPC and TPI. Further work is need to understand the relationship between this state, previously observed metastability in CIGS thin films and the impact of associated defects on device performance.

References

[1] J.W. Boucher, D.W. Miller, C.W. Warren, J.D. Cohen, B.E. McCandless, J.T. Heath, M.C. Lonergan, S.W. Boettcher, "Optical response of deep defects as revealed by transient photocapacitance and photocurrent spectroscopy in CdTe/CdS solar cells," *Solar Energy Materials and Solar Cells*, **129**, 57-63 (2014).

[2] J. Li, D. R. Diercks, T. R. Ohno, C. W.Warren, M. C. Lonergan, J. D. Beach, and C. A. Wolden, Sol. Energ. Mat. Sol. C. **133**, 208 (2015).

[3] C.W. Warren, J. Li, C.A. Wolden, D.M. Meysing, T.M. Barnes, D.W. Miller, J.T. Heath, M.C. Lonergan, "The Effect of Cu on the sun-bandgap density of states of CdTe Solar Cells," *2015 Applied Physics Letters, **106**, 203903 (2015)*.

[4] C.W. Warren, D.W. Miller, F. Yasin, J.T. Heath, "Characterization of bulk defect response in Cu(In, Ga)Se2 thin-film solar cell using DLTS," *2013 IEEE 39th Photovoltaic Specialists Conference (PVSC)*, pp. 0170-0173, 16-21 June 2013.

BAPVC Annual Project Report

Project Title: Non-Equilibrium Processing of CdTe Absorbers
PI: Colin A Wolden, Colorado School of Mines
E-mail: cwolden@mines.edu

Summary:
The fundamental roles of ZnTe in promoting high efficiency and improved durability in CdTe solar cells were elucidated using high resolution TEM imaging and atom probe tomography (APT). It is shown that rapid thermal activation creates a ~50 nm interface region characterized by strong CdTe-ZnTe interdiffusion and Cu segregation to defects and grain boundaries in the CdTe, forming $Cu_{1.4}Te$ clusters encased in Zn. It is proposed that these changes passivate interface states, improving series resistance and limiting Cu migration which is a key to long term stability.

Key Accomplishments:
A critical question is how the composition and structure of the ZnTe:Cu back contact was altered during the RTP process used for optimal activation. Figure 1 display TEM images before and after processing, as well as the composition profile after activation. The as-deposited ZnTe:Cu is uniform, nanocrystalline, with little evidence of intermixing with adjacent layers. After RTP a bilayer structure is formed with substantial grain growth adjacent to the gold metallization layer and the formation of an amorphous layer in contact with CdTe, suggesting ZnTe-CdTe interdiffusion. This is confirmed by elemental profiling, and it is suggested that interdiffusion passivates defects and reduces the impact of the back contact, resulting in improved voltage.

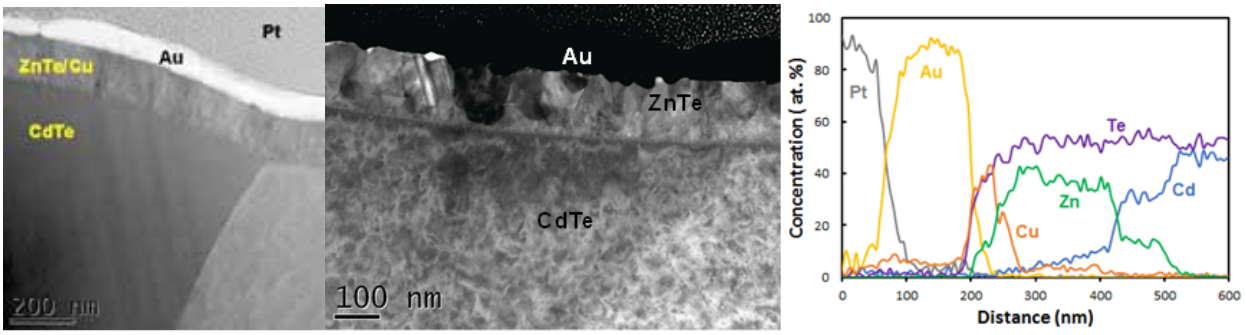

Figure 1. HR-TEM images of back contact region before RTP, after RTP, and plot showing EDAX profiles of elemental composition through the back contact region after RTP.

Nanoscale imaging revealed that much of the Cu segregates to the metallization layer as shown in Fig. 1c, and defects and grain boundaries in the CdTe are passivated by forming Cu_xTe clusters that as shown in **Figure 2**. Moreover the released Zn during the formation of these clusters accumulates at the surface, forming core-shell structure as revealed by APT. This provides the molecular level explanation for the macroscopic measurements that show that the amount and extent of Cu diffusion in these device is orders of magnitude less than expected. Copper, a fast diffuser, has been implicated as a contributor to device degradation. It is believed that the sequestration of copper into these zinc-encased structure limits electromigration and may account in part for the improved stability reported for CdTe modules using ZnTe back contact buffer layers.

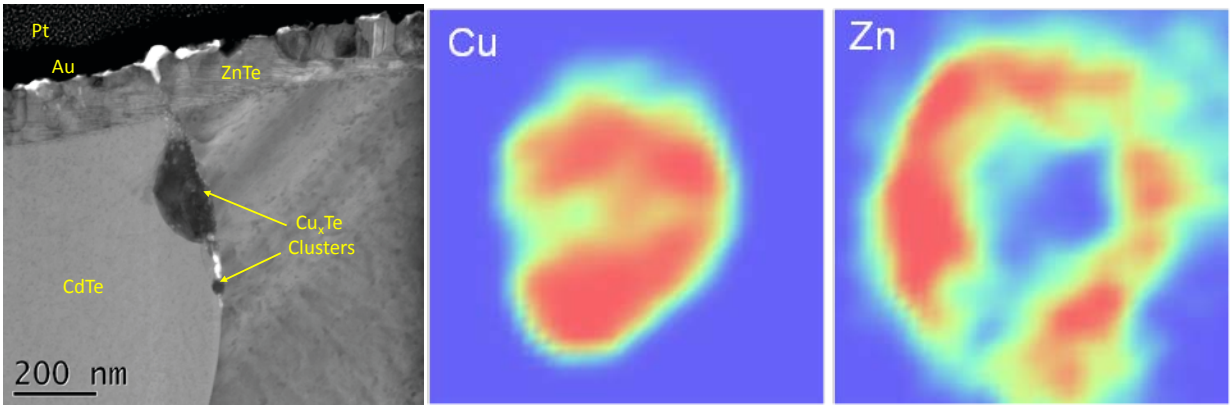

Figure 2. HR-TEM image of back contact region after RTP showing the presence of Cu_xTe aggregates, and 2D contour plots obtained by APT from one of the clusters confirm their core-shell nature.

The stability of unencapsulated devices produced in house have been subjected to accelerated liftetime testing (ALT) as a function of temperature and illumination. **Figure 3** plots the results of ALT testing at 85 ºC for dark and illuminated samples. The stability is quite good up to a 100 hours under these severe stress conditions, particularly under illumination. The J_{sc} and V_{oc} values remain largely unchanged, with losses reflecting decreases in fill factor, with development of rollover, particularly in devices stressed in the dark.

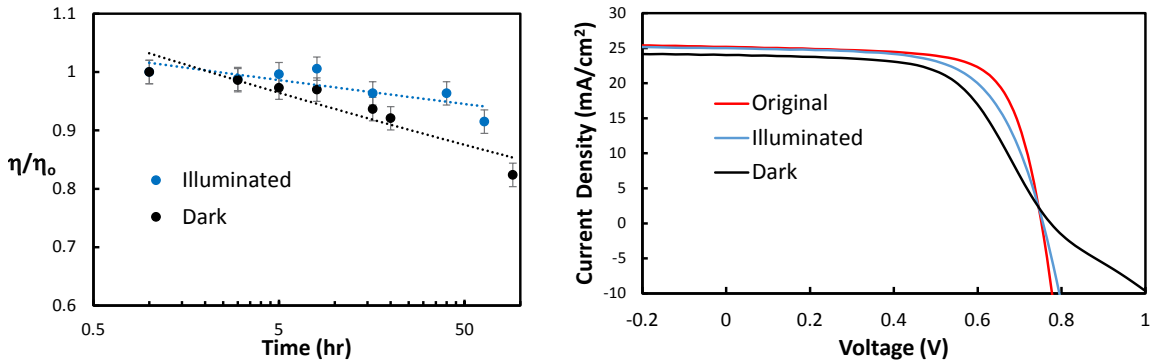

Figure 3. Results of ALT testing at T = 85 ºC showing change in efficiency and representative J-V curves before and after ALT as a function of illumination.

Future Work: There are several areas of ongoing and future work that are being pursued in parallel including the following activities:

- Doping CdTe with group V elements: Recently P-doped source material has been produced and it is demonstrated that significant P is incorporated in final devices.
- Elimination of $CdCl_2$: Preliminary work has yielded ~9% efficient devices without $CdCl_2$, and it is expected that this value may be improved significantly with future study.
- Engineered Heterojunction: The unique evolution of sputtered CdS:O during high temperature device processing has been discerned in collaboration with BAPVC partners at UO and others. This has spurred new work directed at directly engineering the heterojunction without need for post-processing.
- Stability: In collaboration with BAPVC partners at Georgia Tech the stability of novel encapsulants for CdTe solar cells is being examined.

BAPVC Annual Project Report

Project Title: Laser Processing to Improve CdTe Thin Film Photovoltaics Efficiency and Manufacturing

PI: M.A. Scarpulla – University of Utah
E-mail: scarpulla@eng.utah.edu

Summary:

The project focused on post deposition laser processing of CdTe absorbers. Laser driven cadmium chloride treatment of CdTe was achieved by using a continuous wave infrared laser with a dwell time of 15 s. Also, effects of laser treatment on the surface passivation was investigated. Reduction of surface states resulted in un-pinning of the Fermi energy and reduction in surface recombination velocity were observed following laser treatment of CdTe with and without chlorine passivation.

Key Accomplishments:

$CdCl_2$ treatment of CSS deposited CdTe on glass was carried out by using a 1064 nm continuous wave infrared laser. Photoluminescence studies showed a strong A-center peak associated with chlorine passivation on laser treated samples accompanied by a quenching of defect states. Figure 1 shows the spectrally resolved photoluminescence (PL) at 10 K from laser treated CdTe with and without $CdCl_2$. Significant increase in PL yield was observed for laser treated samples accompanied by quenching of the DP peak at 1.55 eV. A prominent 1.43 eV peak, generally associated with A-center, was observed in the laser treated sample in presence of $CdCl_2$. These signatures are also seen in conventional $CdCl_2$ treated samples indicating that the laser process affects similar changes to point defects. This was achieved with a laser dwell time of 40 s on CdTe samples deposited on glass. Similar results were achieved on CdTe samples deposited on alumina with a laser dwell time of 15 s. This work was presented at the recent 42nd IEEE Photovoltaic Specialists Conference [1].

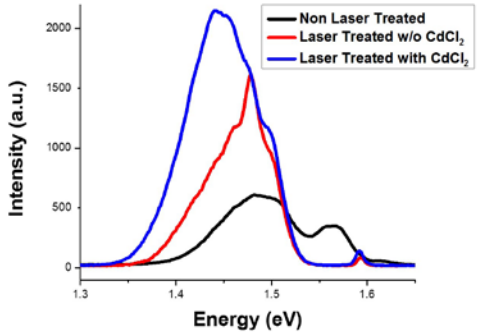

Fig. 1. 10 K PL spectra of laser treated CdTe on glass with and without $CdCl_2$

Surface photovoltage spectroscopy (SPS) and time resolved photoluminescence (TRPL) were used to investigate the effects of laser treatment on CdTe solar cell stacks. The studies showed that a laser dwell time of 20 s with a power density of 250 W/cm^2 is sufficient to reduce surface Fermi level pinning of CdTe by reducing surface defects. Figure 2 shows the SPS of as-deposited and laser treated CdTe stacks (Glass/TCO/CdS/CdTe). Removal of the local minimum just above 1.5 eV

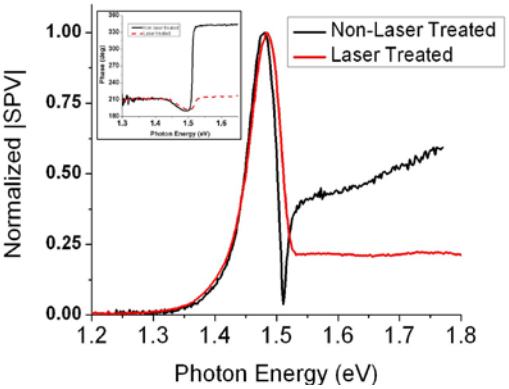

Fig. 2. SPS of as-deposited and laser treated CdTe. Inset shows the SPS phase spectra.

for laser treated samples is attributed to a reduction in number of surface states (reduced Fermi-level pinning). The sub-bandgap photon energies probe both the bulk and surface, while the super-gap energies probe only the depletion width induced by surface Fermi level pinning. This interpretation is supported by the SPS phase spectra (inset of Figure 2) which shows a phase change only near the bandgap and the laser treated sample surface in-phase with the bulk. Single photon TRPL was carried out at 10 K. This experiment is known to be very sensitive to surface recombination so the fact that the TRPL lifetime increases from 7 ns in non-laser treated samples to 15 ns in laser treated samples is also consistent with a reduction in surface recombination. This work was published in Journal of Applied Physics [2].

Future Work:

In the next period, we will focus on studying the use of laser annealing to activate group-V dopants in CdTe as well as investigating athermal effects of light on defect equilibrium and diffusion.

References:

[1] S. Misra, M.I. Khan, V. Palekis, C. Ferekides and M.A. Scarpulla, "*Continous wave laser assisted post deposition chlorine treatment of CdTe*", 2015 IEEE 42nd Photovoltaic Specialists Conference, June 2015. (in press)

[2] B.J. Simonds, V. Kheraj, V. Palekis, C. Ferekides and M.A. Scarpulla, "*Reduction of Fermi level pinning and recombination at polycrystalline CdTe surfaces by laser irradiation*", Journal of Applied Physics **117** 225301 (2015).

BAPVC Annual Project Report

Project Title: Laser Processing to Improve CdTe Thin Film Photovoltaics Efficiency and Manufacturing

PI: **Chris Ferekides; University of South Florida**
E-mail: ferekide@usf.edu

Summary:
This is a collaborative project between the University of South Florida (USF) and the University of Utah. The main goal is to develop high throughput laser-based solar cell processing techniques to improve manufacturability and performance, and lower the manufacturing costs of CdTe thin film PV. Work during year 2 focused on the development of post-deposition Laser-based $CdCl_2$ heat treatments (HT) using a NIR laser (808 nm) donated by Intevac. The baseline solar cell structure being utilized for this project is*: glass/TCO/CdS/CdTe/Back contact.*

Key Accomplishments:
A 60 Watt dual diode 808nm laser is being used for the laser based $CdCl_2$ HT. An X-Y stage was installed to control the speed and direction of the device/cell exposed to the laser beam. Initial results showed poor cell performance due to large temperature gradients (≈10-15 °C/mm) across the laser beam area (0.6 x 0.6 cm^2). This problem was addressed by upgrading the original optics resulting in a rectangular shaped laser beam with size 3 x 0.8 cm^2 and smaller temperature gradient (≈2 °C/mm); the laser annealing apparatus is shown in Fig. 1.

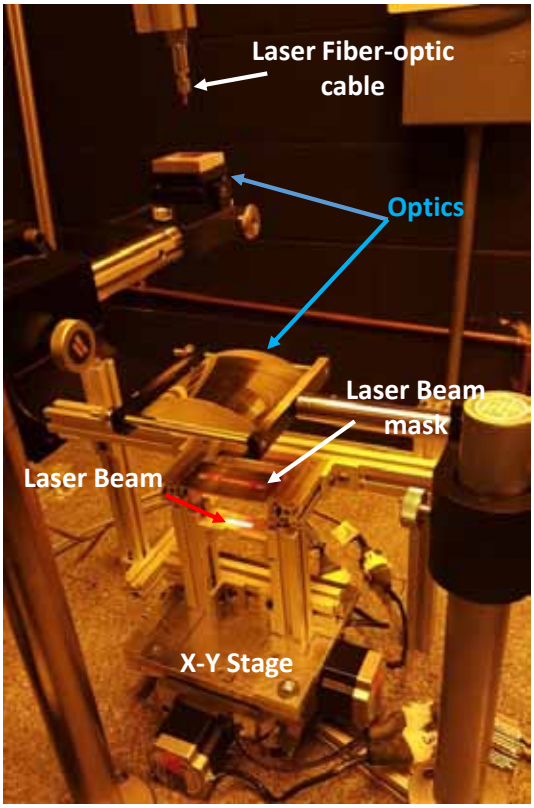

Figure 1. NIR Laser Setup

Devices were initially laser treated under a stationary beam to establish optimum conditions of laser power density. This approach was taken due to difficulties to directly measure the sample temperature. Figure 2 shows the spectral response data for devices treated for 5 and 15 minutes for various laser power densities. CdS thinning is observed at high power densities and long anneal times as seen by the increase in SR at short wavelengths (500 nm). There is also a shift in the SR at long wavelengths (>800 nm) due to bandgap narrowing from sulphur diffusion into CdTe (forms $Cd_{1-X}S_XTe$). These effects are also observed for cells treated using the conventional thermal $CdCl_2$ HT.

To simulate a typical manufacturing process, devices were *moved* under the laser beam with the use of an X-Y stage. Scan times (exposure of the cell under the laser beam) were varied from 1 to 7 minutes. Devices treated at low power densities exhibit the same behavior as with an as-deposited sample (implying that these devices were *under-treated*). The effects of the $CdCl_2$

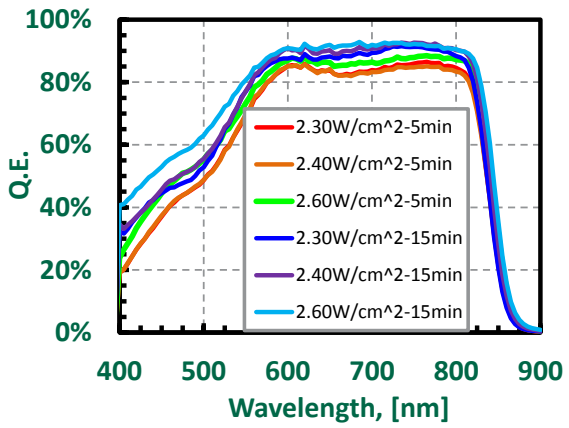

Figure 2. SR data for laser treated CdTe solar cells under different power densities and anneal times

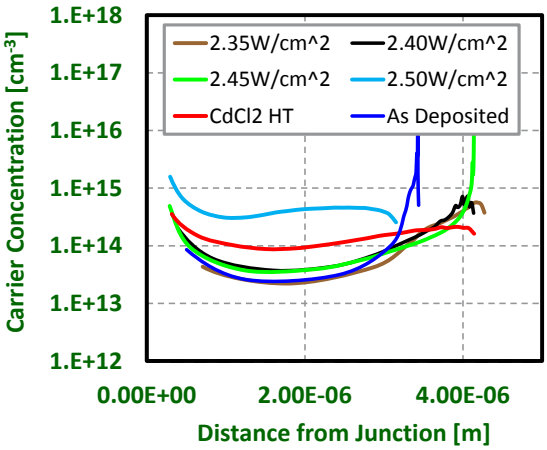

Figure 3. Net-doping concentration vs. laser power density

"activation" are realized at the highest power densities; presumably the improvement in the electronic properties of CdTe - increased carrier lifetime - resulted in improved carrier collection and therefore higher V_{OC} and FF.

It is also noteworthy that the net doping levels of Laser treated samples exhibit a correlation with power density. Doping concentration increases as laser power density increases (see Fig. 3). Even though higher doping than the conventional $CdCl_2$ treated devices was achieved this was not accompanied by an increase in V_{OC} as one would expected, suggesting that other mechanisms are more dominant.

The best cell fabricated to-date demonstrated an efficiency of 13.3% (V_{OC}=800mV, J_{SC}=23.3mA, FF=71.0%). The limiting factor for higher performance is the low V_{OC}'s 790-800 mV when compared to state of the art values of 840-850 mV. The V_{OC} limiting mechanism is currently under investigation.

Future Work:

Future work will focus on: (a) understand what causes the V_{OC} limitation and (b) further optimization of the Laser-based $CdCl_2$ treatment.

BAPVC Annual Project Report

Project Title: Grain Boundary Engineering in Solution-Processed CdTe Solar Cells
PI: A. Paul Alivisatos
E-mail: alivis@berkeley.edu

Summary:
The Alivisatos group has developed a new method for systematically controlling the grain structure in thin film CdTe solar cells. By printing successive layers of nanocrystal inks, we are able to make films in which a single grain spans the thickness of the device. First, the group synthesized a CdTe-Cl nanocrystal building block. By controlling the concentration of the nanocrystal solution and the number of layers in a layer-by-layer sintering method, they have shown that the resulting film morphology can be tuned from a grainy, porous structure, to a dense film with columnar grains. Solar cells incorporating the columnar film exhibit nearly a 10-fold improvement in efficiency improved over devices incorporating grainy films.

Key Accomplishments:
Cadmium telluride (CdTe) solar cell performance relies on the CdTe film microstructure. The most efficient devices require exposure to chloride in a multistep process making grain structure control difficult. The Alivisatos group is seeking to engineer a CdTe nanocrystal (NC) building block that can be deposited from solution and subsequently sintered as a method to control film microstructure for device optimization.

The Alivisatos group has successfully synthesized a solution stable building block. This carefully designed material is a CdTe NC decorated with surface chloride, seen in the far left of **Fig 1**. The nanocrystal is colloidally stabilized with octylamine, a labile ligand that is removed upon heating above 300°C. The group has shown that the CdTe-Cl building block solution can be deposited and subsequently sintered into a film with grain size range 50-150 nm at a low temperature and quick time of 350C and 30s, also shown in **Fig 1**.

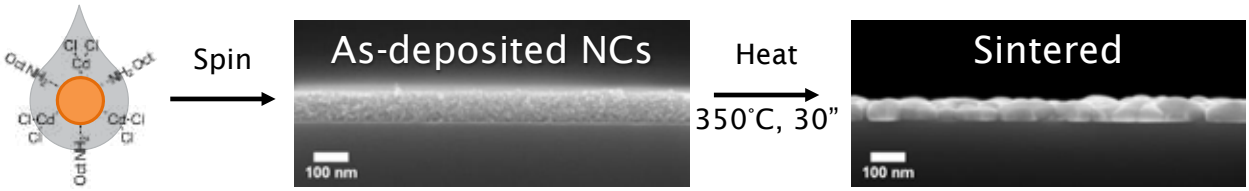

Figure 1: Sintering scheme of a single layer of deposited CdTe-Cl NCs; center and right images: SEM

The Alivisatos group has demonstrated film morphology control by controlling the NC concentration ([NC]). CdTe films were sintered into thick films by a layer-by-layer process as illustrated in the first row of **Fig 3**. First, a NC layer is deposited from solution and sintered. The consecutive NC layer fills the voids and upon sintering and increases the film thickness. Grain morphology in these films was manipulated by changing the [NC] as shown in Fig 2. Solutions with high [NC] produced porous and grainy films while low [NC] yielded continuous films with a columnar grain structure.

[NC]	0.48 mM	0.24 mM	0.12mM
#	4 layer	8 layer	16 layer

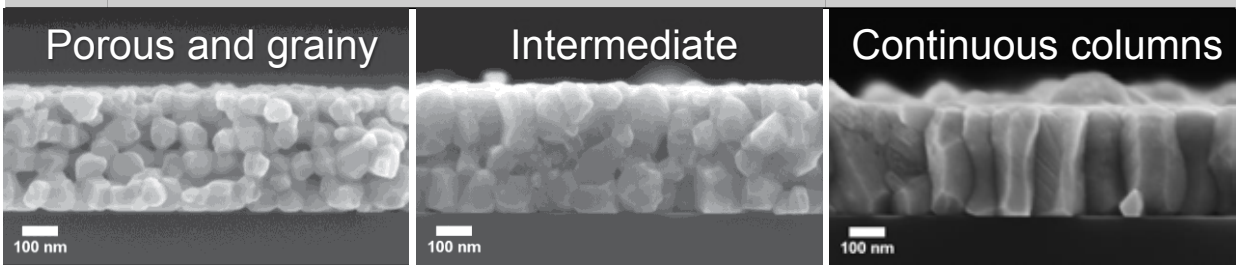

Figure 2: Cross sectional SEM images showing grain morphology as a function of [NC].

The Alivisatos group has established the relationship between grain structure and solar cell performance. Since grain boundaries disrupt charge transport in crystalline materials, the group hypothesized that devices incorporating columnar films will have better performance than those with a grainy texture. The group fabricated simple devices in which the CdTe layer was deposited on an ITO substrate, paired with n-ZnO and capped with aluminum (see **Fig 3** for scheme.) Solar cells with a columnar film performed up to 10x better than devices with a grainy structure, as shown in **Fig 4**. To increase hole transport, solar cells with columnar films sintered in air (oxygen source, facilities p-type doping) provided an addition boost to performance and double the device efficiency.

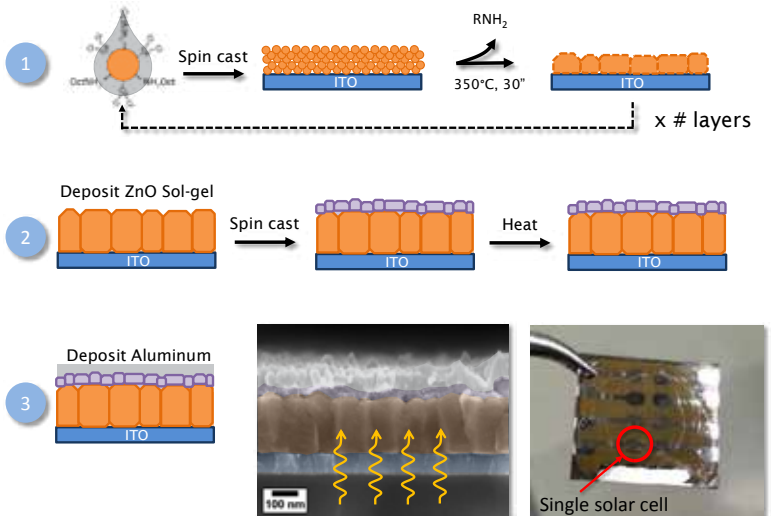

Figure 3: Solar cell fabrication scheme

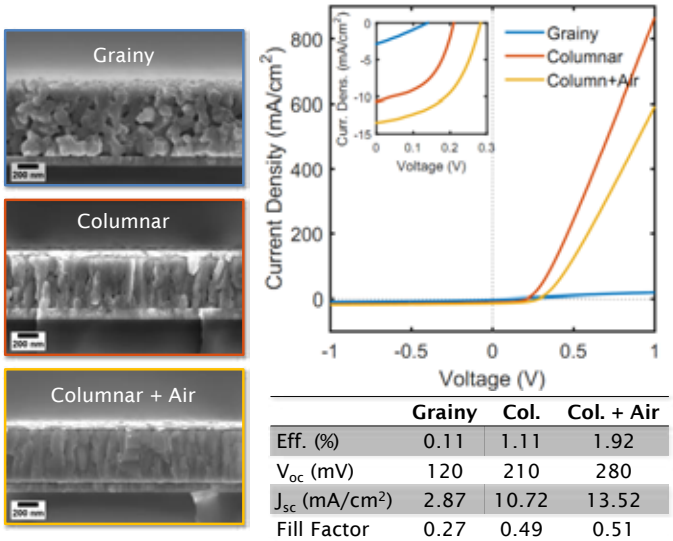

	Grainy	Col.	Col. + Air
Eff. (%)	0.11	1.11	1.92
V_{oc} (mV)	120	210	280
J_{sc} (mA/cm²)	2.87	10.72	13.52
Fill Factor	0.27	0.49	0.51

Figure 4: Solar cell device performance

Future Work:

The next steps in this project is to optimize the sintered CdTe films for solar cells. We have a CdTe-Cl building block that can be sintered layer-by-layer into continuous, columnar films. Devices will be optimized using column width and doping profiles. We will modulate column width using sintering temperature. For doping, we will look to oxidation regents that can be added to the solution instead of air such as pyridine oxide. Film structure and composition will be characterized by EDS and XRD while performance will be characterized by scanning probe techniques such as kelvin probe and c-AFM.

BAPVC Annual Project Report

Project Title: In Situ Characterization of Grain Growth in Thin Film Semiconductors
PI: Prof. Delia J Milliron
E-mail: milliron@che.utexas.edu

Summary:
This project focuses on the development of thin film absorbers from a solution-processed nanocrystal of multicomponent copper chalcogenide-based compound semiconductor such as CIGS, CZTS and CIS. The nanocrystals film can be subsequent transformed into large grain thin film by thermal annealing. The group is deliberately making nanocrystal with hexagonal phase (Wurtzite), which is a metastable structure for these materials with the hope to leverage the transformation to the stable phase will trigger grain growth effectively. Further surface functionalization of these nanocrystal with elements that drive grain growth, like selenium and sodium, thereby result in "in situ selenization" upon annealing. Thin film growth during thermal annealing is studied by In-situ X-ray diffraction, Raman, XPS, TEM and SEM and the resulting microstructures are now being correlated with optoelectronic properties of the materials.

Key Accomplishments:
Over the last two year the group has been developing a versatile colloidal approach to synthesize high quality compound semiconductor nanocrystals [Cu_2ZnSnS_4, $CuInGaS_2$, Cu-In-Zn-S, $CuInS_2$, $Cu_2ZnSn(S_{1-x}Se_x)_4$, etc.] with tight control of shape, size, composition and crystal phase. Specifically, the group has developed a synthesis in which the shape (spherical and rod) and crystal structure of nanocrystals is precisely controlled by reaction conditions – the novelty of this work was the synthetic achievement of hexagonal Wurtzite phase alloyed copper chalcogenide (CIGS and CZTS), which is a metastable structure for these materials. The group has experimentally demonstrated that the use of metastable phase nanocrystal helps in inducing the grain growth under thermal treatment due to metastable to stable conversion. By doing *in-situ* and *ex-situ* XRD studies, this transformation was revealed as being very fast and happening within few minutes of annealing, and thin films of absorber materials with average grain sizes up-to one micron (see Figure) can be achieved not only at low temperature but also without the need of traditional high temperature selenization process. The resulting thin films have been further analyzed with Raman, XPS, PL and SEM to understand the quality of the absorber material. During this study of grain growth using metastable nanocrystals, we have found that we can control more precisely the nucleation and growth regime during annealing by simply using different shapes (rod and sphere) of nanocrystals with similar composition. Further, we have functionalized the surface of our nanocrystals with chalcogenidometallate clusters (ChaMs) consisting of elements that drive grain growth, like selenium, thereby resulting in "*in situ selenization*" upon annealing. By controlling the nanocrystal loading in the ChaMs matrix (Figure), we have achieved not only the polycrystalline thin films with micron size grains but also compositional tunability through ion exchange process of Se with S, which is similar to high temperature selenization process. Resulting absorber material has been characterized with Raman, XRD and PL to confirm the material composition and properties.

Two papers have been published and one more submitted. We expect to publish a complete report about the phase transformation-driven grain growth later this year.

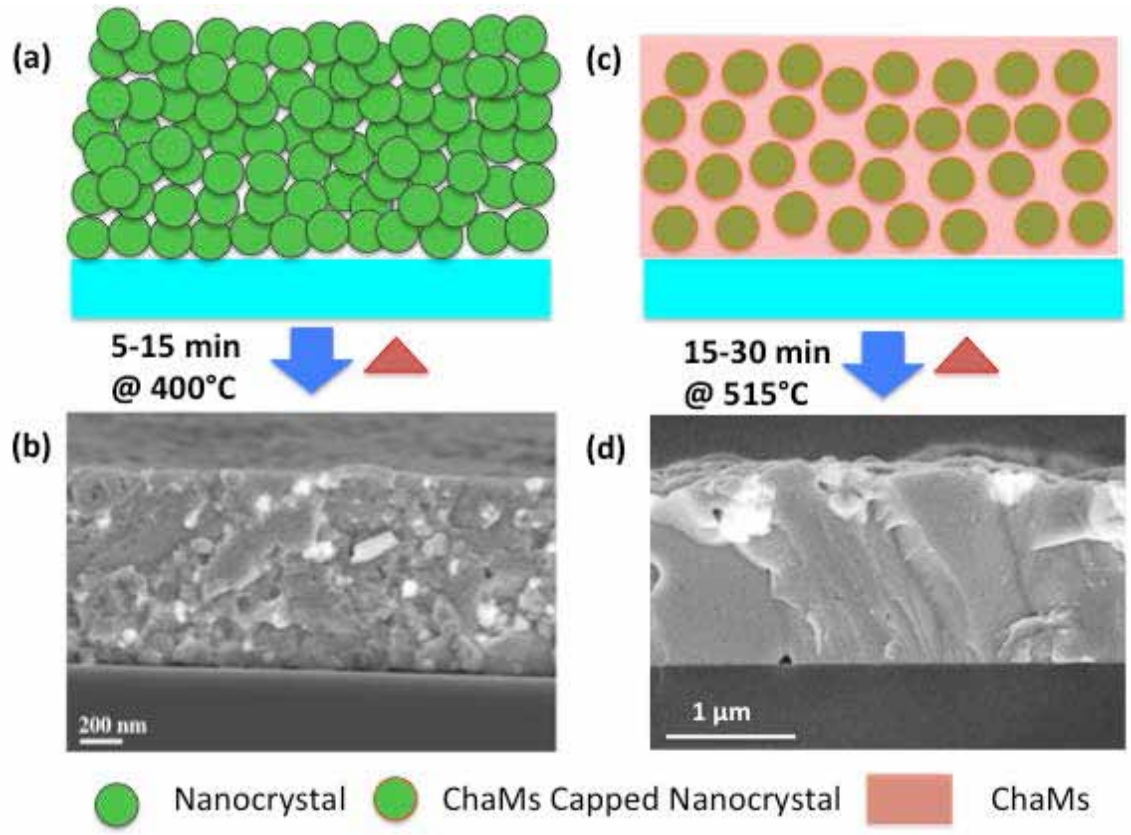

Figure. (a) & (b) Thermal treatment of a nanocrystal film containing metastable nanocrystal results in grain growth. **(c) & (d)** Surface functionalized nanocrystals embedded in a ChaMs matrix consisting of elements that drive grain growth.

Future Work:

In the coming year, we will continue our focus in optimization of film thicknesses with controlled composition and grain growth over device scale area for the fabrication of full PV devices. The optoelectronics properties (hall measurement and PL) of the resulting polycrystalline thin film deposited with and without ChaMs on the substrate will also be investigated. We will further try to introduce other dopants such as antimony in the nanocrystal (during synthesis) or on the surface through ChaMs to understand their effect on the selenization process. This will be studied by using RTP developed by Mike Toney's group at SLAC (BAPVC member) and employing their in-situ x-ray diffraction facility, which will be further accompanied with ex situ SEM analysis and Raman spectroscopy to understand the course of selenization of absorber material.

BAPVC Annual Project Report

Project Title: Applying Cation-Exchange Chemistry to Nanowire Arrays for Efficient Solution-Processed Solar Cells

PI: P. Yang – UCB
E-mail: p_yang@berkeley.edu

Summary:

This group has developed solution-processed sulfide-based nanowire array solar cells that take advantage of improved charge collection and light-trapping effects in nanowire arrays. Within the past year, this group has achieved power conversion efficiencies approaching 4%. This group is also developing low temperature processing techniques for $CH_3NH_3PbX_3$ nanorod array absorber layers that can be applied for photovoltaic devices.

Key Accomplishments:

In the past year, this group has demonstrated CdS- Cu_2S core-shell nanorod array photovoltaics with efficiencies approaching 4%, and a full description of this project has been recently published.[1] In brief, the fabrication of these solar cells is shown in figure 1a. These photovoltaics are based on CdS nanorod arrays grown by a hydrothermal method on an FTO substrate. After protection layers are added to prevent shorting of the p-type Cu_xS to the n-type contact, the CdS nanorod array can be dipped into an aqueous Cu^+ solution to perform cation exchange to yield an array of CdS-Cu_xS core-shell nanorods. The phase and thickness of the Cu_xS can be controlled by varying the cation exchange temperature and time. A plot of the *I-V* curve of a champion device is shown in figure 1b. Contrary to reports on planar devices, the performance of the device is stable after a period of about one month of storage in an inert atmosphere.

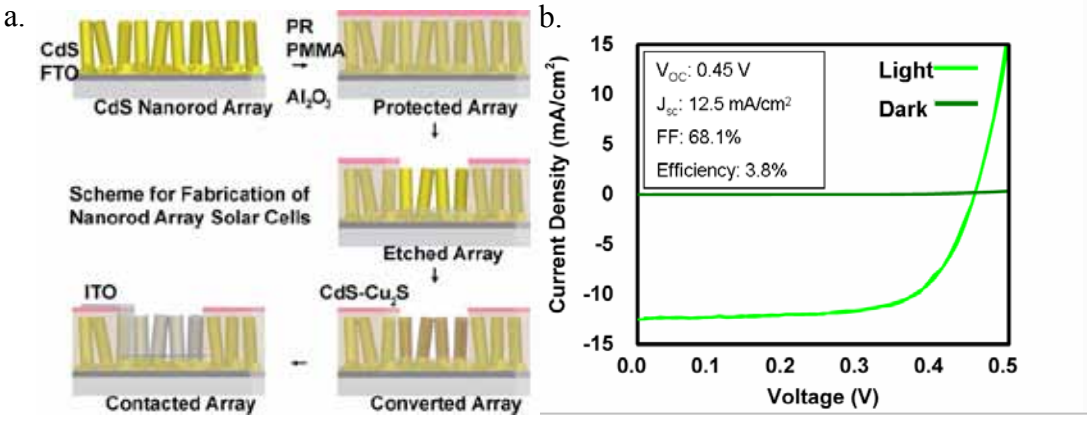

Figure 1. CdS-Cu_2S core-shell nanorod array photovoltaic. a) Schematic for device fabrication. b) *IV* characteristic of a champion device.

[1] Wong, A.B.; Brittman, S.; Yu. Y.; Dasgupta, N.; Yang, P. *Nano Lett.*, **2015**, 15, 4096-4101.

This group is also developing other new methods for the low temperature processing of nanostructured absorber layers for photovoltaics. This group has recently synthesized hybrid perovskite nanorod arrays with a composition of $CH_3NH_3PbBr_3$, and this group has shown that is it possible to use a vapor phase anion exchange technique to transform this material into $CH_3NH_3PbI_3$ nanorod arrays as shown in Figure 2.

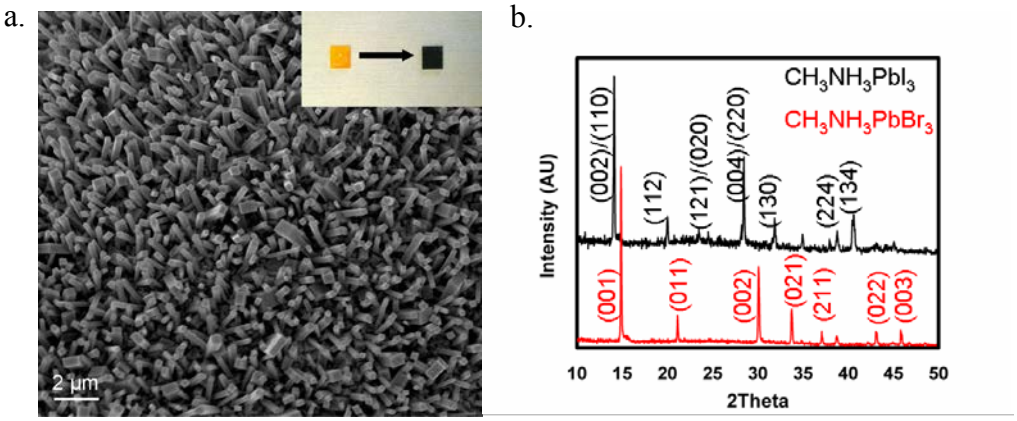

Figure 2. Characterization of $CH_3NH_3PbX_3$ nanorod arrays. a) Scanning electron microscopy image of a $CH_3NH_3PbI_3$ nanorod array after conversion from the as-grown $CH_3NH_3PbBr_3$ nanorod array. b) Powder X-ray diffraction of $CH_3NH_3PbBr_3$ nanorod array and $CH_3NH_3PbI_3$ nanorod array after anion exchange.

Future Work:

Future work will build on the successful fabrication of nanowire photovoltaic devices. This group will optimize performance by tuning the geometry and morphology of the nanowire absorber layer, by controlling the chemistry of the hole and electron transport layers, and by optimizing the design of the electrical contacts to increase device performance beyond current levels.

Thrust: Encapsulation and Reliability

Key Challenges

A key challenge for PV module and system reliability is the fact that many of the mechanisms of observed degradation modes are not well understood. This thrust seeks to identify and characterize degradation mechanisms, facilitate the design and standardization of accelerated testing protocols, and provide the fundamentals for the design of improved PV materials and product designs. In particular, we will: (1) characterize the stability and reliability of PV materials and interfaces, including barrier-films and encapsulants; and (2) develop an understanding of the coupled thermo-mechanical, electro-chemical, and photo-chemical degradation mechanisms that determine the reliability and operational lifetimes of PV technologies.

Existing Projects in our Thrust

- *Reliability and Operational Lifetimes for BAPVC Technologies,* Reinhold Dauskardt (Stanford)
- *PV Module Performance and Lifetime Prediction: Inserting New Technologies Without Lifetime Penalty,* Roger French (Case Western)
- *Novel polymer-nanocrystal composite barrier layers*, Rachel Segalman, Jeffrey Urban (Berkeley)
- *Tailoring Electrostatic Interactions to Produce Hybrid Barrier Films for Photovoltaics*, Bernard Kippelen, Samuel Graham (Georgia Tech)

Potential New Areas of Interest

- Expansion of current work to characterize, model and predict coupled thermo-mechanical and photo-chemical degradation processes in PV technologies to include electro-chemical processes like those responsible for *potential induced degradation (PID)*.
- *Increased interaction with other thrusts* to support reliability and degradation characterization and modeling with particular interests in emerging perovskite, ultra-thin silicon, CdTe and InP PV, along with transparent conductors.
- Development of *multi-layer thin-film mechanics and degradation models* for cell, interconnect, and encapsulant interfaces in PV module packaging technologies, both cell-based and monolithically-integrated.
- Connecting these models with *detailed transport models* for photons, electrons, phonons, and ions in a hierarchical fashion, in order to predict other failure modes.
- *Analysis and development of a database* of thermo-mechanical, electro-chemical, and photo-chemical degradation properties of materials for benchmarking BAPVC innovations, to guide field testing, and inform computer simulations.
- Refinement and redesign of standardized reliability testing capabilities for the broader BAPVC community, re-designing testing for field exposed samples, and calibration/validation of kinetic degradation models and lifetime prediction procedures using in-service and field-exposed data.

BAPVC Annual Project Report

Project Title: Photovoltaic Encapsulant and Backsheet Debonding
PI: Reinhold Dauskardt
E-mail: dauskardt@stanford.edu

Summary:

A metrology was developed to measure adhesion in solar module interfaces without the need for active crack monitoring. Coupled with previously developed fracture-mechanics metrologies, it was used to characterize interfacial debond as a function of temperature and relative humidity. Accelerated environmental testing of the backsheet structure revealed a dramatic drop in adhesion at the PVF/PET after exposure to damp heat. An investigation of the encapsulant lamination process identified a critical cure time and surface preparation procedures that improved the adhesion at the EVA/glass interface.

Key Accomplishments:

The Dauskardt group developed a simplified, mechanics-based adhesion metrology that is both crack-length independent and requires minimal data analysis and specimen preparation. To quantify encapsulation adhesion, Ti/glass/EVA/glass/Ti square adhesion coupons were fabricated as shown in Fig. 1. When loaded by a corner, the coupons debond at a constant mechanical force (P_c) and the energy of adhesion G_c (J/m^2) can be easily calculated with $G_c=P_c^2/(4B)$, where B is the cross-section bending stiffness (per unit width) of the bilayer substrate (Ti/glass). A representative load-displacement curve for a square test coupon is shown in Fig. 2. The value of P increases upon initial loading, plateaus during steady-state debonding at P_c, and decreases abruptly when the debond line reaches the middle of the coupon. G_c measurements of EVA larger than 200 J·m^2 were common and were attributed to (1) cavitation ahead of the debonding-tip and (2) crazing and bridging behind the debonding-tip. It is important to note that the high energy deformation processes (cavitation and crazing) are not measurable in any of the currently-available peeling techniques.

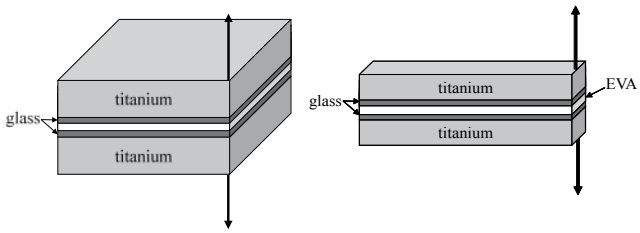

Fig.1. [left] Square corner coupon loaded in tension by a corner. A sheet of encapsulation (EVA, shown in white) was thermally bonded between two glass (150 μm) square substrates bonded to secondary titanium (830μm) substrates as shown. [right] Double cantilever beam with bilayer (Ti/glass) substrates.

This metrology was extended to quantify adhesion in other module laminates using both lab-made coupons and full-size solar modules, both with square and beam-shaped substrates. It was found that that adhesion of the backsheet structure decreased from 1000 to 30 J/m^2 as a consequence of exposure to an accelerated *damp-heat* treatment (80°C and 80%RH). As shown in Fig. 3,the debond energy decreased dramatically from 1000 to 27 J/m^2 (indicating increased propensity for failure) within the first 750 hrs and remained constant during the last 250 hrs of the damp-heat treatment. The loss in debond energy corresponded to a change in the backsheet

debond path, which was partially cohesive in the PVF in specimens aged for t < 750hrs (remnants of the PVF film were left on the debonded PET surface) and was exclusively adhesive at the PVF/PET interface in specimens aged for 750 and 1000 hrs.

EVA/glass adhesion was characterized with respect to lamination cure time and substrate surface treatments. Concerning cure time, EVA/glass adhesion increased (0.48 to 1.5 kJ/m^2) during the first 9 min of post-lamination treatment at 140°C, then decreased with further exposure, implying that there exists a critical time at temperature for which adhesion is optimized. Regarding surface treatment, triple rinsing the glass substrate with acetone + IPA + UV ozone yielded a G_c of 1 kJ/m^2 whereas using a tricholorobenzene degreaser treatment yielded a G_c of 0.5 J/m^2. The triple rinse + UV yielded the largest G_c due to more efficient covalent bonding of the ionomer to glass; the residual thin film left by the tricholorbenzene lead to lower values of G_c. In both cleaning treatments, thicker encapsulations yielded larger values of G_c. All specimens exhibited cavitation, crazing and bridging, as expected when G_c > 200 J/m^2.

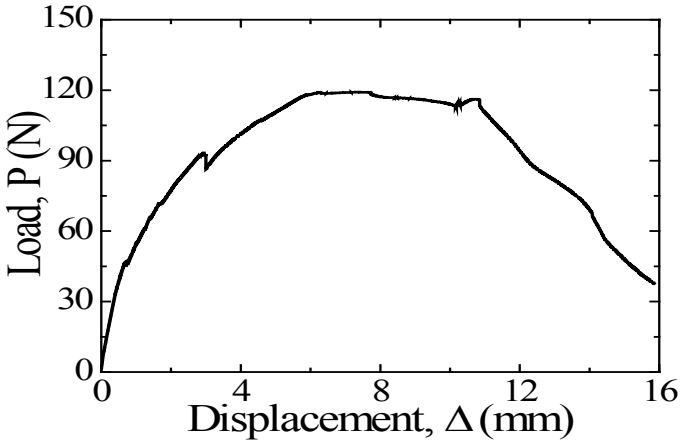

Fig.2. Load-displacement curve for EVA/glass debonding obtained by loading the square adhesion coupon by a corner. The value of *P* increased with initial loading, plateaued during steady-state debonding at P_c, and decreased abruptly when the

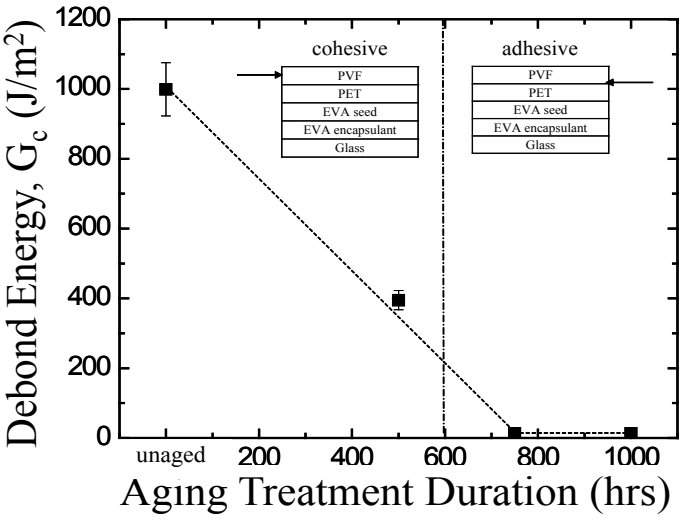

Fig.3. Backsheet adhesion vs. duration of aging treatment at 85°C and 85% RH. Arrow in stacking diagram indicates debond path location: partially cohesive in PVF after 0 and 500 hrs of treatment and strictly adhesive at the PVF-PET interface after 750 and 1000 hrs.

Future Work:

The Dauskardt group will characterize the effects of encapsulation material, (e.g. EVA, ionomer, polyolefin), on the debond energy and encapsulant debonding kinetics. The group will continue to develop multi-layer thin-film mechanics and degradation models for cell, interconnect, and encapsulant interfaces in PV module packaging technologies. Additionally, the group will refine the developed reliability testing capabilities for the broader BAPVC community, re-designing testing for field exposed samples and calibration/validation of kinetic degradation models and lifetime prediction procedures using in-service and field-exposed data.

BAPVC Annual Project Report

Project Title: PV Module performance & Lifetime Prediction: Inserting New Technologies Without Lifetime Penalty
PI: Roger H. French, Kenneth D. Singer, Jiayang Sun, Guo-Qiang (GQ) Zhang
E-mail: roger.french@case.edu

Summary:

A data science approach is being developed for the performance and lifetime prediction (PLP) tool for real-world exposed modules and mini-modules exposed to accelerated exposures to elucidate key degradation modes including corrosion of screen printed silver. The PLP tool is being developed using semi-supervised generalized structural equation modeling (semi-gSEM) for statistical analytics, which generates visual representation of the strength of relationships between stress and responses.[1]

Key Accomplishments:

The PLP tool has been developed to include automated diagraming of degradation pathways and relationships between stress, mechanisms/modes, and responses. The semi-gSEM methodology has been published on Git as an open source package (1C). PyCRADLE GUI was developed to ingest data into E-CRADLE. Nagios was developed to monitor real-world data streams and a databook to keep metadata in Hadoop.

A statistical model was developed using 60 modules of 20 different brands exposed in Cleveland, OH using time series data. Data cleaning procedure was developed and data was integrated into E-CRADLE. Hierarchal clustering showed that the brand effect had less of an impact than the mounting configuration of the model. A mixed effect model was developed to understand the relationship between variables, which include power produced, temperature, irradiance, and model brand. The pairwise plot for this model is shown in Figure 1.[2]

Screen printed corrosion is being investigated to understand the mechanism of degradation and its relationship to overall power loss.[3] This accelerated study protocol includes multi-factor exposures to relate the stress to the degradation mechanism. Mini-modules fabricated by the DuPont Silicon Valley Technology Center. These mini-module samples were finished at the SDLE center and were prepared for testing by adding junction boxes and modifying cable lengths. The prepared modules were used to develop and establish three lab instruments and measurement techniques (EL Imaging, I-V Curves, and Confocal Raman Microscopy) for the non-destructive characterization of electrical and chemical properties of mini-modules. Electroluminescence image of a mini-module exposed to

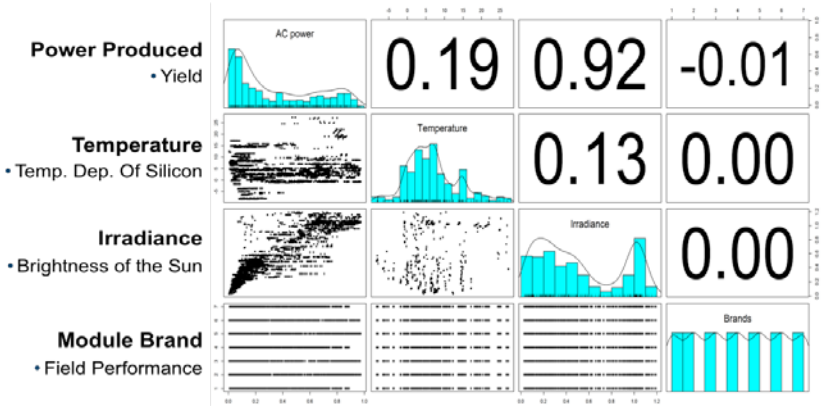

Figure 1: Pairwise plot for the mixed effect module for real-world exposed modules.

damp heat accelerated exposure shows degradation attributed to silver corrosion in Figure 2. Raman spectra are shown in Figure 3 for different segments of the module. R code was developed to facilitate data handling of the three file types produced by the measurement techniques (jpg, xml, spc), and additional code was developed to automate ANOVA modeling of Gage R&R experimental results. Sources of variation being contributed by the measurement techniques themselves were investigated with several rounds of these experiments and corrective measures were designed and implemented.

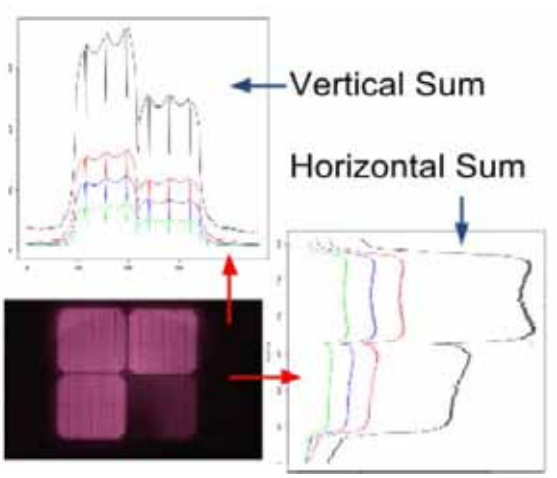

Figure 2: Quantitative image analytics applied to electroluminescence of a mini-module exposed to 1000 hrs of damp heat.

Degradation of transparent conductive oxides (ITO, AZO, FTO) was studied subjecting them to environmental and material stressors. Optical, electrical and surface sensitive TCO property metrics were analyzed and different degradation mechanisms observed.[4]

Future Work:

The next iteration of the semi-gSEM methodology (sgSEM v 0.5) will be able to understand the contribution of multiple stressors and stress levels on the performance loss

In time series analysis additional data will be analyzed to further refine the mixed effects model of real-world PV module degradation. Additionally, the time series data analysis will begin to elucidate information within the dataset to help predict module performance.

Future work on the Screen Printed Silver Corrosion in PV Modules project begins with applying the developed measurement techniques to baseline the mini-module samples prior to beginning environmental exposures. While the dataset is being generated, figures of merit that summarize each datatype will be identified through a combination of literature and observed results, and automatically extracted from the accumulating raw data files. The distilled dataframe of these variables will be analyzed with the semi-gSEM technique to create statistical models describing the rates and functional forms of the observed mechanistic degradation modes and pathways in the two styles of mini-module due to the various stressors present in the exposure conditions, which is the overall goal of this project.

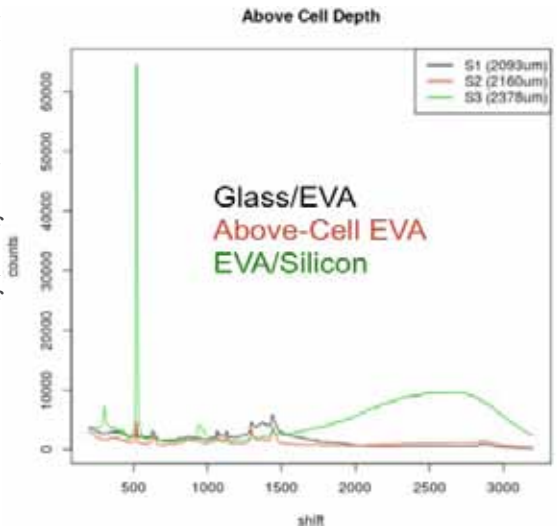

Figure 3: Confocal Raman spectra at various depths in a mini-module, demonstrating the ability to non-destructively probe chemical degradation.

References

1. French, Roger H., et. al, "Degradation Science: Mesoscopic Evolution and Temporal Analytics of Photovoltaic Energy Materials," Current Opinion in Solid State and Materials Science, 2015.
2. Hu, Yang, 2014, Thesis, CWRU.
3. Wheeler, N. R. et. al, SPIE 9563-32, 2015.
4. Mirletz, H. M, et al. Sol. En. Mat, & Cells, 2015.

BAPVC Annual Project Report

Project Title: Composite encapsulation layers
PI: Jeffrey Urban
E-mail: jjurban@lbl.gov

Summary:

The group has developed encapsulating layer PV modules using a composite of polymer and water-scavenging nanocrystals. In the first phase, the composite of block copolymer and hygroscopic nanocrystals was used, probing the role of the composite structure and nanocrystals. In this final phase of the project, we build upon both lessons learned from the first phase and feedback from the consortium to move to more scalable systems that can be deployed to partners. Specifically, the group is using more commercially available polymeric system in the second phase with water-scavenging metal organic framework (MOF) molecules.

Key Accomplishments:

The group utilized a self-assembly of block copolymer (poly(styrene-*b*-2-vinylpyridine), PS-P2VP) to modulate the structure of the films. The block copolymer is comprised of hydrophilic (P2VP) and hydrophobic (PS) parts, and its self-assembly results in either spherical (PS-P2VP(S)) or lamellar (PS-P2VP(L)) structure, depending on the ratio of two parts (Figure 1). In both cases, water-scavenging hygroscopic nanocrystals (MgO) are incorporated into hydrophilic blocks. Water vapor molecules are blocked by the hydrophobic layer firstly, and the permeated molecules are absorbed by hydrophilic parts and water-scavenging nanocrystals. Particularly, this water-absorbing process is reversible; hence, the scavenged water molecules can be "breathed-out" again without saturation of the absorbing sites.

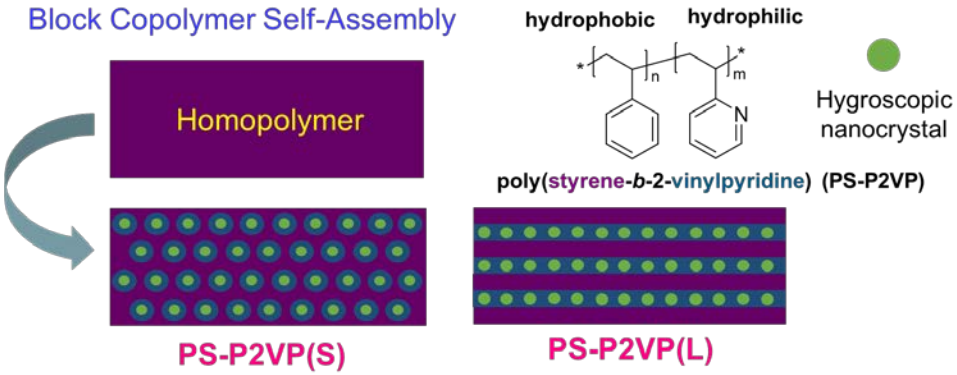

Figure 1. A schematic of the composite films: PS-P2VP(S) and PS-P2VP(L)

Water Vapor Transmission Rate (WVTR) studies showed that our block copolymer system is much more efficient as a barrier layer than the original hydrophobic homopolymer (PS) film, even though the hydrophilic parts are added, which can be attributed to the well-defined internal structure. In addition, the incorporation of hygroscopic nanocrystals (MgO) raised the water-vapor blocking ability of the film to a higher level. Morphologically, it was observed that the sphere structure is more efficient than lamellar.

	WVTR ($g \cdot m^{-2} \cdot day^{-1}$)	WVTR ($g \cdot mil \cdot m^{-2} \cdot day^{-1}$)
PS-P2VP (S)	5.882	$3.076*10^{-3}$
PS-P2VP-MgO (S)	5.719	$2.118*10^{-3}$
PS-P2VP (L)	6.355	$3.285*10^{-3}$
PS-P2VP-MgO (L)	6.184	$2.845*10^{-3}$
PS		7.286

Figure 2. WVTR studies of the composite films

In the first phase, the group learned that the composite of a spherical structure led to more efficient water vapor-blocking; hence, in the second phase they moved to more commercially available base materials as multi-lamellar structures do not offer a clear benefit but only increase cost. The new encapsulating barrier is a composite comprised of hydrophobic COC polymer (cyclic olefin copolymer) and water scavenging MOF nanocrystal to improve the environmental stability and processability, and also functionality and price. The basic idea is an extension of the previous work comprised of PS-P2VP block copolymer and MgO nanoparticle, in which hygroscopic inorganic nanoparticle were incorporated into the copolymer. Already we have fabricated some initial composites for testing at large scale using doctor-blading, and obtained transparent films. Moisture and adhesion tests are underway.

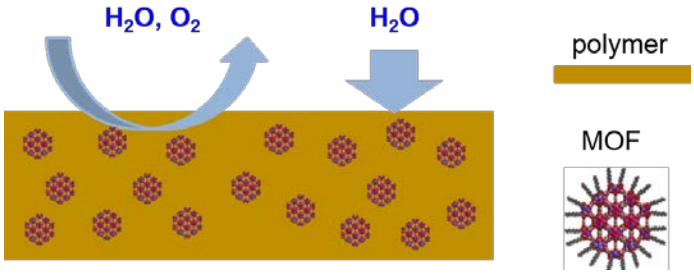

Figure 3. Schematic of the novel composite barrier layer material to under development

Future Work:

The key barrier in this system is to disperse MOF nanocrystal in the polymer matrix, and the group has been working to enhance the dispersibiliy of MOF in hydrophobic solvent. The composite film of COC polymer and MOF with different crystal size will be fabricated using doctor blading, and WVTR value will be measured. Furthermore, the group will test the protection ability of the COC/MOF films by coating the encapsulating materials on different photovoltaics, and will understand bonding/failure mechanisms. (Collaborations underway with Prof. Dauskardt, Prof. Salleo)

Key Publication:

"Enhanced water vapor blocking in transparent hybrid polymer-nanocrystal films", Eun Seon Cho, Christopher M. Evans, Emily C. Davidson, Megan L. Hoarfrost, Miguel A. Modestino, Rachel A. Segalman, and *Jeffrey J. Urban, *ACS Macro Lett.,* **4**, 70-74 (2015).

BAPVC Annual Project Report

Project Title: Tailoring Electrostatic Interactions to Produce Hybrid Barrier Films for Photovoltaics

PI: Bernard Kippelen and Samuel Graham, Georgia Institute of Technology
E-mail: kippelen@gatech.edu

Summary:
In this program, the Kippelen/Graham groups at Georgia Tech have developed barriers coatings using a combination of vacuum deposition methods (PECVD and ALD) that were tested on various photovoltaic systems ranging from crystalline Si to organic photovoltaics. Encapsulation of devices has been achieved by using either a direct deposition process of the barrier layers onto the device or by using indirect methods where the barrier is laminated to the device structure. During the past year, barriers with various structures including ALD nanolaminates, and PECVD/ALD hybrid structures have been studied and characterized in terms of effective water vapor transmission rate measured during damp heat testing. All of these structures were tested using optical Ca tests. High performance was achieved through control of the mechanical properties and film architecture.

Key Accomplishments:

I. Integration of Hybrid Barriers With Perovskite (with McGehee Group, Stanford), CdTe Solar Cells (with Wolden Group, Colorado School of Mines): The performance of the newly developed hybrid barrier films was tested on perovskite solar cells fabricated in the McGehee group at Stanford. The barrier films were prepared on PEN substrates at Georgia Tech and used to encapsulate the devices as shown in Figure 1. The SiN_x film was deposited using plasma-enhanced chemical vapor deposition (PECVD), and the Al_2O_3 and TiO_2 films were deposited using atomic layer deposition (ALD). Afterwards, the prepared barrier films were applied on the perovskite solar cells using a UV-curable adhesive. While good stability was observed in packaged perovskite cells stored in ambient laboratory conditions (see Fig. 1b), the cells were found to degrade rapidly under continuous light soaking experiments possibly caused by a reaction between the UV-curable epoxy and the perovskite layer.

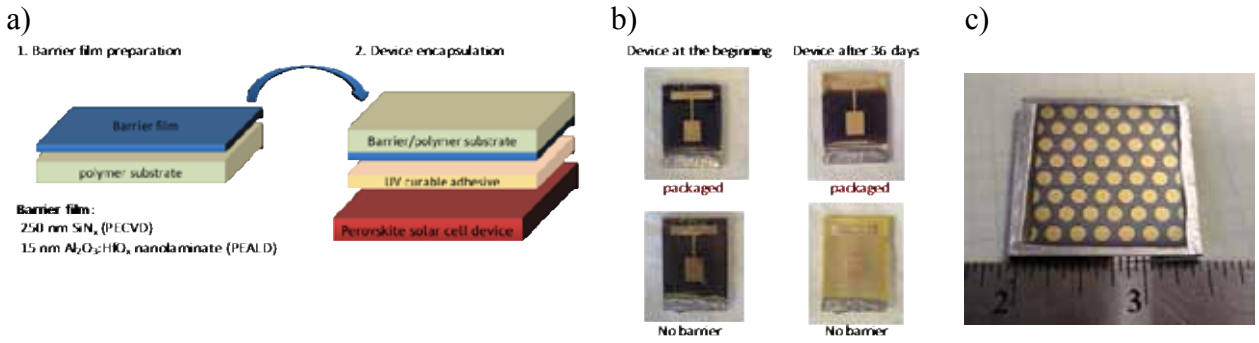

Figure 1: a) Device encapsulation procedure for perovskite solar cells; b) Photographs of encapsulated cells and reference cells stored under ambient conditions; c) Photograph of CdTe solar cells encapsulated using the direct deposition of hybrid barrier layers.

The performance of the hybrid barrier films was also evaluated on CdTe solar cells received from the Wolden Group at the Colorado School of Mines. As an initial test, the barrier film was directly deposited onto the CdTe solar cells (see Fig. 1c) and no degradation in performance was observed after the encapsulation process. Studies are underway to test the lifetime of these cells under harsh damp hear environmental conditions.

II. Reducing the Impact of Residual Stress on the Mechanical Reliability of Hybrid Barrier Films: The Kippelen/Graham groups have shown that the use of polymer layers to passivate particle defects on the surface of devices prior to the growth of atomic layer deposition (ALD) barrier films can result in the spontaneous cracking of the barrier layers. Such cracking renders the performance of the barrier film unacceptable. For this study, two barrier architectures were grown on fluorinated polymer (Cytop) coated Ca sensors that were used to monitor the permeation of moisture and oxygen (Fig. 2a). The cracking in ALD Al_2O_3 and HfO_2 nanolaminates deposited on Cytop planarization layers increased with increasing thickness of the Cytop layer (Fig. 2b). This is due in part to the high tensile residual stresses that exist in low temperature deposited ALD film combined with the stress concentration around particle defects, and the reduction to constraint of channel cracking in the ALD layer with thicker polymer films. By inserting a compressively stressed SiNx layer between the ALD layer and the Cytop (Figure 1), the cracking of the barrier films on Cytop was eliminated.

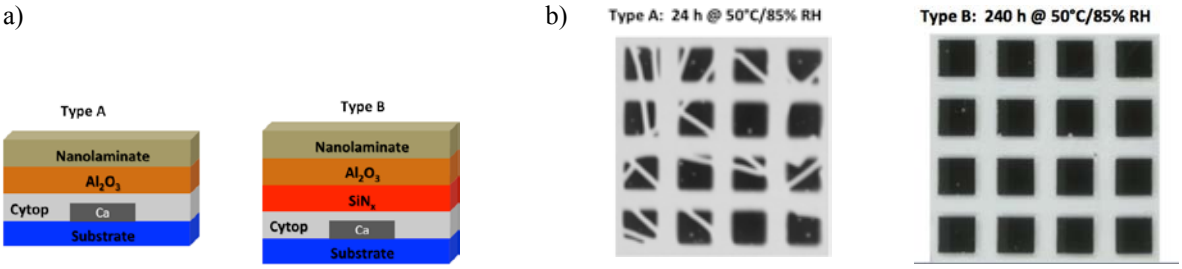

Figure 2: a) Structures of the two multilayer barrier film architectures studied. Type-A: ALD barrier deposited directly onto Cytop layer; Type-B: ALD layer deposited on SiN_x layer on Cytop. b) Type A barrier film on Ca sensors on glass with a 1000 nm Cytop polymer layer. and a Type B barrier film on Ca sensors on glass with SiNx and a 1000 nm Cytop polymer layer. Sample structure Type A is after 24 h at 50°C/85% RH where the Ca degradation along the crack defects are clearly visible. Sample structure Type B is after 240 h at 50°C/85% RH.

Future Work:
While the barriers developed in this program show good performance, these hybrid barrier structures are complex in nature, and methods to further reduce the processing time and complexity are needed for broader adoption by industry. Following the leads from previous studies on multilayer barrier films, the Kippelen/Graham groups will focus on testing PECVD SiNx/Polymer multilayers where the polymer layer consists of a nanocomposite. The polymer nanocomposites incorporate metal-organic frameworks (MOFs) that have been chosen for their low permeability for water vapor, low cost, and their thermal and chemical stability. Initial testing of these films is underway.

Bay Area Photovoltaic Consortium
McCullough Building
476 Lomita Mall
Stanford, CA 94305-4045
http:/bapvc.stanford.edu